

Self-assembly of Low Molecular Weight Gellants in the Presence of Surfactants

Inaugural-Dissertation

zur Erlangung des Doktorgrades
der Mathematisch-Naturwissenschaftlichen Fakultät
der Heinrich-Heine-Universität Düsseldorf

vorgelegt von

Filiz Yapici

aus Düsseldorf

Düsseldorf, Dezember 2019

aus dem Institut für Molekulare Physikalische Chemie
der Heinrich-Heine-Universität Düsseldorf

Gedruckt mit Genehmigung der
Mathematisch-Naturwissenschaftlichen Fakultät
der Heinrich-Heine-Universität Düsseldorf

Berichtersteller:

1. Prof. Dr. Claus A.M. Seidel
2. Prof. Dr. Wolfgang von Rybinski

Tag der mündlichen Prüfung:

21.01.2020

“Be the change you want to see in the world”

Ghandi (1869 - 1948)

For my family

Content

1	Zusammenfassung	9
2	Summary	14
3	Introduction	19
3.1.	State of the Art	19
3.1.1.	Studies on the Interactions between Surfactant Molecules and LMWGs	20
3.1.1.1.	Gelation Behavior in Organic Solvents	20
3.1.1.2.	Gelation Behavior in a Water System	22
3.1.2.	Importance of the History of Gel	23
3.1.3.	Rheological Studies	24
3.2.	Motivation and Objectives	25
4	Theoretical Background	27
4.1.	Physicochemical Properties of Surfactants	27
4.2.	Low Molecular Weight Gellants	30
4.2.1.	Definition	30
4.2.2.	Formation of a Gel Network	31
4.2.3.	Coassembly Models	34
4.3.	Methods	34
4.3.1.	Cryogenic-Transmission Electron Microscopy	34
4.3.2.	Dynamic Light Scattering	36
4.3.3.	Rheology	38
5	Experimental Methods	42
5.1.	Chemicals	42
5.2.	Sample Preparation	42
5.3.	Cryogenic-Transmission Electron Microscopy	43
5.4.	Surface Tension Measurements	45
5.5.	Dynamic Light Scattering	46

5.6. Rheology	46
6 Results and Discussion.....	48
6.1. Gelation Behavior of DBC in a Water System	48
6.1.1. Phase Transition Temperature	48
6.1.2. Characterization of the Phase Transition and Properties of Gel	51
6.1.2.1. Optical Microscopy	51
6.1.2.2. Cryogenic-Transmission Electron Microscopy.....	52
6.1.2.3. Surface Tension Measurements.....	53
6.1.2.4. Kinetics of the Sol-Gel Phase Transition	54
6.2. Study of the Gelation Behavior of DBC in the Presence of LAS.....	63
6.2.1. Molecular Interactions below the Critical Gelation Concentration	64
6.2.1.1. Surface Tension Measurements.....	64
6.2.2. Molecular Interactions above the Critical Gelation Concentration.....	66
6.2.2.1. Phase Transition Temperature	66
6.2.2.2. Optical Microscopy	75
6.2.2.3. Cryogenic-Transmission Electron Microscopy.....	76
6.2.2.4. Kinetics of the Sol-Gel Phase Transition	83
6.3. Study of the Gelation Behavior of DBC in the Presence of C₁₂₋₁₈E₇.....	103
6.3.1. Molecular Interactions below the Critical Gelation Concentration	103
6.3.1.1. Surface Tension Measurements.....	103
6.3.2. Molecular Interactions above the Critical Gelation Concentration.....	105
6.3.2.1. Phase Transition Temperature	105
6.3.2.2. Rheological Study.....	108
6.4. Comparison of the Gelation Behavior of DBC in the Presence of LAS and C₁₂₋₁₈E₇	110
6.5. Study of the Gelation Behavior of L-Tyr-L-Tyr in the Presence of LAS.....	113
6.5.1. Gelation Behavior of L-Tyr-L-Tyr in a Water System	115
6.5.2. Molecular Interactions in Mixture with LAS	117

6.5.2.1.	Phase Transition Temperature	117
6.5.2.2.	Microscopic Images	121
6.5.2.3.	Kinetics of the Sol-Gel Phase Transition	126
6.6.	Comparison of the Gelation Behavior of DBC vs.	
	L-Tyr-L-Tyr	135
7	Outlook	145
8	Abbreviations	146
9	List of Figures	148
10	List of Tables	158
11	References	162
12	List of Presentations	173
13	Acknowledgements	174
14	Eidesstattliche Erklärung	175

1 Zusammenfassung

Niedermolekulare Gelbildner mit einer molaren Masse von weniger als 1000 Da können durch eine thermo-reversible, nicht-kovalente Selbstorganisation ein stabiles dreidimensionales Netzwerk aus Fasern oder Aggregaten^{[1]–[10]} bilden, welches das Lösungsmittel immobilisieren kann^{[11],[12]}.

Sie werden hauptsächlich in organischen Lösungsmitteln oder mit Wasser mischbaren Co-Lösungsmitteln eingesetzt. In Studien zu niedermolekularen Gelbildnern in wässrigen Systemen ohne Co-Lösungsmitteln werden die genauen Verfahren zur Herstellung der Gele für rheologische Messungen und der Einfluss von Tensidmolekülen auf die Dynamik der Bildung von Gelnetzwerken in wässrigen Systemen in der Literatur nur unzureichend beschrieben.

Die vorliegende Studie hat einen neuen Weg für ein besseres Verständnis der Gelierungseigenschaften von Hydrogelatoren in Gegenwart von Tensidmolekülen aufgezeigt, da systematische Untersuchungen für zwei verschiedene Arten von niedermolekularen Gelbildnern unter definierten Scher- und Präparationsbedingungen durchgeführt wurden.

Zusätzlich können Vorhersagen für den Gelierungsprozess in Gegenwart von Tensidmolekülen gemacht werden.

In dieser Arbeit für Hydrogelatoren wurde der Einfluss von Tensidmolekülen auf den Gelierungsprozess, einschließlich der Induktions-, Gelierungs- und Gleichgewichtsphasen, unter Verwendung von Rheologie untersucht. Daher war es notwendig, eine Herstellungsmethode mit definiertem Temperaturprofil und definierten Scherbedingungen zu entwickeln.

Die Morphologie des Gelnetzwerks wurde auch durch Lichtmikroskopie- und kryogene Transmissionselektronenmikroskopie- (cryo-TEM) Messungen charakterisiert. Um Informationen über den Einfluss der Molekülstruktur der Hydrogelatoren zu erhalten, wurden die Gelierungseigenschaften von zwei verschiedenen niedermolekularen Gelbildnern in Gegenwart von Tensidmolekülen im wässrigen System untersucht. Ein Modell für die Bildung des Gelnetzwerks für das ternäre System aus Gelator, Tensid und Wasser wird vorgeschlagen.

Herstellung von Gelen

Zur Herstellung der Gele wurde eine abgewogene Menge des Gelators in einem Wassersystem oder einer wässrigen Tensidlösung in einem Fläschchen hergestellt und dann in einen Heiz-Thermomixer gestellt. Die Probe wurde erhitzt und geschüttelt, bis eine klare Lösung erhalten wurde. Die Temperatur wurde auf eine Temperatur abgesenkt, bei der sich die Probe in der Solphase befand, sodass keine Gelbildung auftrat. Für rheologische Messungen war es wichtig, dass die Gelbildung nicht im Fläschchen, sondern im Spalt des Rheometers erfolgt. In dieser Studie wurde festgestellt, dass bei Auftreten einer Gelierung in dem Fläschchen die Rheologie eher auf den Selbstheilungscharakter des Gels als auf das tatsächliche Gelierungsverhalten abzielte, da ein Spatel für den Transfer des Gels in das Rheometer verwendet worden war, was zu einer Zerstörung des Gelnetzwerks führt.

Um das Gelierungsverhalten zu untersuchen, ohne dass das Gelnetzwerk durch äußere Kräfte gestört wurde, wurde die Probe in der Solphase in das Rheometer überführt, so dass die Gelierung in dem Spalt des Rheometers als außerhalb des Rheometers auftrat. Das Gelierungsverhalten wurde unter definierten Scherbedingungen untersucht.

Gelierungsverhalten von DBC in Gegenwart von LAS und C₁₂₋₁₈E₇

H₂O-LAS-DBC

Es wurde festgestellt, dass DBC (N,N'-Dibenzoyl-L-Cystin) in einem wässrigem System und sogar in Mischung mit LAS (Natrium-n-Alkylbenzolsulfonat) gelieren kann. Oberhalb der kritischen Gelierungskonzentration von 4,46 mM wurde festgestellt, dass die Zugabe von LAS zu dem DBC-in-Wasser System die DBC Induktions- und Gelierungsphasen stark beeinflusste.

In der Induktionsphase wurde herausgefunden, dass die Bildung von Gelnetzwerken bei niedrigen LAS-Konzentrationen gefördert und bei hohen LAS-Konzentrationen verzögert wurde.

Es wurde angenommen, dass die Förderung der Bildung von Gelnetzwerken auf die verbesserte Dispersion von DBC Partikeln durch Tensidmoleküle während des Heizprozesses der Probenpräparation zurückzuführen war. Dies könnte zur Bildung kleinerer Aggregate durch die Abnahme der Grenzflächenspannung zwischen den Gelatoraggregaten und der Wasserphase geführt haben, was den Nukleationsprozess der Gelatoraggregate erleichtern könnte.

Die Verzögerung könnte der Diffusion von Gelatormonomeren zugeschrieben werden, die durch Tensidmizellen behindert wurden, da unter Verwendung verschiedener Annahmen ein dicht gepacktes System von Mizellen berechnet wurde.

Als weiterer Aspekt könnte die Verzögerung der Bildung des Gelnetzwerks auf eine sterische Hinderung der Gelatoraggregate zurückzuführen sein, da LAS-Moleküle auf ihrer Oberfläche so adsorbieren, dass die Moleküle nicht direkt miteinander interagieren könnten. Diese Barriere muss für den Nukleationsprozess der Gelatoraggregate überwunden werden.

Die Gelierungsphase in Gegenwart von Tensiden wurde durch Anwendung der von *Huang et al.*^[13] vorgeschlagenen *Dickinson*-Gleichung untersucht. Dabei wurde herausgefunden, dass der zur Beschreibung der Gelierungskinetik in der *Dickinson*-Gleichung enthaltene D_r -Parameter für alle Systeme gleich war, obwohl der Gelator in Abwesenheit und Gegenwart von Tensiden experimentell eine sehr unterschiedliche Kinetik zeigte. Die *Dickinson*-Gleichung ist daher nicht geeignet, diese Systeme zu beschreiben. Es wurde daher ein qualitatives Modell entwickelt, dass die Wechselwirkungen mit dem Gelator berücksichtigt.

Die Bestimmung der $t-t_g$ -Werte für einen konstanten G' -Wert zeigte, dass die Gelierungsrate mit zunehmender LAS-Konzentration verringert wurde, die mit den cryo-TEM-Aufnahmen korrelierte, als eine feinere Gelnetzwerkstruktur mit steigender LAS-Konzentration gebildet wurde. Das Netzwerk wurde aus faserartigen Aggregaten mit einer Dicke von bis zu 280 nm aufgebaut; bei hohen Tensidkonzentrationen wurde eine feinere Netzwerkstruktur von entweder festen Fasern oder faserartigen Aggregaten mit einer Dicke von bis zu 100 nm gebildet. Dies legt nahe, dass die Bildung feiner Netzwerkstrukturen länger dauert als die Bildung robuster Strukturen.

In der Gleichgewichtsphase wurde festgestellt, dass die $G'(\infty)$ -Werte bei hohen Tensidkonzentrationen geringfügig höher waren als bei niedrigen Tensidkonzentrationen, was mit der Bildung eines feineren Gelnetzwerks korreliert, wenn die Tensidkonzentration erhöht wird.

Zum ersten Mal wurde gezeigt, dass die Förderung und Verzögerung der Bildung des Gelnetzwerks durch die Zugabe des gleichen Tensidmoleküls erfolgt und dass die Verzögerung nicht zu einer Abnahme der G' -Werte führt.

H₂O-C₁₂₋₁₈E₇-DBC

In Mischung mit C₁₂₋₁₈E₇ (Fettalkoholethoxylat) wurde die Bildung des DBC-Gelnetzwerks für Tensidkonzentrationen von bis zu 1,72 mM gefördert. Oberhalb dieser Konzentration trat Phasenseparation oder Kristallisation auf.

Die Gelierungsphase konnte aufgrund der schnellen Gelierungskinetik nicht untersucht werden.

In der Gleichgewichtsphase, waren die $G'(\infty)$ -Werte höher als die des binären Systems H₂O-DBC, was darauf hindeuten könnte, dass sich in Gegenwart des Niotensids eine feinere Gelnetzwerkstruktur bildet als in Abwesenheit von Tensidmolekülen.

Der Vergleich der beiden Systeme zeigt, dass die Gelnetzwerkbildung in Mischung mit C₁₂₋₁₈E₇- oder LAS-Molekülen im niedrigen Tensidkonzentrationsbereich von bis zu 1,72 mM gefördert wird, da in Mischung mit Tensidmolekülen höhere $T_{\text{sol-gel}}$ -Werte ermittelt wurden als im binären wässrigen System. In der Gleichgewichtsphase wurden für das DBC-in-C₁₂₋₁₈E₇-System höhere $G'(\infty)$ -Werte gefunden als für das DBC-in-LAS-System, was auf eine feinere Gelnetzwerkstruktur in Mischung mit C₁₂₋₁₈E₇ als in einer Mischung mit LAS hindeuten könnte.

Gelierungsverhalten von L-Tyr-L-Tyr in Gegenwart von LAS

L-Tyr-L-Tyr (3,6-bis(4-hydroxybenzyl)piperazin-2,5-dion) konnte nur in Gegenwart von LAS ein Gelnetzwerk bilden. In Abwesenheit von Tensidmolekülen konnte keine Gelierung erzeugt werden.

In der Induktionsphase wurde die Gelbildung bei hohen Tensidkonzentrationen durch Abkühlen mit einer Geschwindigkeit von 5 K/min verzögert. Bei schneller Abkühlung mit 10 K/min wurde keine Verzögerung der Gelbildung beobachtet.

Studien zur Wirkung von LAS-Molekülen auf die Gelierungsphase haben gezeigt, dass die Gelierungsrate bei unterschiedlichen Abkühlungsraten innerhalb ähnlicher $t-t_g$ -Bereiche liegt. Es gab keinen klaren Trend, der den Anstieg der LAS-Konzentration mit der Gelierungsrate korrelierte.

Als die Bildung des Gelnetzwerks in der Gleichgewichtsphase abgeschlossen war, wurden durch Abkühlen der Probe mit einer Geschwindigkeit von 5 statt 10 K/min geringfügig höhere $G'(\infty)$ -Werte erhalten. Es wurde kein deutlicher Trend bei den $G'(\infty)$ -Werten festgestellt, der mit den cryo-TEM-Aufnahmen korrelierte. Es wurde gefunden, dass eine feine Gelnetzwerkstruktur von entweder festen Fasern oder faserartigen Aggregaten mit einer Dicke von bis zu 60 nm gebildet wurde. Die Morphologie änderte sich nicht mit zunehmender LAS-Konzentration.

Daraus kann geschlossen werden, dass, wenn die Induktions- und Gelierungsphasen nicht stark von Tensidmolekülen beeinflusst werden, ein ähnliches Verhalten auch in der Gleichgewichtsphase beobachtet werden kann, wenn die Bildung des Gelnetzwerks abgeschlossen ist.

Der Vergleich der beiden Gelatoren hat gezeigt, dass die Induktions-, Gelierungs- und Gleichgewichtsphasen von DBC stärker von LAS beeinflusst wurden als die von L-Tyr-L Tyr.

Es wurde angenommen, dass die L-Tyr-L-Tyr-Netzwerkstruktur aus festen Fasern und die DBC-Netzwerkstruktur aus faserartigen Aggregaten bestand, da sich herausstellte, dass die L-Tyr-L-Tyr-Gelierungsrate größer war als von DBC in Gegenwart von LAS. Es zeigte sich, dass die faserartigen Aggregate gegenüber Tensidmolekülen empfindlicher waren als die festen Fasern.

Dies wurde aus den folgenden Ergebnissen geschlossen: 1) Die Bildung des DBC-Gelnetzwerks bei hohen LAS-Konzentrationen wurde durch Abkühlen mit unterschiedlichen Geschwindigkeiten verzögert anstatt nur mit einer Geschwindigkeit von 5 K/min, 2) das Minimum vom G' -Wert während des Übergangs von der Induktions- zu der Gelierungsphase war für DBC stärker ausgeprägt als für das ternäre L-Tyr-L-Tyr-System, 3) die DBC-Gelierungsrate nahm mit zunehmender LAS-Konzentration ab, wobei für das L-Tyr-L-Tyr-in-LAS-System kein eindeutiger Trend festgestellt wurde, und 4) die DBC $G'(\infty)$ -Werte stiegen bei hohen LAS-Konzentrationen an, wobei für L-Tyr-L-Tyr kein eindeutiger Trend mit einem Anstieg der LAS-Konzentration gefunden wurde.

Aus den Befunden kann geschlossen werden, dass der Gelierungsprozess von niedermolekularen Gelbildnern durch Tensidmoleküle gesteuert und das Gelierungsverhalten in der Gleichgewichtsphase aus den Befunden aus der der Induktions- und Gelierungsphase vorhergesagt werden kann.

2 Summary

Low molecular weight gellants (LMWGs) with a molecular mass of less than 1000 Da, are capable of thermo-reversible, non-covalent self-assembly to form a stable, three-dimensional network of fibers or aggregates^{[1]–[10]} that is able to immobilize the solvent^{[11],[12]}.

They are mainly used in organic solvents or mixed with water-miscible co-solvents. In studies of LMWGs in water systems without any co-solvents, the exact procedure for preparing the gels for rheological measurements and the influence of surfactant molecules on the dynamics of gel network formation in water systems, are poorly reported in the literature.

The present study has shown a new way for a better understanding of the gelation properties of hydrogellants in the presence of surfactant molecules as systematical investigations were performed for two different types of LMWGs under defined shear and preparation conditions.

In addition, predictions for the gelation process in the presence of surfactant molecules can be made.

In this work for hydrogellants, the influence of surfactant molecules on the gelation process, including the induction, gelation, and quasi-equilibrium stages, using rheology was studied. Therefore, it was necessary to develop a preparation method with defined temperature profile and defined shear conditions.

The gel network's morphology was also characterized using optical microscopy and cryogenic transmission electron microscopy measurements. To get information about the influence of the molecular structure of the hydrogellant, the gelation properties of two different LMWGs in the presence of surfactant molecules were investigated in the water system. A model for the gel network formation of the ternary system gellant and surfactant in water is proposed.

Preparation of Gels

To prepare the gels, a weighed amount of the gelling agent in a water system or aqueous surfactant solution, was prepared in a vial and then placed in a thermomixer. The sample was heated and shaken until a clear solution was obtained. The temperature was lowered to a temperature, at which the sample was in the sol phase so that no gelation occurred. It was important for rheological measurements that gelation occurred within the rheometer's gap rather than in the vial. In this study, it was found that when gelation occurred in the vial, it was the gel's self-healing character rather than real gelation behavior that the rheology was monitoring, because a spatula had been used for the transfer of the gel into the rheometer, leading to the destruction of the gel network.

To study the gelation behavior without the gel network being disturbed by external forces, the sample was transferred into the rheometer as it was, in the sol phase, so that gelation occurred within, rather than outside, the gap. The gelation behavior was studied under defined shear conditions.

Gelation Behavior of DBC in the Presence of LAS and C₁₂₋₁₈E₇

H₂O-LAS-DBC

It was found that DBC (N,N'-dibenzoyl-L-cystine) was able to gel in a water system and even when mixed with LAS (sodium-n-alkyl-benzene sulfonate). Above the critical gelation concentration of 4.46 mM, it was found that the addition of LAS to the DBC-in-water system strongly influenced the DBC induction and gelation stages and, to a lesser extent, the quasi-equilibrium stage.

In the induction stage, it was found that gel network formation was promoted at low LAS concentrations and delayed at high LAS concentrations.

It was believed that the promotion of gel network formation was due to the enhanced dispersion of DBC particles by surfactant molecules, during the sample preparation heating process. This could have led to the formation of smaller aggregates due to the decrease in the interfacial tension between the gellant aggregates and the water phase, which could facilitate the gellant aggregates' nucleation process.

The delay could be attributed to the diffusion of gellant monomers being hindered by surfactant micelles, as, using various assumptions, a densely packed system of micelles was calculated.

As a further aspect, the delay in gel network formation could be attributed to steric hindrance of gellant aggregates due to LAS molecules being adsorbed on their surface in such a way that the molecules are unable to interact directly with one another. This barrier must be overcome for the aggregates' nucleation.

The gelation stage in the presence of surfactants was studied by the application of the *Dickinson* equation, proposed by *Huang et al.*^[13]. It was observed, that the D_f parameter of the *Dickinson* equation, describing the kinetic behavior of the gelation process, was found to be identical for all studied systems although the gelling agent showed different kinetic behavior in the absence and presence of surfactant molecules. Therefore, the *Dickinson* equation is not suitable for describing the kinetic behavior of these systems. As such, a qualitative model was developed including the interactions between gellant and surfactant molecules.

The determination of the t_{tg} values for a fixed G' value showed that the gelation rate was decreased by an increase of the LAS concentration, which correlated with the cryo-TEM images, as a finer gel network structure was formed by an increase of the LAS concentration. The network was built up of fiber-like aggregates with a thickness of up to 280 nm; at high surfactant concentrations, a finer network structure of either solid fibers or fiber-like aggregates, with a thickness of up to 100 nm, was formed. This suggests that it takes longer to form fine network structures than rough structures.

In the quasi-equilibrium stage, the $G'(\infty)$ values were found to be slightly greater at high surfactant concentrations than at low surfactant concentrations, which correlates with a finer gel network being formed when the surfactant concentration is increased. For the first time it was shown that the promotion and delay of gel network formation occurred by the addition of the same surfactant molecule and that the delay did not lead to a decrease of G' values.

H₂O-C₁₂₋₁₈E₇-DBC

In a mixture with C₁₂₋₁₈E₇ (fattyalcohol ethoxylate), the DBC's gel network formation was promoted for surfactant concentrations of up to 1.72 mM. Phase separation or crystallization occurred above this concentration.

The gelation stage could not be studied due to fast gelation kinetics.

In the quasi-equilibrium stage, the $G'(\infty)$ values were higher than those of the binary system H₂O-DBC, which could give an indication that a finer gel network structure is formed in the presence of the non-ionic surfactant, rather than in the absence of surfactant molecules.

To compare both systems, the gel network formation was promoted in a mixture with C₁₂₋₁₈E₇ or LAS molecules within the low surfactant concentration range, of up to 1.72 mM, as greater $T_{\text{sol-gel}}$ values were determined in a mixture with surfactant molecules than in a water system. In the quasi-equilibrium stage, higher $G'(\infty)$ values were found for the DBC-in-C₁₂₋₁₈E₇ system than for the DBC-in-LAS system, which could indicate a finer DBC gel network structure in a mixture with C₁₂₋₁₈E₇, rather than in a mixture with LAS.

Gelation Behavior of L-Tyr-L-Tyr in the Presence of LAS

L-Tyr-L-Tyr (3,6-bis(4-hydroxybenzyl)piperazine-2,5-dione) was only able to form a gel network in the presence of LAS. Gelation could not be produced in the absence of surfactant molecules.

In the induction stage the gel formation at high surfactant concentrations was delayed by cooling at a rate of 5 K/min. With fast cooling, 10 K/min, no delay in gel formation was observed.

From studies of the effect of LAS molecules on the gelation stage, it was shown that the gelation rate was found to be within similar $t-t_g$ ranges at different cooling rates. There was no clear trend correlating the increase in the LAS concentration to the gelation rate.

When the gel network formation was completed in the quasi-equilibrium stage, slightly higher $G'(\infty)$ values were obtained by cooling the sample at a rate of 5 instead of 10 K/min. A clear trend in the $G'(\infty)$ values was not found, which correlates with the cryo-TEM images as the formation of a fine gel network structure of either solid fibers or fiber-like aggregates with a thickness of up to 60 nm, was found. The morphology did not change when the LAS concentration was increased.

It can be concluded that if the induction and gelation stages are not strongly influenced by surfactant molecules, a similar behavior can also be observed in the quasi-equilibrium stage, when the gel network formation is completed.

The comparison of both gelling agents showed that the induction, gelation, and quasi-equilibrium stages of DBC were more influenced by the presence of LAS than by that of L-Tyr-L-Tyr.

It was believed that the L-Tyr-L-Tyr network structure was made up of solid fibers and that the DBC network structure consisted of fiber-like aggregates, as the L-Tyr-L-Tyr gelation rate was found to be greater than that of DBC in a mixture with LAS.

It appeared that the fiber-like aggregates were more sensitive to surfactant molecules than the solid fibers.

This was concluded from the following results: 1) The DBC gel network formation at high LAS concentrations was delayed by cooling at different rates instead of only at a rate of 5 K/min, 2) the minimum of G' value during the transition from the induction to the gelation stage, was more pronounced for the DBC than for the L-Tyr-L-Tyr ternary system, 3) the DBC gelation rate decreased with an increase in the LAS concentration, whereby no clear trend was found for the L-Tyr-L-Tyr-in-LAS system, and 4) the DBC $G'(\infty)$ values increased at high LAS concentrations, whereby no clear trend was found for L-Tyr-L-Tyr with an increase in the LAS concentration.

From the findings, it is possible to conclude that the gelation process of LMWGs can be controlled by surfactant molecules and that the gelation behavior in the quasi-equilibrium stage could be predicted from the findings from the induction and the gelation stages.

3 Introduction

3.1. State of the Art

Low molecular weight gellants (LMWGs), which are small molecules with a molecular mass of less than 1000 Da, belong to the group of supramolecular gels as they are capable of spontaneous, thermo-reversible, non-covalent self-assembly into a three-dimensional network of fibers or aggregates^{[1]–[10]} which is able to immobilize the solvent^{[11],[12]}.

In 1891, *Meunier*^[14] found the first LMWG, dibenzylidene sorbitol (DBS), which is now used in cosmetic products. In 1892, *Brenzinger*^[15] reported on N,N'-dibenzoyl-L-cystine (DBC) whereby, in 1921, *Cortner*^[16] described this substance as the first small molecule gellant, which was able to gel in a water system. However, research into the characterization of gelation properties started with LMWG 12-hydroxystearic acid (12-HSA), in 1912^[17].

Due to their advantages over the commonly used polymeric thickeners, such as their thermo-reversible self-assembly process driven by non-covalent interactions rather than covalent interactions, they have become more and more interesting in the literature to researchers. Apart from their thermo-reversibility, LMWGs have further advantages over polymeric thickeners, such as their biocompatibility^[18], which is particularly important for drug delivery, their self-healing character^[19], for example, for technological and biological applications, and their efficiency at very low gellant concentrations, such as 0.1 wt-%^[16].

LMWGs are categorized as hydrogellants when the surrounding medium is water, organogellants when the surrounding medium is an organic solvent such as decane, DMSO and ionogels when the surrounding medium is an ionic solvent, such as 1-butyl-3-methylimidazolium bromide^{[20]–[22]}.

The effect of additives, including electrolytes^[23], polymers^[24], other LMWGs^[25] and surfactants^{[26]–[29]}, on the gelation behavior of LMWGs was characterized using physical methods. Optical, electron, scanning electron and atomic force microscopy were performed to study the morphology of the gel networks. Rheological and calorimetric measurements were performed to gain insights into their structural behavior.

The investigations were completed using scattering (SAXS - small-angle X-ray scattering, SANS - small-angle neutron scattering, DLS - dynamic light scattering) and spectroscopic methods (Fluorescence, UV/VIS, MS, NMR and IR)^[30].

LMWGs are used in different applications, such as in the fields of drug delivery and tissue engineering. In drug delivery systems^[31], they are mainly used as scaffolds for therapeutic drug delivery as they are biocompatible which makes them easier for the body to degrade. It was found that the antibiotic vancomycin functionalized with pyrene as a hydrogellant shows more activity than vancomycin itself.

In the field of tissue engineering^[32], they are used as bioactive molecules and are able to promote the wound healing.

3.1.1. Studies on the Interactions between Surfactant Molecules and LMWGs

Research on the interactions between surfactant molecules and LMWGs, has gained immense attention in the literature^{[33],[34]}, as the study of surfactant molecules in mixtures with polymeric thickeners has shown that phase separation occurs or mixed assemblies are formed.

3.1.1.1. Gelation Behavior in Organic Solvents

In the presence of surfactant molecules, three different scenarios were found in organic solvents:

1. Promotion of Gel Network Formation
2. Disturbance of Gel Network Formation
3. No Influence on Gel Network Formation

Promotion of Gel Network Formation

The influence of additives leading to an improvement in the gelation properties of a gel, such as increasing the elasticity of the gel network, or the formation of higher-ordered structures, can be interpreted as the promotion of a gel network formation^[35].

In 2006, *Xing* et al.^[33] found that the addition of non-ionic surfactants to organogellants, could increase the elasticity of the gel network. They found that the addition of the surfactant polyethylene glycol sorbitan monooleate, can promote the gel network formation of the LMWGs N-lauroyl-L-glutamic acid di-n-butylamide-in-isooctadecanol and lanosterol-in-benzyl benzoate system, by promoting fiber tip-branching.

In 2009^[28], it was shown for the ternary system, propylene glycol-sorbitan monolaurate-N-lauroyl-L-glutamic acid, that a spherulitic network was formed in the absence of sorbitan monolaurate, whereby by adding a sorbitan monolaurate below its cmc, a comb-like network was formed due to the adsorption of surfactant molecules on the fibers' side surfaces, which then changed into a spherulitic network again with a further increase in the surfactant concentration above the cmc. The surfactant was used as a "topological modifier", which was able to weaken or strengthen the gel network.

In 2016, *Chen* et al.^[36] found that the addition of sorbitan monolaurate and t-octylphenoxypolyethoxyethanol to the binary gel of DMSO-2,3-di-n-decycloxyanthracene, increased the elasticity of the gel network during the gel network transformation from a spherulitic fiber network to an interconnected fiber network, due to the adsorption of sorbitan monolaurate on the side surface, and of t-octylphenoxypolyethoxyethanol on the fiber tip surface, of gellant fibers.

Disturbance of Gel Network Formation

The influence of additives leading to a weakening of the gels' gelation properties, such as decreasing the phase transition temperature, delaying gel formation or the formation of thinner fibers, can be understood as the disturbance of gel network formation^[37].

That gel formation was delayed in the presence of surfactant molecules, was discovered in 2018^[38]. It was suggested that the addition of sorbitan monooleate or polyethylene glycol sorbitan monooleate into the binary system of DMSO-2,3-di-n-decycloxyanthracene, leads to the delay of 100 seconds in gel network formation, which was assumed to be due to the solubilization of gellant monomers in surfactant micelles, or the adsorption of surfactant molecules on air bubbles or dust particles, instead of gellant monomers. Moreover, the addition of surfactant molecules led to the formation of fibers that were thinner than when these molecules were absent.

No Influence on Gel Network Formation

When a gel's gelation properties do not change in the presence of additives, then this can be described as an "orthogonal self-assembled" system^{[39],[40]} in which the gel network and a second, self-assembled structure, such as micelles^[26], vesicles^[26] or lamellar phase^{[41]–[43]}, can coexist within a single system without their features and properties being impacted.

In 2014, *Laupheimer*^[43] found, in research on the H₂O/n-decane-tetraethylene glycol monodecylether-12-hydroxyoctadecanoic acid quaternary system, that the gel network formed by the LMWG and the microemulsion formed by the non-ionic surfactant, coexisted within a one phase system without influencing each other.

In 2017, it was shown, by *Fu*^[44], that DBC shows an "orthogonal self-assembled behavior" in the presence of the gemini surfactant N'-((methylazanediy)bis(ethane-2,1-diyl))bis(N,N'-dimethyldodecan-1-aminium) in a solvent mixture of H₂O/DMSO.

3.1.1.2. Gelation Behavior in a Water System

When surfactant molecules were present, two scenarios were found in a water system without any co-solvents:

1. Disturbance of Gel Network Formation
2. No Influence on Gel Network Formation

Disturbance of Gel Network Formation

In 2009, *Brizard*^[34] found that adding the cationic surfactant cetyltrimethylammonium tosylate (CTAT) to the H₂O-1,3,5-cyclohexyltricarbosamide derivative system, led to a decrease in the sol-gel transition temperature. It was assumed that this could be due to the solubilization of gellant monomers in surfactant micelles, or to the shortening of gellant fiber length by CTAT molecules, which favor the end-capping of gellant fibers.

In 2013, *Nebot*^[29] found that adding the ionic surfactant, sodium dodecyl sulfate (SDS), reduced the elasticity of the gel network, due to the incorporation of gellant monomers into micelles. The authors proposed a mixed micelle model, consisting of gellant monomers and surfactant micelles, which would lower the stability of the gel network. The reduction in the gel network's elasticity was also found by *Koitan*^[43], in 2017,^[45] as lamellar phases were gelled with 12-hydroxyoctadecanoic acid.

It was presumed that the reduction in the gel network's elasticity might be because a quantity of the gelling agent could be used as a co-surfactant, which would offer a lower number of gellant monomers for self-assembly into a three-dimensional gel network. Another belief was that the lamellar phase could act as a "better solvent" for the LMWG than n-decane, which was used as a solvent in the absence of surfactant molecules, as the organogellant 12-hydroxyoctadecanoic was unable to gel in a water system.

The change of morphology in the presence of surfactants, was also constituted in 2012^[46] by the addition of SDS to the binary system made up of water and an amphiphilic tris-urea derivative. Nonetheless, thinner fibers were formed with increased surfactant concentration than in the absence of surfactants, because without the addition of surfactant molecules, a gel could not be formed in a water system.

No Influence on Gel Network Formation

In 2003, *van Esch* et al.^[26] found that the gelation properties of 1,3,5-cyclohexyltricarboxamide derivatives do not change in the presence of ionic or non-ionic surfactants. Even when surfactant molecules were present, the gel network's morphology and the gelling agent's phase transition temperature were not influenced by the surfactant molecules.

3.1.2. Importance of the History of Gel

Cooling Rate

Information, like the dissolution temperature of the LMWG, the final temperature of gel network formation or the cooling rate, is not often provided, even though, in 1994^{[45], [47]} it was reported that, for an azobenzene-linked cholesteryl gellant, the cooling rate could influence the morphology of the gel network. It was shown that right-handed helices were formed by fast cooling and left-handed helices by slow cooling.

Moreover, in 2000^[48], it was reported that the probability of gel network formation was higher when cooled at higher cooling rates, than at lower cooling rates.

In 2010^[49], it was found that depending on the solvent, a critical cooling rate for the LMWG 12-hydroxystearic acid (12-HSA) in mineral oil existed. The authors claimed that when cooling the sample at rates below 5 K/min, a limited branched network occurred, compared to a more branched network when cooling at higher cooling rates.

Preparation of Gel

A further aspect was reported by *Du et al.*^[50], that heating a sample to higher temperatures than the dissolution temperature, or heating it for longer, can lead to a precipitate rather than a well-dissolved solution. Nevertheless, it can often be seen in the literature^[30] that the gels were prepared by dissolving the gelling agent with a heat gun or in a water or oil bath until a transparent solution had been obtained, whereby it is not known whether the LMWG was solubilized or dispersed.

The controlled preparation of gel networks was widely investigated by *Li et al.*^[33] in 2006. They described the preparation of a gel in detail. They reported the gelling agent's dissolution temperature and cooling rate and discovered, for example, that by cooling a sample of the LMWG N-lauroyl-L-glutamic acid di-n-butylamide-in-isooctadecanol system, at a higher rate, the formation of thinner and more branched fibers was promoted.

3.1.3. Rheological Studies

Different methods of gel preparation for rheological studies are reported in the literature^[29]. It can often be seen that the gels were prepared in a vial and then stored for few hours, or a day, at 298 K before being transferred into the rheometer with a spatula. Hence, the gel network was damaged by the external force driven by the spatula, so that it is unclear whether the real structural behavior of the gel was studied or, instead, its self-healing property.

On the other hand, *Liu et al.*^[33] transferred the sample to the rheometer when it was in the sol phase, so that the gelation occurred in the rheometer's gap rather than in the vial, in order to prevent any external forces.

In addition, in 2012, *Yuan*^[51] reported that the gelation process of the LMWG N-lauroyl-L-glutamic acid di-n-butylamide-in-ethylene glycol system, could be controlled by the gap size. For a gap size of less than 500 μm , the size of the gel network was independent of the temperature and the gellant concentration. However, the gel formation was delayed due to the increased viscosity of the confined mixture, which complicated the nucleation and growth of fibers and increased the resistance of the gel network^[52]. For a larger gap size above 500 μm , the size of gel network was dependent on the temperature and gellant concentration, and the extended gel structures could be formed with a gap of 1200 μm .

Kinetics of Gel Network Formation

The kinetic studies on LMWGs in the organic solvents, diisooctyl phthalate and isooctadecanol, were begun in 2002 by *Liu et al.*^{[53],[54]}. The influence of surfactant molecules on the kinetic behavior of LMWGs were begun in 2016^[55] for the organogellant, 2,3-di-n-decycloxyanthracene, in the presence of sorbitan monolaurate, and t-octylphenoxypolyethoxyethanol in a DMSO system, and were continued in 2018^{[36],[38]} by the addition of a sorbitan monooleate and polyethylene glycol sorbitan monooleate to the same binary system. It was found that the addition of sorbitan monolaurate and t-octylphenoxypolyethoxyethanol promoted the gel network formation, due to the adsorption on the gellant fibers, which led to increased elasticity during and at the end of, gel network formation. In contrast, the addition of sorbitan monooleate and polyethylene glycol sorbitan monooleate led to a delay in gel network formation and to reduced elasticity during and at the end of, gel network formation.

3.2. Motivation and Objectives

The research on LMWGs has concentrated on the synthesis of new LMWGs of different substance classes, or on the completed gel network for the use in different applications. However, the importance of the history of a gel network's formation for its morphology and gelation properties, such as its structural behavior, is much less frequently reported. Although the importance of a gel's history was reported in the literature^[47] at the beginning of the 1990s, it has either been neglected in the literature or the authors have only been interested in the design of new molecules or in the completed gel network.

As a next point, it has been discussed in the literature^{[56],[57]} that symmetric 2,5-diketopiperazines (DKPs), with the same amino acid composition, tend to precipitate rather than self-assemble into a gel network. To promote the self-assembly behavior, either asymmetric DKPs^[58] were synthesized or the symmetric DKPs were treated with ultrasound in order to promote the gellant monomers' aggregation by influencing their translational and rotational molecular movements^[59]. However, this resulted in the formation of thinner fibers^[58]. Furthermore, it has been shown in the literature^{[46],[60],[61]} that LMWGs, like β -cyclodextrin^{[60],[61]} and tris-urea derivative^[46], can only self-assemble into a gel network in the presence of surfactants.

Or, for example, N-octylgluconamide has a low lifetime stability in a water system due to the slow transition from tail-to-tail micellar bilayers to head-to-tail crystalline sheets, whereby the life time stability can be increased by the addition of surfactants, due to hydrophobic interactions and hydrogen bonding.

The gelation properties of low molecular weight organogellants have been widely studied in the literature; in contrast, the studies on low molecular weight hydrogellants without any co-solvent, have been poorly reported. The majority of the LMWGs available are based on organic compounds without additional polar groups, so that they are usually not soluble in a water system without the addition of water-miscible organic solvents, such as DMSO, to pre-dissolve the LMWG aggregates, which then form a gel network when hot water is added to the system and allowed to cool to 298 K, whereby, aqueous gels are then formed instead of hydrogels^[30].

Therefore, the goal of this work was to study for hydrogellants the influence of surfactant molecules on the gelation process, including the induction, gelation, and quasi-equilibrium stages, using rheology under defined preparation and shear conditions.

The gel network's morphology should also be characterized using optical microscopy and cryogenic transmission electron microscopy measurements.

The objectives of this work are: 1) to understand the influence of different types of surfactant molecules on the three gelation process stages, 2) to create a model description of these influences, and 3) the targeted monitoring of the influence of surfactant molecules on the gelation behavior of LMWGs.

To get information about the influence of molecular structure of the hydrogellant, it is interesting to investigate the gelation properties of two different LMWGs, in the presence of surfactant molecules in the water system.

The gelation properties of a more hydrophilic compound, DBC, and of a more hydrophobic DKP, 3,6-bis(4-hydroxybenzyl)piperazine-2,5-dione (L-Tyr-L-Tyr)^[62], which was synthesized in the institute of organic chemistry at the university of Bremen, should be compared with each other in a water system and in a mixture with surfactants.


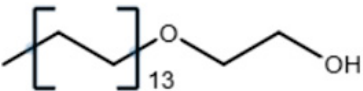

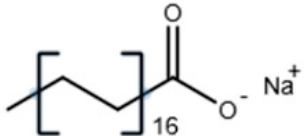

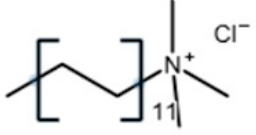

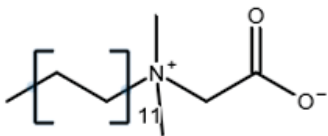
4 Theoretical Background

4.1. Physicochemical Properties of Surfactants

Surfactants are amphiphilic compounds which have a hydrophilic (polar) and hydrophobic (non-polar) character. They are able to decrease the interfacial and surface tension of the surrounding aqueous medium by adsorbing at the air-liquid interface, whereby the hydrophobic part is directed to the air phase and the hydrophilic part to the liquid phase ^[62].

They can be divided into different classes according to their hydrophilic part, as outlined in Table 4-1.

Table 4-1 Different classes of surfactants taken from reference [63].

Class	Schematic illustration	Examples
Non-ionic		
Anionic		
Cationic		
Zwitter-ionic		

Surfactant molecules can form different aggregates in aqueous solutions, depending on the surfactant concentration and temperature, as shown in Figure 4-1.

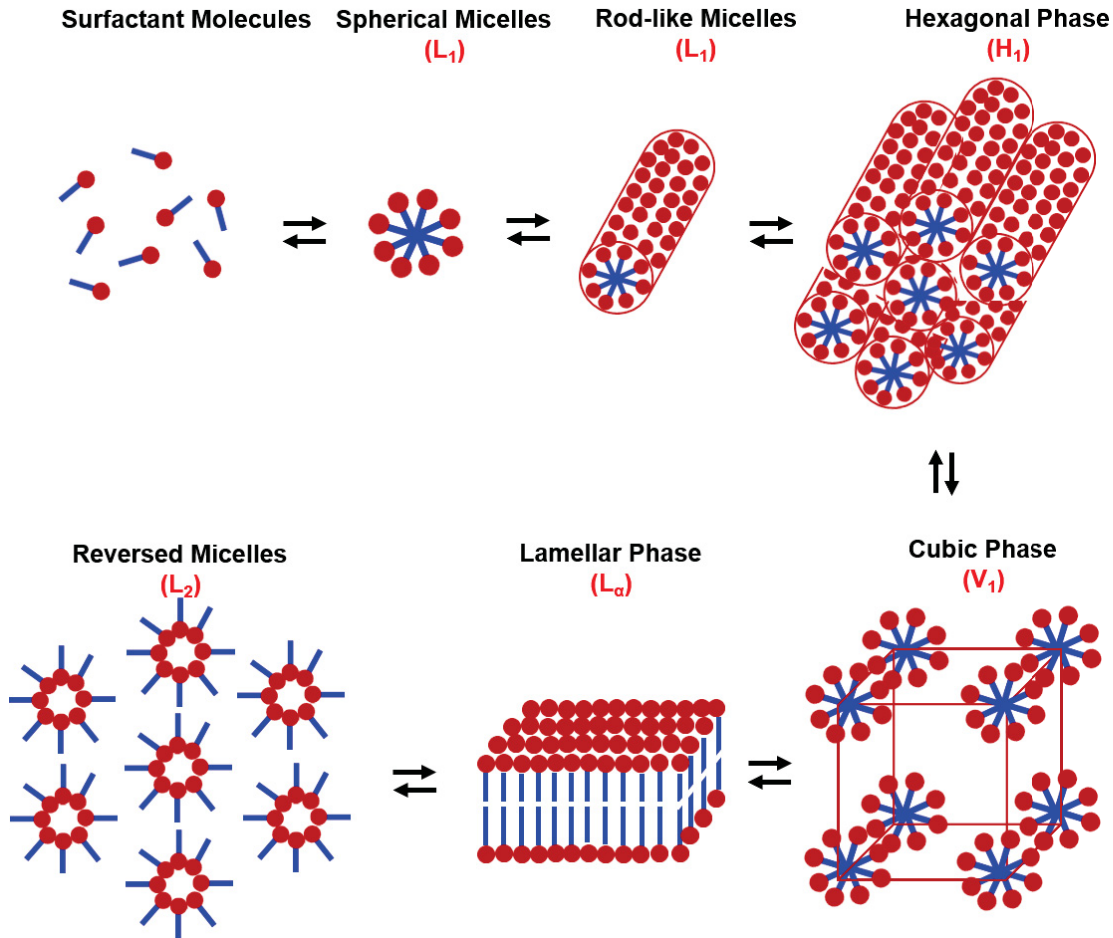


Figure 4-1 Schematic illustration of the aggregates formed by surfactant molecules with increasing surfactant concentration or temperature (according to reference [63]).

With increasing surfactant concentration or temperature, the individual surfactant molecules adsorb at the air-water interface, until the surface is completely occupied by them. Above the critical micelle concentration (cmc), the individual surfactant molecules form aggregates in solution. In the micellar phase (L_1), aggregates, such as spherical or rod-like micelles, are formed, which then aggregate further to form cylindrical micelles packed as hexagons (H_1), cubes (V_1), plates (L_a) or reversed micelles (L_2).

The phase behavior of a non-ionic surfactant, $C_{12}E_6$, is outlined in Figure 4-2.

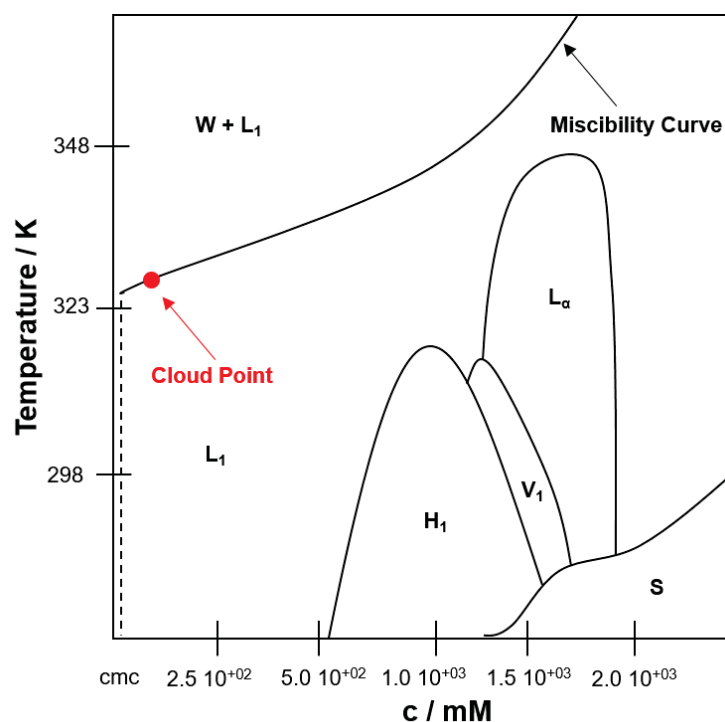


Figure 4-2 Phase behavior study of the binary system $H_2O-C_{12}E_6$ (data were taken from reference [64]) (cmc – critical micelle concentration, W – water, L_1 – spherical micelles, H_1 – hexagonal phase, V_1 – cubic phase, L_α – lamellar phase, S – solid).

With increasing surfactant concentration, it is possible to see a phase sequence from micellar (L_1) up to lamellar phase (L_α). The surfactant is no longer soluble in water in the solid phase.

A miscibility gap arises when the L_1 phase is heated, which is related to the phase separation into two immiscible phases consisting of one surfactant-rich (L_1) and one surfactant-poor, liquid phase (W), so that a turbid solution is formed. The appearance of phase separation through the heating of the micellar phase, is due to the dehydration of the non-ionic surfactant's polar head-group, leading to enhanced micelle-micelle interaction^{[65],[66]}.

In practice, the temperature at which the transition from the one-phase to the two-phase region occurs, is called the cloud point. Commonly, from an application perspective, the cloud point is defined as the phase boundary to the two-phase region^[67] and is determined at a surfactant concentration of 1 wt-%^[68].

4.2. Low Molecular Weight Gellants

4.2.1. Definition

Low molecular weight gellants (LMWGs) are small molecules with a molecular mass of less than 1000 Da, that are capable of thermo-reversible self-assembly in organic, aqueous or ionic solvents, to form a three-dimensional gel network of fibers or aggregates, in which the solvent is trapped in the mesh by capillary forces and surface tension^{[11],[69]}. They can be considered to be viscoelastic systems^{[12],[20],[70]}. LMWGs are also described as physical gels, molecular gels or self-assembled fibrillar networks (SAFINs), not to mention that LMWGs can also self-assemble into solid fibers, spheres, ribbons or sheets^{[1]–[10],[71]}.

The gel network is held together by non-covalent interactions, such as electrostatic interactions, hydrogen bonding, π - π stacking and van-der-Waals forces^[72]. LMWGs are amphiphilic compounds composed of a hydrophilic moiety, a hydrophobic aromatic group or long hydrocarbon chains and, to increase the gelation capability, groups transmitting non-covalent interactions^{[73],[74]}.

However, the formation of a gel network is considered to be an empirical science, as the LMWGs' design does not always lead to the formation of a gel network^{[73]–[75]}. It could be seen in the literature^[73] that a cholic-acid derivative, which was capable of self-assembly in organic solvents, did not form a gel network in the same medium when the structure was modified by adding a further hydroxyl group. Therefore, the balance between the hydrophilic and hydrophobic groups must be ensured in order to promote the formation of a gel network.

4.2.2. Formation of a Gel Network

LMWGs' self-assembly into three-dimensional gel networks, can be divided into three structures, the primary, secondary and tertiary structures^[11], as illustrated in Figure 4-3.

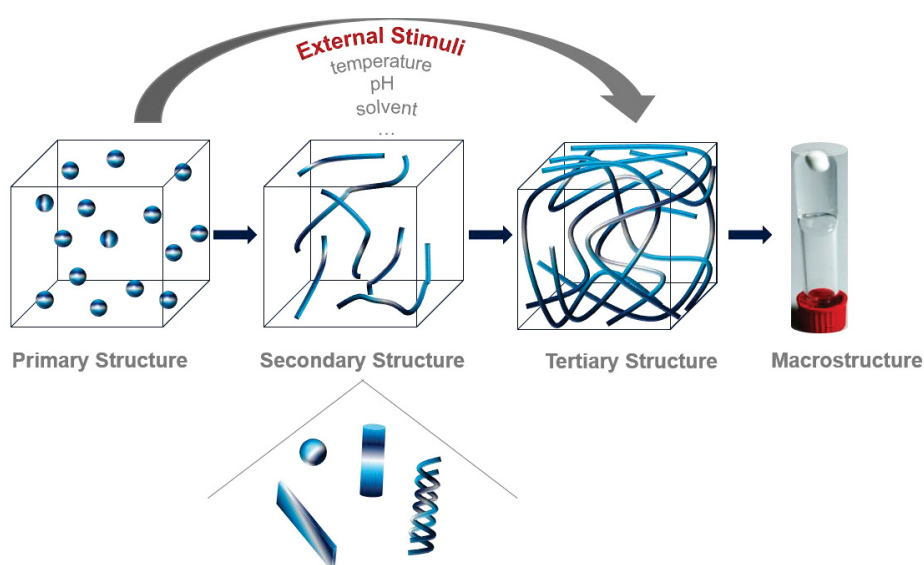


Figure 4-3 Schematic illustration of the hierarchical self-assembly of low molecular weight gellants (LMWGs) (according to reference [11]).

One or two-dimensional interactions occur in the primary structure, Å° to nm-scale. The secondary structure, nm to µm-scale, can be interpreted as the aggregates' morphology, during which one-dimensional fibers, tapes, belts, twists, tubes or spheres can be formed^[71]. In the tertiary structure, µm to mm-scale, the gellant aggregates interact with one another, due to non-covalent interactions, and form a continuous gel network of fibers or aggregates. It has been stated in the literature^{[1]–[10]} that the gel network could be made up of solid^[1], rod-like^[5], bundled^[5], curved^[8], separated^[2], twisted^[6], entangled^[7] or ribbon like^[3] fibers. The aggregates' gel network could be formed from spherical^[7], rod-like^[9] or lamella-like^[10] aggregates.

According to literature^{[76],[77]} on the formation of a gel network based on solid fibers, the gel network structure is related to the distribution of nodes and edges. Nodes are the junctions and the fibers, which form connection between the junctions, are the edges, which could be of either a transient or permanent nature^{[76],[77]}, as depicted in Figure 4-4.

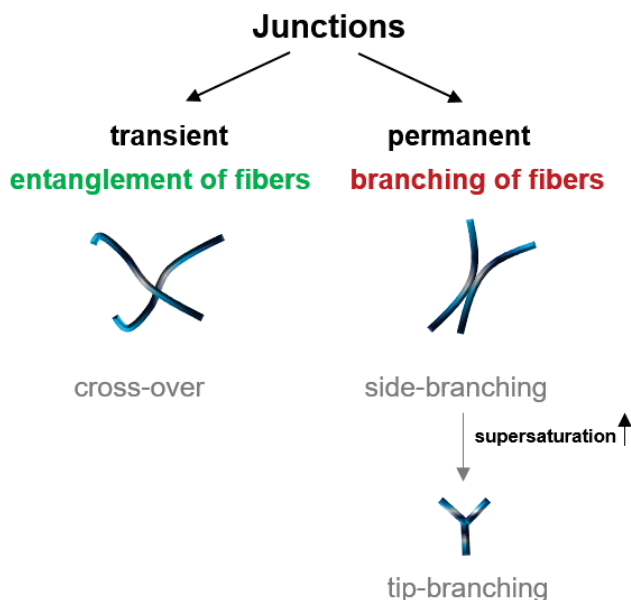


Figure 4-4 Schematic illustration of different types of junctions (according to references [53],[78]–[80]).

When a gel network consists of fibers which are entangled and physically cross over each other, then the gel network is made up of transient junctions^{[78],[81]}. Alternatively, if the fibers arise from rigid branching, then the gel network is made up of permanent junctions^[53]. A gel network with permanent junctions is stronger than one with transient junctions^{[81]–[84]}. Depending on the supersaturation, two types of branching can exist in permanent junctions, either side-branching or tip-branching. A low supersaturation, meaning gel network formation at a high temperature for a constant gellant concentration or the formation of a gel network with a low gellant concentration^[79], favors side-branching, whereby this can be switched to tip-branching by either increasing the supersaturation or by increasing the cooling rate^{[79],[80],[83],[85]}, thus a stronger gel network is formed by tip-branching. However, increasing the supersaturation above a certain value could lead to the transition from a permanent to a transient gel network structure^[86]. Therefore, the supersaturation plays a key role in the formation of a gel network^{[24],[82]}.

The gel network consists of a minor component, the gelling agent, and major component, the solvent^[87].

LMWGs have a high hydrophobicity and the hierarchical self-assembly into a gel network is a result of the transition from a favored environment, where it is highly soluble, to an unfavored environment, where it is poorly soluble and it therefore self-assembles^[88].

This transition can be ensured by external stimuli, such as the heating-cooling cycle, changes in pH or solvent polarity, or the addition of surfactants. The LMWG is solubilized or dispersed by heating; cooling decreases the solubility so that it self-assembles and forms a gel network^[89]. The transition from the sol to the gel phase, is known as the sol-gel-transition temperature $T_{\text{sol-gel}}$. Depending on the surrounding medium or the compound's chemical structure, precipitation or crystallization could occur instead of a gel network, as discussed in the literature^{[56],[57]}. Therefore, gel network formation is described as an inhibited crystallization or precipitation process^{[11],[90]}.

In terms of the effect of pH, the LMWG is dissolved better at one pH than another and is then able to form a gel network^[91]. When triggering the gelation with solvent polarity, the LMWG is first dissolved in an organic solvent and water is then added to the mixture.

As this is not favored by the LMWG, it self-assembles^[92]. Further external stimuli for promoting gel network formation are discussed in the literature^[50].

4.2.3. Coassembly Models

Three different types of coassembly models exist for LMWGs when they are in contact with amphiphilic compounds, such as surfactant molecules^[37].

Orthogonal self-assembly is defined as the selective and simultaneous assembly of molecules in the molecular scale, into higher-ordered structures in the nm-scale, in a single system without interference with the properties and features of the individual components^{[39],[40]}. Accordingly, the following properties and features do not change when LMWGs come into contact with surfactant molecules:

- Morphology of the Gel Network^{[26],[27],[37],[44],[93]}
- LMWG's Phase Transition Temperature^{[26],[93]}
- Critical Micelle Concentration^{[26],[93]}

Cooperative self-assembly is defined as the assembly of molecules into higher-ordered structures, in a single system with interference with the properties and features of the individual components, which results from either the formation of a complex structure from component 1 or 2, or the formation of mixed structures of the components^[35].

Disruptive self-assembly is defined as the complete or partial inhibition of the formation of higher-ordered molecular structures in a single system, so that the components mutually influence one another^[37].

4.3. Methods

4.3.1. Cryogenic-Transmission Electron Microscopy

By using transmission electron microscopy measurements (TEM), it is possible to visualize structures with a resolution of the order of 0.2 to 0.5 nm.

According to *De Broglie*^[94], the wavelength of electrons is given by the equation:

$$\lambda = \frac{h}{m * v} \text{ [nm]} \quad \textbf{4-1}$$

with the *Planck's* constant h , mass m and the velocity v .

It can be concluded that an increase in the velocity leads to a shorter wavelength, and as such, to a higher resolution.

A schematic illustration of a TEM's electron beam is shown in Figure 4-5.

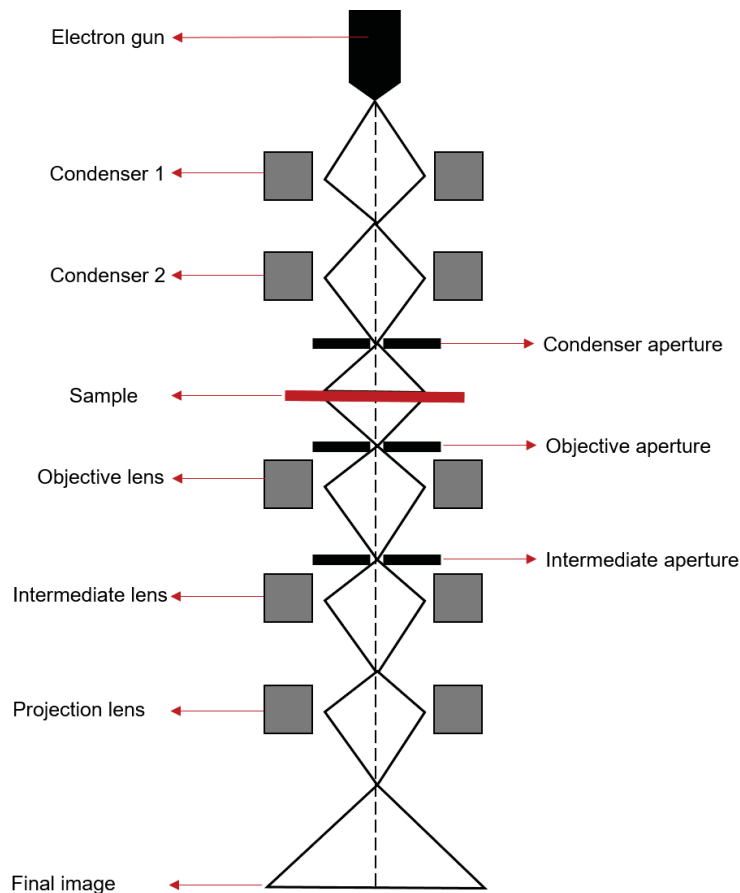


Figure 4-5 Schematic illustration of the electron beam of a transmission electron microscope (redrawn from reference [95]).

A thin layer of the sample is irradiated using a high electron beam with up to 100 keV of energy. The electron beam is produced, under vacuum conditions, by the electron gun which consists of an electron emitting cathode, a filament surrounded by a “Wehnelt” grid, which produces electrons, and an anode. The condenser lenses restrict the electron beam and project it onto the viewing screen. The electrons can both penetrate the sample atoms and interact with their nuclei through *Coulomb* force, which would lead to an elastic scattering or they interact with the electrons of the sample atom, which would lead to an inelastic scattering. The transmitted electrons are then focused by the objective lens to a charge-coupled device camera.

The term “*cryogenic*” (cryo) is related to the preparation of the sample, which allows the sample’s morphology to be visualized in the frozen-hydrated state. To prepare the sample for cryo-TEM, a thin film of the sample is prepared on a copper grid and then frozen in liquid ethane or propane, using a high cooling rate, to the temperature of liquid nitrogen. The high cooling rate is necessary to prevent the formation of ice

crystals^[96]. After the freezing process, the excess liquid ethane or propane is removed with a filter paper and the sample is then placed into a cryo holder and transferred into the electron microscope.

Further information on the fundamentals of cryo-TEM is outlined in the literature ^{[95],[97]–[99]}.

The morphology of the gel network structure of LMWGs in the absence and presence of surfactant molecules was studied by using cryo-TEM measurements. The gel preparation and the conditions for the imaging measurement are outlined in Chapter 5.3.

4.3.2. Dynamic Light Scattering

Dynamic light scattering (DLS), which is also known as photon correlation spectroscopy (PCS) or quasi-elastic light scattering (QELS), is a tool for determining the hydrodynamic particle diameter based on measuring the *Brownian* motion of particles, driven by the thermal stochastic collision of the particles with molecules of the surrounding aqueous medium, and then applying the *Mie* theory^[100]. The *Mie* theory^[100] was established in 1908 and relates to the absorption and light scattering of isotropic spherical particles of any diameter larger than the wavelength of the laser.

From the speed of the *Brownian* motion known as the diffusion coefficient D , the hydrodynamic diameter can be determined by using the *Stokes-Einstein* equation^[101] given by:

$$D = \frac{k_B * T}{6 * \pi * \eta * r} \text{ [m}^2\text{/s]} \quad \mathbf{4-2}$$

with the *Boltzmann* constant k_B , temperature T , viscosity η and the hydrodynamic radius r .

According to the *Stokes-Einstein* equation, it can be concluded that the *Brownian* motion of small particles is faster than that of large particles. The particles' time-dependent movement is monitored during the measurement. The movement of large particles leads to similar particle positions and, in contrast, the movement of small particles leads to different particle positions.

When the sample is irradiated with the monochromatic laser light, the particles scatter light in all directions, which can lead to the phenomenon of constructive interference of waves, if they are in phase thus forming a wave with a larger amplitude, or that of destructive interference of waves if the waves cancel each other out.

The scattered intensity of particles can be expressed by the second-order autocorrelation function:

$$g_2(\tau_D) = \frac{\langle I(t) * I(t + \tau_D) \rangle}{\langle I(t) \rangle^2} \quad 4-3$$

with the scattered intensity I , the time t and the delayed time τ_D .

The second-order autocorrelation function can be converted into a first-order electric field autocorrelation function $g_1(\tau)$ to obtain the information on the measured fluctuations^[102] with the *Siegert* equation:

$$g_2(\tau_D) = 1 + \beta * |g_1(\tau_D)|^2 \quad 4-4$$

with the correction factor β .

For mono-disperse particles, the first-order autocorrelation function can be expressed by an exponential decay function:

$$g_1(\tau_D) = e^{-Dq^2\tau} \quad 4-5$$

with the scattering vector q , which is given by:

$$q = \frac{4 * \pi}{\lambda} \sin \frac{\theta}{2} \quad 4-6$$

with the wavelength of the scattered light λ and the scattering angle θ .

Further information on the theory of DLS measurement can be obtained from the literature^{[103]–[105]}.

In this work, the hydrodynamic particle diameter of micelles was determined by DLS measurements. The measurement conditions are shown in Chapter 5.5.

4.3.3. Rheology

Rheology is the study of deformation and flow of matter, which studies the relationships between the forces applied and the resulting deformations^[106]. The root, “*rheo*”, has its origins from the Greek word, “*rhein*”, which means “*to flow*”, and is a type of deformation. The fundamentals of rheology can be taken from the literature^{[107]–[109]}.

For rheological studies, the sample is placed between two plates of which the lower plate is stationary, and the upper is movable. If a shear stress is applied to a system, there can be different responses to the stress applied, depending on the type of solvent. The shear stress is defined as the force applied over an area.

Newton’s Law

According to *Newton’s Law* the ratio of the shear stress τ to the shear rate $\dot{\gamma}$ is a proportionality constant, namely viscosity:

$$\eta = \frac{\tau}{\dot{\gamma}} \text{ (T = const.) [Pa s]} \quad \mathbf{4-7}$$

Viscosity can be described as the flow resistance, which is independent of the shear force applied, even when a strong force or long loading processes exist.

Newton’s Law can be illustrated by a dashpot model. When a shear stress is applied, the dashpot’s piston moves simultaneously with the shear load and stops when the shear force is removed, thus it does not revert to its original state, which is due to the deformation energy being lost during the load process.

Hooke’s Law

According to *Hooke’s Law*, the ratio of the shear stress to the shear strain, γ_s , is a proportionality constant, which is the storage modulus:

$$G' = \frac{\tau}{\gamma_s} \text{ (T = const.) [Pa]} \quad \mathbf{4-8}$$

The storage modulus can be defined as the stiffness of an elastic material.

Hooke’s Law can be illustrated by a spring model. When a shear stress is applied, the spring moves simultaneously with the shear load, returning immediately and completely to its initial state when the shear force is removed, because the deformation energy is stored in the system during the load process.

Oscillating shear rheometry

For viscoelastic systems, which can be understood as combining viscous and elastic behavior, the system's elastic behavior is described by the storage modulus, G' , hence the deformation energy is reversibly stored in the system. The system's viscous behavior can be described by the loss modulus, G'' , hence the deformation energy is irreversibly lost during the load process.

Both parameters can be determined using oscillating shear rheometry.

A sinusoidal shear strain with the amplitude, $\gamma_{s,0}$, is applied to the system and then the resulting sinusoidal shear stress with the amplitude, τ_0 , and the phase shift angle, δ , are measured, as illustrated in Figure 4-6.

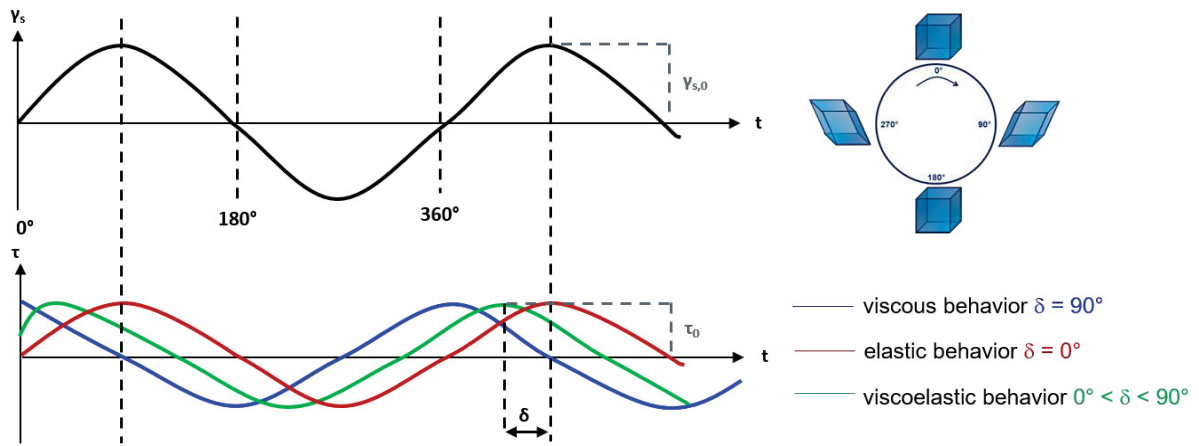


Figure 4-6 Visualization of the applied sinusoidal shear strain and shear stress response of samples showing viscous, elastic, and viscoelastic behaviors (according to reference [110]).

For a *Newtonian* fluid, the applied shear strain and the shear stress response occur out of phase, as the phase shift angle, δ , is 90° .

For a *Hookean* solid, the applied shear strain and the shear stress response occur in phase, as the phase shift angle is 0° .

Thus, for a viscoelastic system, the combination of the viscous and elastic behavior leads to a shift of the phase angle between 0° and 90° .

The applied sinusoidal shear strain can be expressed by the equation:

$$\gamma_s(t) = \gamma_{s,0}(t) * \sin(\omega t) \quad 4-9$$

with the maximum amplitude γ_0 , the angular frequency ω and the time t .

The shear stress response to the applied shear strain, is given by:

$$\tau(t) = \tau_0(t) * \sin(\omega t + \delta) \quad 4-10$$

with the maximum amplitude τ_0 and the phase shift angle δ .

For a *Newtonian* Fluid, the phase shift angle was 90° and it follows from *Newton's* law, as shown in equation 4-7 that the equation 4-9 must be derived according to the time, as shown by:

$$\frac{\gamma_s(t)}{dt} = \gamma_{s,0}(t) * \omega * \cos(\omega t) \quad 4-11$$

According to the equation 4-7 the response of the shear stress to the applied sinusoidal shear strain can be expressed by:

$$\tau(t) = \eta * \gamma_{s,0}(t) * \omega * \cos(\omega t) \quad 4-12$$

For a *Hookean* solid, according to equation 4-8, the response of the shear stress to the applied sinusoidal shear strain is:

$$\tau(t) = G' * \gamma_{s,0}(t) * \sin(\omega t) \quad 4-13$$

For a viscoelastic system, the complex modulus G^* , which is defined as the system's total resistance against the applied shear strain, will be introduced in the complex plane, as illustrated in Figure 4-7.

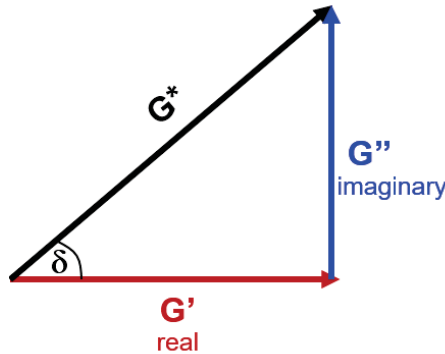


Figure 4-7 Illustration of the relationship between the complex modulus G^* , storage modulus G' and loss modulus G'' (according to reference [110]).

As previously mentioned, the elastic character of a viscoelastic system can be expressed by the storage modulus G' and the viscous character by the loss modulus G'' . Furthermore, it has been shown that for a *Hookean* solid, the applied shear strain and the shear stress response occur in phase, so that the storage modulus G' can also be called the “in phase” or the “real part” of a viscoelastic system.

In contrast, for a *Newtonian* fluid, the applied shear strain and the shear stress response occur out of phase, therefore, the loss modulus G'' is also called the “out of phase” or the “imaginary part” of a viscoelastic system.

The relationship between G^* , G' and G'' is expressed by the equation:

$$G^* = G' + iG'' \quad \mathbf{4-14}$$

with the complex number i and complex modulus G^* .

To calculate the G' and G'' values, first the complex modulus, G^* , is calculated from the raw data of the measurement which is the shear stress, τ , and the shear strain, γ_s , given by the equation:

$$G^* = \frac{\tau(t)}{\gamma_s(t)} \quad \mathbf{4-15}$$

According to trigonometrical laws, the storage modulus G' and loss modulus G'' can be then calculated by:

$$G' = G^* * \cos \delta = \frac{\tau(t)}{\gamma_s(t)} * \cos \delta \quad \mathbf{4-16}$$

$$G'' = G^* * \sin \delta = \frac{\tau(t)}{\gamma_s(t)} * \sin \delta \quad \mathbf{4-17}$$

The phase shift angle is zero for an elastic behavior and it follows that G' is equal to G^* and that G'' is zero.

The phase shift angle is 90° for a viscous behavior and it follows that G' is zero and that G'' is equal to G^* .

The structural behavior of LMWGs in the absence and presence of surfactant molecules was studied by oscillating shear rheology measurements. The measurement conditions are outlined in Chapter 5.6.

5 Experimental Methods

5.1. Chemicals

Table 5-2 Used chemicals with their trade names, purities and suppliers. The compound L-Tyr-L-Tyr was synthesized by *Dominik Goebel*, one of Prof. *Nachtsheims's* PhD students at the university of Bremen.

Name	Trade name	Purity / %	Supplier
water	-	bidistilled	-
Sodium-n-alkyl-benzene sulfonate (C ₁₀₋₁₃ -LAS)	Disponil LDBS	56	BASF
Fattyalcohol ethoxylate (C ₁₂₋₁₈ E ₇)	Dehydol LT7	≥ 99	BASF
N,N'-dibenzoyl-L-cystine (DBC)	-	≥ 98	Sigma-Aldrich
3,6-bis(4-hydroxybenzyl)piperazine-2,5-dione (L-Tyr-L-Tyr)	-	-	-

5.2. Sample Preparation

To prepare hydrogels in the absence and presence of surfactants, a weighed amount of the gelling agent was dissolved in a water system or an aqueous surfactant solution, by being heated to a temperature of 401 K under excessive pressure in a closed vial, so that the sample was heated to above the boiling temperature of water, which is 373 K at normal pressure of 1.01 bar. To avoid excessive pressure, special vials from the company Dunn Labortechnik GmbH were used; these have pressure relief caps (Figure 5-8) that can prevent excessive pressure above 10.3 bar.

The vials were placed into a thermomixer, from the company Hettich Benelux (Figure 5-8), and shaken with 400 rpm at 401 K until the gelling agent was dissolved in the water or aqueous surfactant solution, so that a clear solution was obtained. To ensure safety in the laboratory, the thermomixer was in the fume cupboard.

The thermomixer temperature was lowered to 358 K before the sample was removed for the measurements.



Figure 5-8 Illustration of the thermomixer from the company Hettich Benelux and the vial consisting of a pressure relief cap from the company Dunn Labortechnik GmbH.

5.3. Cryogenic-Transmission Electron Microscopy

The cryogenic-transmission electron microscopy (cryo-TEM) measurements were performed using a Philips TECNAI 10 transmission electron microscope operated at a voltage of 100 kV. The microscope was equipped with a tungsten point cathode and a CCD camera (Figure 5-9). A 3 mm diameter copper grid was immersed into the sample at 363 K, at which temperature, it was, in the sol phase. Depending on the gel formation kinetics, the copper grid with the sample on its surface, was stored at 298 K for 5, 45 or 60 minutes.

The samples were then frozen in the cryogenic working chamber in liquid propane to a temperature of 103 K and the excess propane was removed with a filter paper.

The components within the working chamber are shown in Figure 5-10.

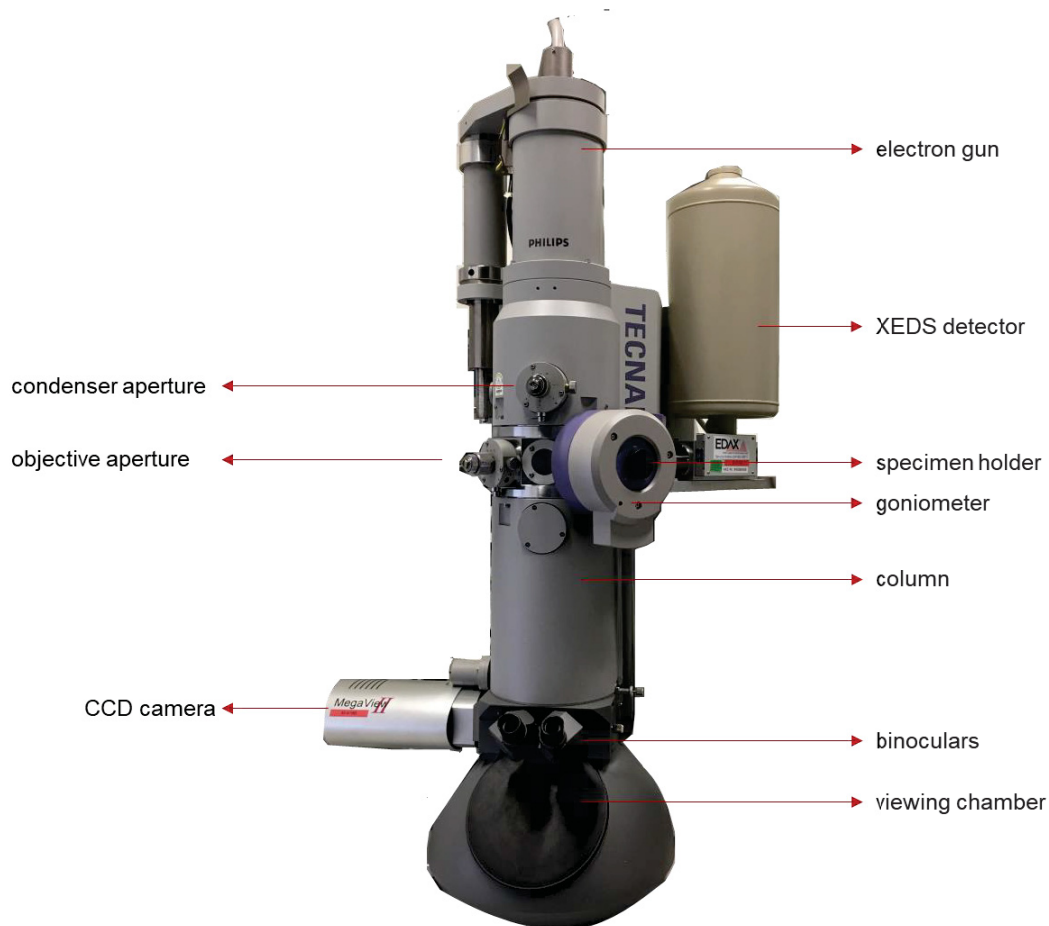


Figure 5-9 Illustration of the components of transmission electron microscope.

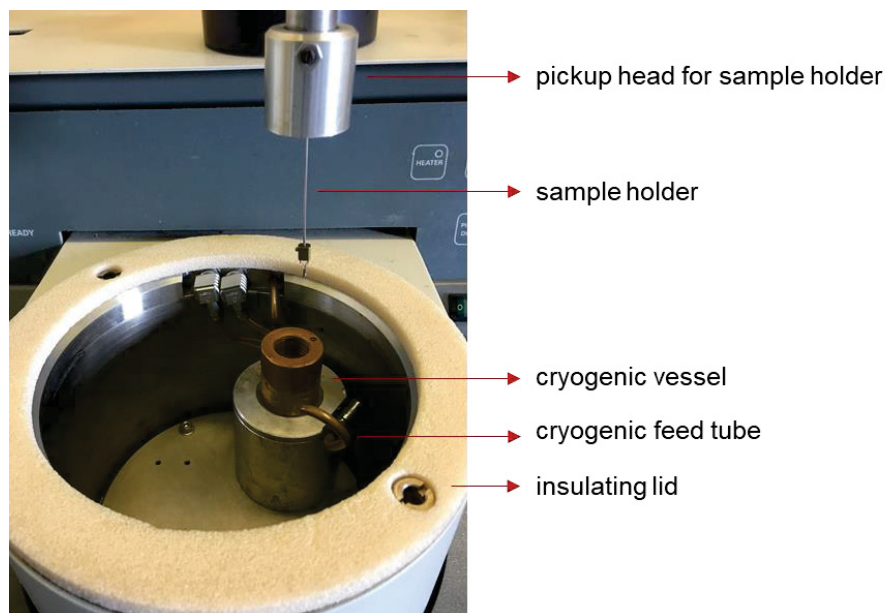


Figure 5-10 Illustration of the cryogenic working chamber.

The sample was placed, under liquid nitrogen, into the cryo-TEM holder at 103 K and transferred into the electron microscope.

5.4. Surface Tension Measurements

The surface tension measurements were carried out with a KRÜSS force tensiometer K100 and the surface tension was measured at 298 K, using the *De Nouy* ring method. The binary systems of H₂O-surfactant were prepared individually for each surfactant concentration and adjusted to an initial pH of 3, 5 or 7. The ternary systems of H₂O-surfactant-DBC were prepared for a constant gellant concentration of 1.11 mM and various surfactant concentrations. The samples for each surfactant concentration were prepared individually from the stock solution of 2.22 mM DBC aqueous solution by dilution with aqueous surfactant solution, and adjusted to an initial pH of 3, 5 or 7.

The initial pH in the binary system of H₂O-LAS was 7, thus hydrochloric acid solution (**2.0 M**) was added to the system to lower the pH. In contrast, the initial pH of the ternary system H₂O-LAS-DBC with a gellant concentration of 1.11, was 3.5, hence, sodium hydroxide solution (**2.0 M**) was added to the system to increase the pH.

The initial pH of the binary system H₂O-C₁₂₋₁₈E₇ was 7, hence, hydrochloric acid solution (**2.0 M**) was added to the system to lower it to an initial pH of 5. However, the initial pH of the ternary system H₂O-C₁₂₋₁₈E₇-DBC was 3.5, hence, to increase the pH to an initial pH of 5, sodium hydroxide solution (**2.0 M**) was added.

The vessel was moved towards the ring and the ring was immersed into the sample with a depth of 3 mm. The force which was needed to move the ring from the liquid into the air phase, was measured with a sensitivity of 0.001 g and a speed of 3 mm/min. The average value for the surface tension was recorded five times when the sample was measured, however the measurement was ended when the standard deviation of the surface tension was 0.1 mN/m.

In this work, the first recorded value was taken as the surface tension, because the measurement was completed later at low surfactant concentrations than at high surfactant concentration. To have the same measurement conditions, the first determined value for surface tension was taken for each surfactant concentration, bearing in mind that the standard deviation of the averaged values was higher than 0.1 mN/m.

5.5. Dynamic Light Scattering

The hydrodynamic diameter of particles in the binary system, H₂O-LAS with varied surfactant concentrations, was measured with a Malvern Zetasizer. The binary systems were prepared at 298 K, transferred into the cuvette and then placed into the Zetasizer. The measurement was repeated at regular 5-minute intervals.

5.6. Rheology

The rheological measurements were performed using a rotational rheometer (Kinexus Rheometer, Malvern Instruments - Figure 5-11) with a plate-and-plate geometry with a diameter of 20 mm and a gap of 800 μm .

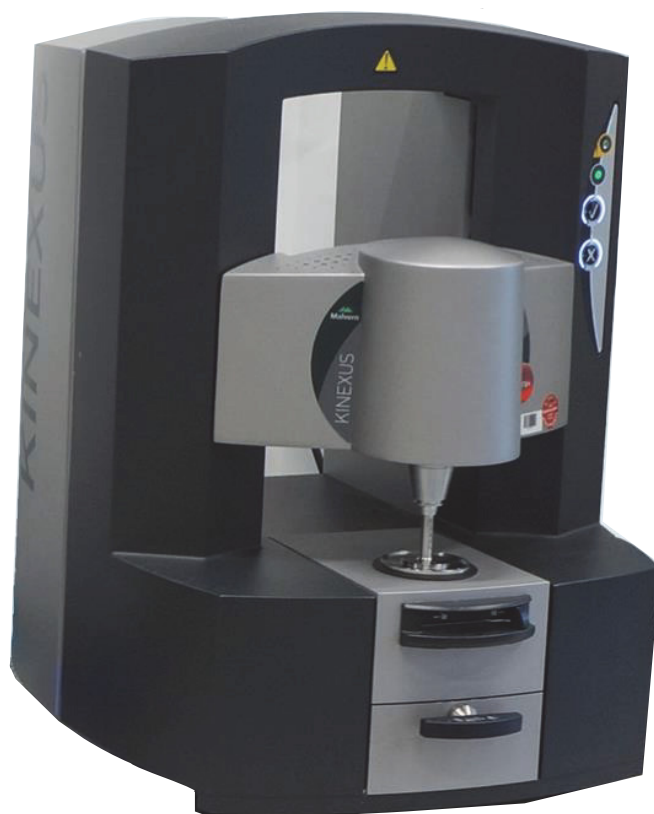


Figure 5-11 Illustration of a rotational rheometer from Malvern Instruments.

Before transferring the sample into the rheometer, the stationary lower plate was thermostatically regulated, using a Peltier element, to a temperature of 353 K. The gap between the lower and upper plates was set to 100 μm for 10 minutes, to prevent abrupt gelation being caused by temperature differences between the sample and the rheometer's upper and lower plates.

The sample was prepared in the thermomixer as described in section 5.2, and after the DBC was dissolved at 401 K, the sample was cooled to 358 K. Hence, if the rheometer's temperature had not been adjusted to 353 K, then the sample could have gelled within a few seconds, before the upper plate could be lowered, because of the abrupt decrease in its temperature when it made contact with the lower plate, which was at 298 K.

As a consequence, the gel could have been damaged by the additional external forces driven from the upper plate, when lowering the upper plate to the desired gap. And even equilibrating the sample for several hours, hence by giving the gel time for self-healing, could not ensure that the initial gel network would reform. To overcome this undesired behavior, the sample transferred into the rheometer in the sol phase and the temperature of the rheometer was adjusted to 353 K to prevent gelation occurring before the 800 μm gap was adjusted. Hence, the gelation occurred inside the gap, rather than outside it.

The transition from the sol to the gel phase, was performed by temperature-sweep measurements with a shear strain of 0.05 %, a frequency of 1 Hz and cooling rates of 1, 2, 5 and 10 K/min. A solvent trap was used to overcome the effects of evaporation during the measurement.

The sol-gel transition temperature, $T_{\text{sol-gel}}$, was determined from the increase in the G' values with decreasing temperature^{[111],[112]}.

To study the gelation process, temperature-sweep measurements were performed and the evolution of the G' values was monitored with a shear strain of 0.05 % and a frequency of 1 Hz.

6 Results and Discussion

6.1. Gelation Behavior of DBC in a Water System

The physicochemical properties of the DBC-in-water system, were investigated both below and above, the critical gelation concentration. The focus was on understanding the gelation process of DBC, leading to the formation of a gel network.

The gelation process was studied using rheology at different cooling rates and the gel network's morphology was investigated using optical microscopy and cryogenic transmission electron microscopy (cryo-TEM) measurements.

6.1.1. Phase Transition Temperature

To determine the phase transition temperature, measurements were performed above the critical gelation concentration of 4.46 mM, which was recognized optically, and corresponds to one gellant molecule per 12000 water molecules in the gel network. No gelation occurred below the critical gelation concentration. In the literature^{[113],[114]}, the critical gelation concentration of DBC in this water system was found to be 3.00^[113] and 2.23 mM^[114].

The measurement of the temperature dependency of G' and G'' values for the 6.69 mM binary system of H₂O-DBC, is shown in Figure 6-12. The concentration of DBC was kept constant at 6.69 mM to prevent evaporation having any effects on the measurements.

When cooling the sample at a rate of 10 K/min, the G' values were nearly independent of the temperature down to a value of 336 K. Below this temperature, the G' values increased sharply from $8 \times 10^{+00}$ to $4 \times 10^{+02}$ Pa, by cooling to 322 K. With a further decrease in the temperature, the G' values reached a plateau, with G' values of $5 \times 10^{+02}$ Pa. The temperature at which the G' values started to be increased by lowering the temperature, was found to be 336 K and was taken as the $T_{\text{sol-gel}}$ value for a cooling rate of 10 K/min.

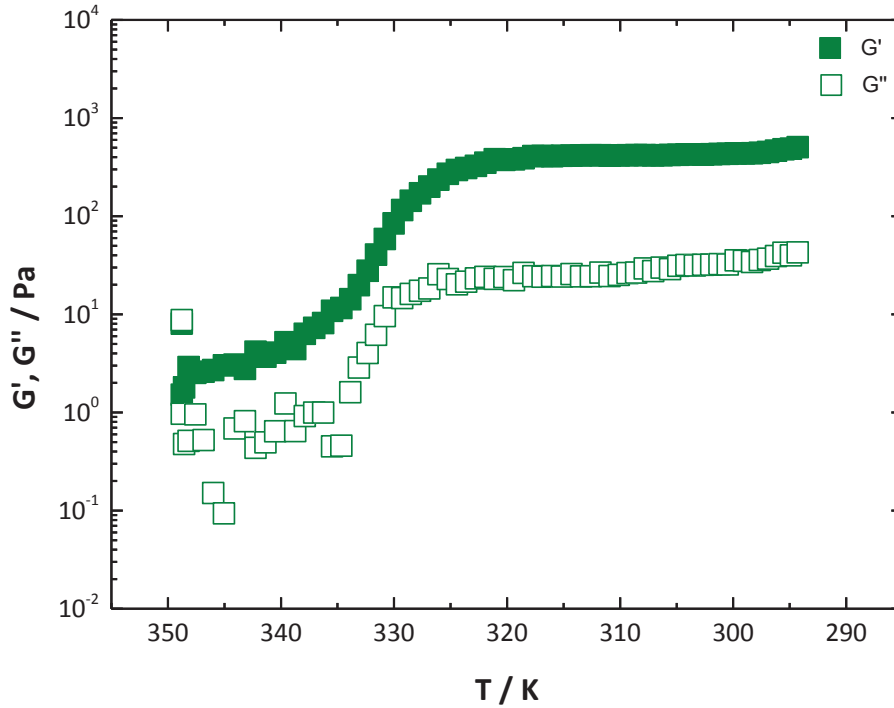


Figure 6-12 Storage modulus G' and loss modulus G'' vs. temperature of the 6.69 mM binary system of H_2O -DBC measured with oscillating shear rheometry at a constant frequency of 1 Hz, a shear strain of 0.05 %, and a cooling rate of 10 K/min, using a parallel plate geometry with a gap of 800 μm .

To study the influence of the cooling rate on the DBC-in-water system's gelation process, the $T_{\text{sol-gel}}$ values for the 6.69 mM binary system of H_2O -DBC were determined for different cooling rates, as shown in Figure 6-13.

When the cooling rate was increased from 1 to 10 K/min, the apparent $T_{\text{sol-gel}}$ values decreased from 353 to 336 K. Due to the $T_{\text{sol-gel}}$ values' dependency on the cooling rate, the determined values were considered to be “apparent” $T_{\text{sol-gel}}$ values for a defined cooling rate.

To determine the “real” $T_{\text{sol-gel}}$ values, the measurement must be performed quasi-statically. Thus, the temperature must be lowered with a very low cooling rate.

By extrapolating the data for a cooling rate of 0 K/min, it was possible to predict the quasi-static equilibrium value of 353 K.

The values determined for cooling rates higher than 0 K/min, could then be interpreted as a superposition of the temperature drop and the kinetic behavior.

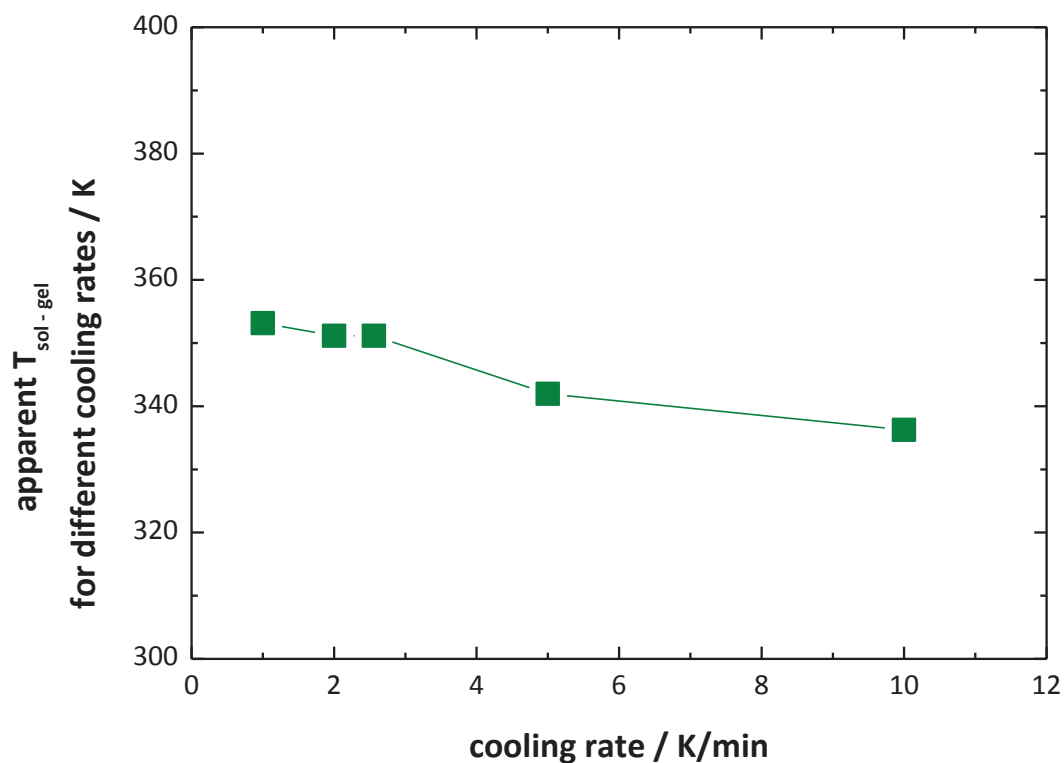


Figure 6-13 Apparent sol-gel transition temperature for different cooling rates, $T_{\text{sol-gel}}$, vs. cooling rate of the binary system H_2O -DBC with 6.69 mM DBC, measured with oscillating shear rheometry at a constant frequency of 1 Hz, and a shear strain of 0.05 %, using a parallel plate geometry with a gap of 800 μm .

6.1.2. Characterization of the Phase Transition and Properties of Gel

6.1.2.1. Optical Microscopy

The gel network morphology of the 6.69 mM binary gel of H₂O-DBC, was studied using optical microscopy, as shown in Figure 6-14.



Figure 6-14 Optical microscopy image of the 6.69 mM binary system of H₂O-DBC. The sample was transferred onto the slide at 353 K and was allowed to cool to 298 K. The image was taken after 20 minutes (scale bar = 100 μm).

It was possible to visualize short, solid fibers with a thickness of between 1 and 2 μm , which were randomly oriented and curved. They appeared to be entangled with each other. It is important to note that diffraction phenomena should be considered when using optical microscopy^[115]. Hence, the fiber thickness obtained from the image could be influenced by diffraction phenomena and should be taken as an “apparent” fiber thickness. In addition, an apparent fiber thickness of between 1 and 2 μm could also be the result of bundles of gel fibers^[83], which will be discussed in section 6.1.2.2.

6.1.2.2. Cryogenic-Transmission Electron Microscopy

Cryogenic-transmission electron microscopy measurement (cryo-TEM) was performed to visualize the gel network structure of the binary gel in a nanometer resolution, as depicted in Figure 6-15.

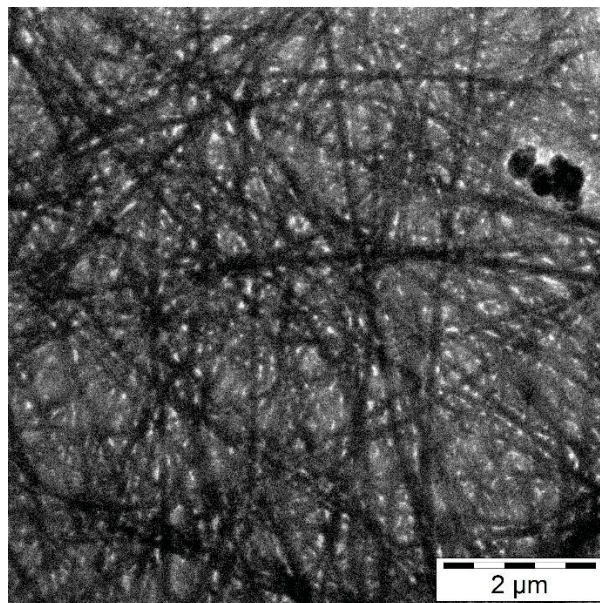


Figure 6-15 Cryo-TEM image of the 6.69 mM binary system of H₂O-DBC. The sample was at first allowed to cool from 363 to 298 K. After standing at 298 K for 5 minutes, the sample was prepared for cryo-TEM.

At first sight, the impression was given that fibers had been formed, however a closer look revealed the formation of fiber-like aggregates of spherulites.

These structures appeared to be randomly oriented and entangled with each other.

The thickness of the fiber-like aggregates was determined to be between 80 and 230 nm, by using imaging software for electron microscopy, “*iTEM*”. In the literature^[116], the gel network morphology of the binary gel H₂O-DBC with a gellant concentration of 4.46 mM, was described as being a network made up of solid fibers. A fiber thickness of between 20 and 60 nm was found.

By comparing the cryo-TEM and the optical microscopy images of DBC, it was found that the short fibers visualized by optical microscopy, which had an apparent thickness of between 1 and 2 μm, presumably resulted from the bundling of fiber-like aggregates. As the thickness of the aggregates measured by TEM, was between 80 and 230 nm, it follows that bundles of fiber-like aggregates with a thickness between 1 and 2 μm could be imaged by optical microscopy.

6.1.2.3. Surface Tension Measurements

The surface tension of the 1.11 mM binary system of H₂O-DBC was investigated to find out whether DBC had surface-active properties. The measurements were performed with a *Du Nouy* ring tensiometer and the results are shown in Table 6-3.

Table 6-3 Surface tension of water and of the binary system H₂O-DBC with a gellant concentration of 1.11 mM at pH values of 3 and 5, measured with a *Du Nouy* ring tensiometer, at 298 K. The samples were prepared individually for each pH.

pH	c / mM	Surface tension / mN m ⁻¹
3	0.00	67.3
3	1.11	56.4
5	0.00	68.3
5	1.11	55.5

Gelation in the sample would hinder the formation of a liquid lamella, which is required when the ring is immersed into the sample to measure the surface tension. Therefore, the gellant concentration was kept constant at 1.11 mM, which is below the critical gelation concentration of 4.46 mM, to ensure that no gelation occurred in the water.

The surface tension of water, at pH 3 and 298 K, was found to be 67.3 mN/m and 68.3 mN/m at pH 5 and 298 K, which was in line with the literature^[117]. When DBC was added to the water system, the solution's pH decreased from 7 to 3.5. Thus, a sodium hydroxide solution (**2.0 M**) was added to the system to adjust the pH to above 3.5.

In the presence of 1.11 mM DBC, the solution's surface tension was found to be 56 mN/m, which was independent of the pH. DBC seemed to be slightly surface-active. DBC's surface-activity could be due to its amphiphilic constitution of hydrophilic cysteine units and hydrophobic groups, such as benzoyl groups, as shown in Figure 6-16.

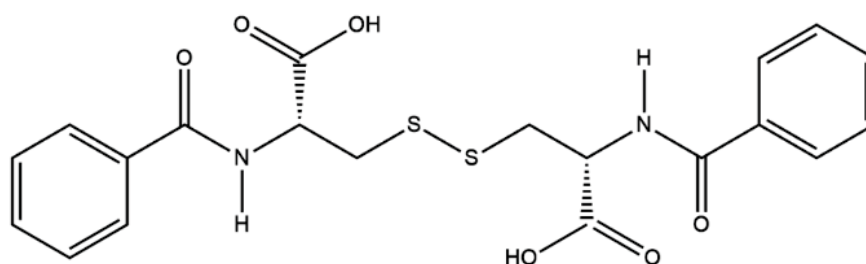


Figure 6-16 Chemical structure of DBC.

The DBC molecules could adsorb at the air-water interface whereby the hydrophobic benzyl groups could be oriented towards the air phase and the hydrophilic core to the water phase, leading to the decrease of the water's surface tension.

However, the gelling agent was not as highly surface-active as typical surfactants, such as LAS^[118], which can lower the surface tension of water by > 33 mN/m.

6.1.2.4. Kinetics of the Sol-Gel Phase Transition

The kinetics of the DBC-in-water system's gelation process were studied using rheology and also by the application of the *Dickinson* equation, proposed by *Huang et al.*^[13]. It is important to mention that, in this study, the investigation was focused on the kinetic behavior of the DBC-in-water system and not on the phase transition temperature. For this reason, the measurements were performed at high cooling rates in order to study the DBC gelation process. The gel formation at low cooling rates was completed at high temperatures, making the study of the kinetic behavior impossible for fast gelation. This is due to the rheometer's temperature restrictions or because the gel solidified due to the evaporation of the solvent for slow gelation.

In the literature^[119], *Dickinson* proposed an equation for studying the gelation process of spherical particles, which form aggregates by cross-linking. This equation was valid under the assumptions that the gel network consisted of fractal-type bonds, which were irreversible, and non-covalent bonds, which were reversible.

In addition, it was presumed that the gelling agent's aggregates were hard and incompressible particles and that their cross-sections were mono-disperse and had similar shapes. Furthermore, the gelation process was considered in the same way as the *Smoluchowski* model for diffusion^[120].

The resulting equation was suitable for characterizing the kinetic behavior of weak gelation processes. For the application of this equation, the data from the gelation stage of the gelation process were fitted in terms of the *Dickinson* equation.

In 2006^[13], this equation was applied to describe the fractal analysis of molecular gelation kinetics of dilute or semi-dilute, formulations determined using rheological measurements. *Huang et al.*^[13] developed an empirical relaxation equation for the determination of the fractal dimension D_f :

$$\ln\left(\frac{G'(t) - G'(0)}{G'(\infty) - G'(0)}\right) = \frac{3 - D_f}{D_f} \ln(t - t_g) + k \quad 6-1$$

with the average values of G' in the induction stage $G'(0)$, gelation stage $G'(t)$, quasi-equilibrium stage $G'(\infty)$, gelation time t_g at $G'(0)$, the time t , the constant k and the fractal dimension D_f , which gives an indication of the compactness of the gel network. The D_f value was determined from the slope of the linear fit of $\ln\left(\frac{G'(t) - G'(0)}{G'(\infty) - G'(0)}\right)$ against $\ln(t - t_g)$ in the gelation stage^{[55],[13],[119]}.

This equation was proposed under the conditions that the gelation process was divided into three stages: the induction, gelation, and quasi-equilibrium stages. In the induction stage, the nucleation and growth of gellant monomers occurs, which does not influence the storage modulus G' greatly. In the gelation stage, the monomers aggregate into fibers, which leads to a sharp increase of G' , and the solvent is completely entrapped in the meshes.

The rearrangements of fibers and junctions lead to further increases of G' , until a three-dimensional gel network of fibers is formed in the quasi-equilibrium stage.

By combining the determined D_f value with optical microscopy measurements *Huang et al.*^[13] defined ranges for D_f values describing the fractal structure of gels.

The following assignments of D_f values to the optical microscopy measurements were made:

Table 6-4 Indications for different D_f values according to references [54],[13],[121]–[124].

D_f	compactness of the gel network
1.0 - 1.5	linear (open) network structure
1.5 - 2.0	less compact network structure
2.0 - 3.0	highly compact network structure
3.0	solid structure

A linear (open) network structure, which could be understood as a tangle of fibers^{[54],[13],[121]}, was proposed for D_f values between 1.0 and 1.5. For D_f values ranging from 1.5 to 2.0, the fractal network's morphology was described as being a less compact network, which could be interpreted as the formation of branched fibers^{[54],[13],[121]}. For a D_f value above 2.0, a highly compact network structure with more branched fibers or fractally rough structures, was proposed^[121] and solid structures were proposed^[121] at a D_f value of 3.0. The highest possible D_f value for describing the morphology of fractal network structures was 3.0, due to proposed empirical relaxation equation, as shown in equation 6-1.

The slope would be negative for D_f values greater than 3.0, which would mean that the G' values decreased with time, which is not reasonable from a physical point of view.

The indications for different D_f values show that a decrease in D_f values is related to the formation of finer network structures, from solid-like structures down to linear network structures.

In 2013, *Wang* et al.^[125] developed an extended equation for analyzing the kinetic data, which was also suitable for concentrated formulations. They showed that for a D_f value of up to 2.0, the assignment of this value to a less compact network structure correlated to the equation proposed by *Huang* et al.^[13]. However, above this value, equation 6-1 was not suitable for describing more branched fractal network structures.

By introducing the scaling factor, α ^[126], they showed that the proposed equation was not only suitable for dilute systems but also for concentrated formulations, such as gellant concentrations of up to 140 mM.

The extended relaxation equation^[125] was given by:

$$\ln \left(\frac{G'(t) - G'(0)}{G'(\infty) - G'(0)} \right)^{1/\alpha} = \frac{3 - D_f}{D_f} \ln(t - t_g) + k \quad \mathbf{6-2}$$

The scaling factor was determined by plotting the G' values against the gellant concentration.

In this study of the analysis of the gelation behavior, the gellant concentration was kept constant at 6.69 mM, as above this concentration, the kinetics of the gel network formation could not be studied using rheological measurements, due to fast gelation. Therefore, dilute gellant systems were studied. The kinetic data were fitted in terms of the *Dickinson* equation proposed by *Huang* et al.^[13], which is suitable for dilute or semi-dilute gellant formulations.

In order to gain a deeper understanding of the *Dickinson* equation proposed by *Huang* et al.^[13], model calculations of G' values were performed for given D_f values, according to the equation:

$$G'(t) = \left[(t - t_g)^{\frac{3-D_f}{D_f}} * e^k * (G'(\infty) - G'(0)) \right] + G'(0) \quad \mathbf{6-3}$$

The $G'(0)$ and $G'(\infty)$ values were kept constant at $8 \times 10^{+00}$ Pa for $G'(0)$ and $5 \times 10^{+02}$ Pa for $G'(\infty)$, taken from temperature-sweep measurements obtained by cooling the binary system H₂O-DBC with a gellant concentration of 6.69 mM, at a rate of 10 K/min (Chapter 6.1.1, Figure 6-12).

The model calculations of the G' values for different D_f values, and the fractal analysis of the kinetic data in terms of the *Dickinson* equation according to equations 6-1 and 6-3, are depicted in Figure 6-17.

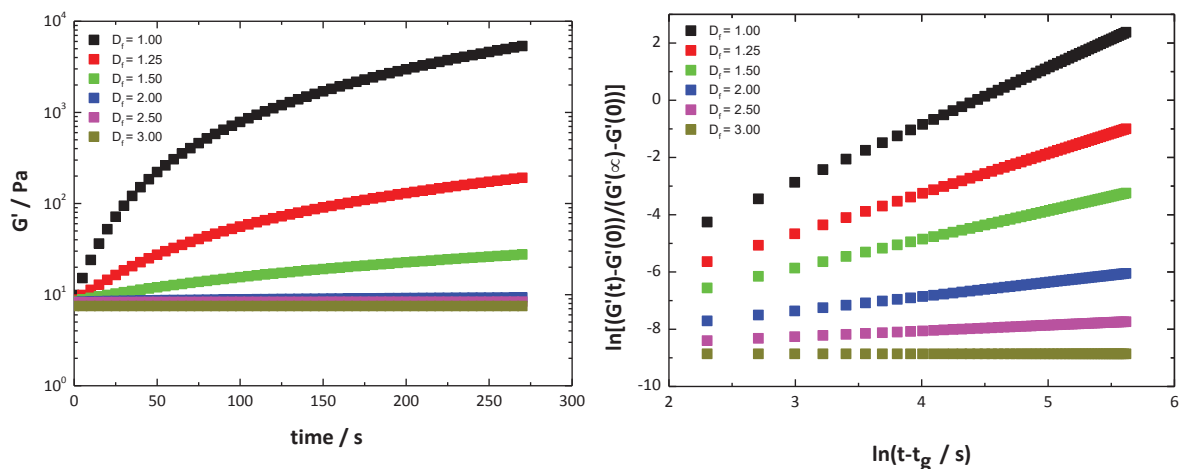


Figure 6-17 Model calculations of the storage modulus G' vs. time for different D_f values, according to equation 6-3 (left), and fractal analysis of the kinetic data in terms of the *Dickinson* equation, according to equation 6-1 (right).

It was found that the rate of increase for the G' values is highly dependent on the given D_f value. With increasing D_f values, the G' values increased more slowly than at low D_f values. Moreover, the given $G'(\infty)$ value of $5 \times 10^{+02}$ Pa, could not be achieved for a D_f value greater than 1.00 within the given timeframe. Even a slight increase of the D_f value from 1.00 to 1.25 meant that the complete gelation process could not be monitored. With a further increase in the D_f value, the G' values are nearly independent of the time, with $8 \times 10^{+00}$ Pa, which shows that no structures are formed.

As mentioned previously, solid structures were formed at a D_f value of 3.00^[121], which was in line with the model calculations, as the G' values were independent of the time. It could therefore be concluded that the structures' growth processes can be better studied at lower D_f values. This could also be related to the formation of fine network structures with higher G' values at low D_f values, compared to solid structures with lower G' values at high D_f values, which do not show a growth process.

For determining the D_f value of the 6.69 mM DBC-in-water system, temperature - sweep measurements were performed at a cooling rate of 10 K/min, as shown in Figure 6-18.

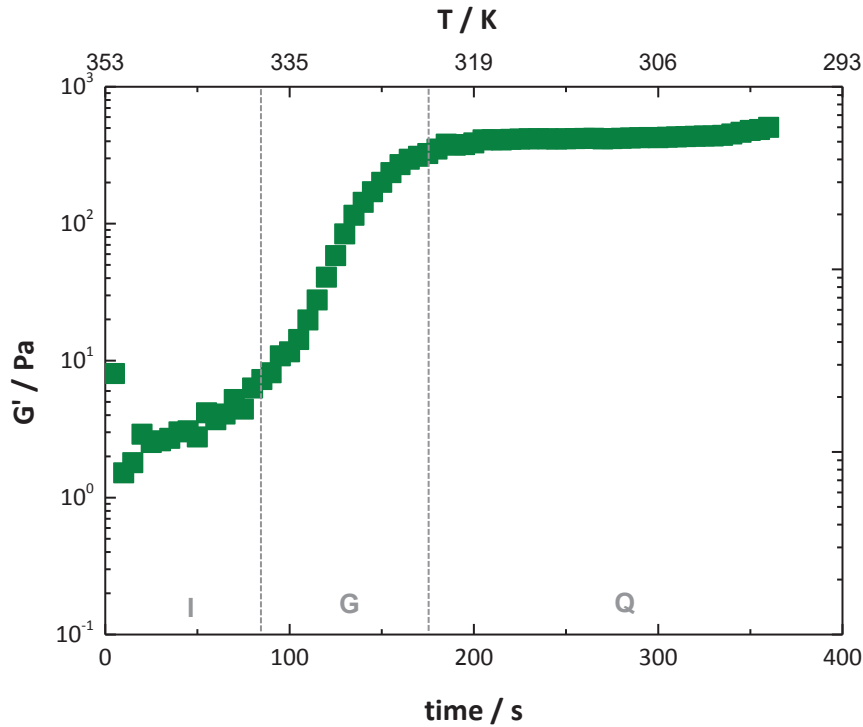


Figure 6-18 Evolution of the storage modulus G' of the 6.69 mM binary system of H_2O -DBC, measured with oscillating shear rheometry at a constant frequency of 1 Hz, a shear strain of 0.05 %, and a cooling rate of 10 K/min, using a parallel plate geometry with a gap of 800 μm (I - Induction stage, G - Gelation stage, Q - Quasi-equilibrium stage).

When cooling the sample at a rate of 10 K/min, the G' values increased slightly from $2 \times 10^{+00}$ to $8 \times 10^{+00}$ Pa, during the induction stage. After the gelation time, which was found to be 90 s, the G' values sharply increased over two orders of magnitudes during the gelation stage, from $8 \times 10^{+00}$ to $4 \times 10^{+02}$ Pa, until the quasi-equilibrium stage was reached after 180 s. At this point, the G' values plateaued at $5 \times 10^{+02}$ Pa, indicating that gel network formation was completed.

The data were fitted in terms of the *Dickinson* equation (equation 6-1).

The following parameters were obtained from the kinetic data for the application of this equation:

Table 6-5 Parameters taken from the kinetic data of the 6.69 mM binary system of H₂O-DBC for applying the *Dickinson* equation (equation 6-1) (t_g – gelation time at $G'(0)$, $G'(0)$ - average values of G' in the induction stage, $G'(\infty)$ - average values of G' in the quasi-equilibrium stage).

Parameter	Value
t_g	90 s
$G'(0)$	$8 \times 10^{+00} \text{ Pa} \pm 8 \times 10^{-01} \text{ Pa}$
$G'(\infty)$	$5 \times 10^{+02} \text{ Pa} \pm 2 \times 10^{+02} \text{ Pa}$

The fractal analysis of the kinetic data, in terms of equation 6-1, is depicted in Figure 6-19.

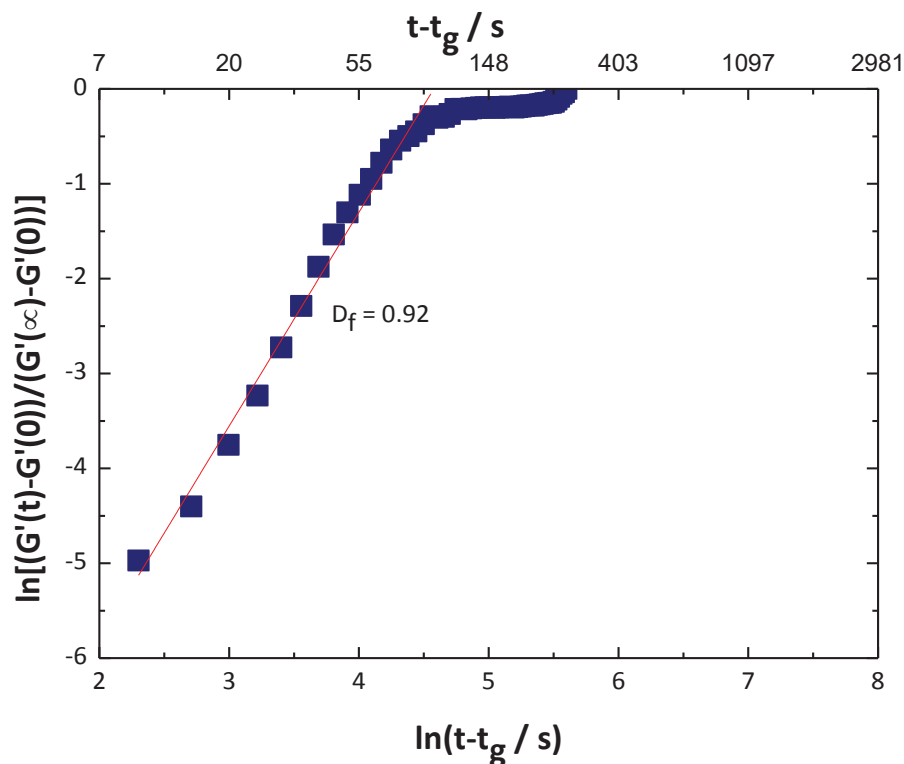


Figure 6-19 Fractal analysis of the kinetic data in terms of the *Dickinson* equation, according to equation 6-1, of the 6.69 mM binary system of H₂O-DBC, measured with oscillating shear rheometry at a constant frequency of 1 Hz, a shear strain of 0.05 %, and a cooling rate of 10 K/min, using a parallel plate geometry with a gap of 800 μm .

A D_f value of 0.92 was determined from the slope of the linear fit of $\ln\left(\frac{G'(t)-G'(0)}{G'(\infty)-G'(0)}\right)$ against $\ln(t - t_g)$, which indicates a growth process in terms of the model calculations performed (Figure 6-17). According to *Huang et al.*^[13], this value would describe a linear (open) network structure.

As mentioned above, the assignment of the D_f values to the network structures, was performed by comparing the D_f values to the optical microscopy measurements.

The morphology of the binary gel visualized by the optical microscopy measurement is shown in Chapter 6.1.2.1 (Figure 6-14). The appearance of randomly oriented, short fibers, which seemed to be tangled with each other, could be imaged. However, the presence of a linear (open) network structure for D_f values between 1.0 and 1.5 (Table 6-4), as proposed by *Huang et al.*, cannot be clearly assigned for the optical microscopy measurement.

In this work, the gel network's morphology was also studied using cryo-TEM measurements (Chapter 6.1.2.2, Figure 6-15); fiber-like aggregates, which were randomly oriented and entangled with each other, were found.

As a result, the indication for a linear (open) network structure seems to be better correlated to the cryo-TEM measurement, than to the optical microscopy measurement.

To study the influence of the gellant concentration on the storage modulus G' , the G' values in the quasi-equilibrium stage were determined using rheological measurements for varied gellant concentrations, as outlined in Figure 6-20.

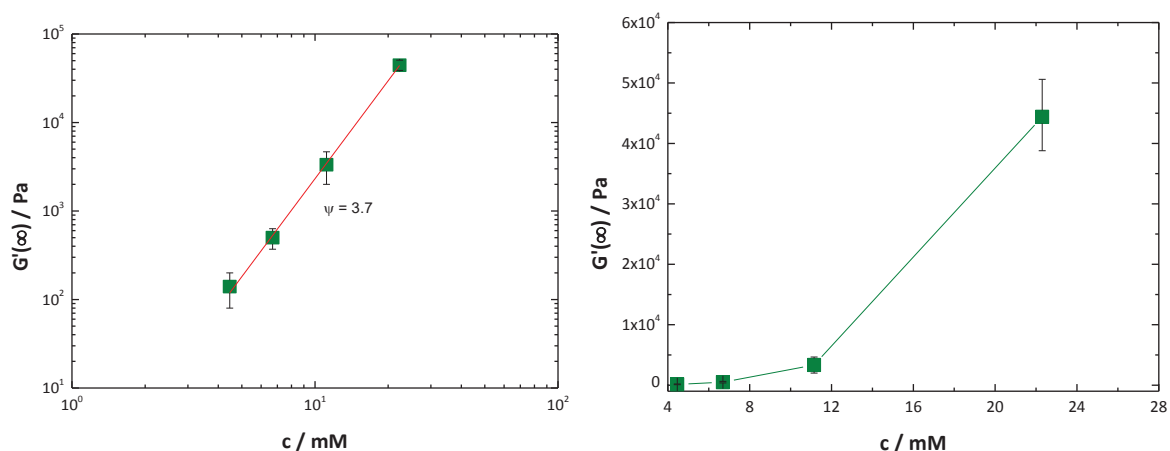


Figure 6-20 Log-log (left) and linear-linear plots (right) of the storage modulus in the quasi-equilibrium stage, $G'(\infty)$, of the binary system H₂O-DBC with varied gellant concentrations, measured at 293 K with oscillating shear rheometry, at a frequency of 1 Hz, and a strain of 0.05 %, using a parallel plate geometry with a gap of 800 μ m. The prepared sample was transferred into the rheometer at 353 K and was cooled to 293 K with a rate of 10 K/min.

When the DBC concentration was increased, the $G'(\infty)$ values increased from $1 \times 10^{+02}$ to $7 \times 10^{+04}$ Pa.

According to a power law function^[127]:

$$G'(\infty) = c^\psi \quad \mathbf{6-4}$$

the scaling exponent ψ could be determined from the slope of the log-log plot of $G'(\infty)$ against the gellant concentration. A scaling exponent of 3.7 was determined for the H₂O-DBC hydrogel.

In the literature^[124], a scaling exponent of 3.7 was found for multiwalled carbon nanotube-epoxy suspensions, which formed compact network structures of polymer-stabilized elastic networks.

A scaling exponent of 2.2 was found for entangled biopolymer networks^[128].

The linear plot of $G'(\infty)$ against the gellant concentration showed that above a DBC concentration of 11.15 mM, there was a much greater increase in G' value than below this concentration. The results showed that to study the kinetics of DBC gel formation, gellant concentrations lower than 11.15 mM had to be studied.

Otherwise, it would not be possible to investigate the gelation process with the induction, gelation, and quasi-equilibrium stages, due to fast gelation kinetics.

6.2. Study of the Gelation Behavior of DBC in the Presence of LAS

The physicochemical properties of DBC were studied in the presence of the anionic surfactant, LAS, both below and above the critical gelation concentration of 4.46 mM. Initially, the surface tension of a ternary system of H₂O-LAS-DBC below the critical gelation concentration was studied, to determine whether the LAS's cmc and surface tension would be influenced by the addition of DBC, which had been found to be slightly surface-active (Chapter 6.1.2.3, Table 6-3).

Thereafter, the apparent $T_{\text{sol-gel}}$ values for different cooling rates of the ternary system with varied surfactant concentrations and with a gellant concentration above the critical gelation concentration, were studied using rheology. The gel network's morphology was visualized by imaging measurements.

Finally, the kinetics on gel network formation were investigated with rheological measurements, and the kinetic data were fitted in terms of the *Dickinson* equation proposed by *Huang* et al.^[13] (Chapter 6.1.2.4, equation 6-1).

6.2.1. Molecular Interactions below the Critical Gelation Concentration

The influence of DBC molecules on the surface tension properties of LAS, was studied using surface tension measurements, which could give an indication of the molecular interactions between the DBC and LAS molecules.

6.2.1.1. Surface Tension Measurements

The surface tension measurements were performed with a *Du Nouy* ring tensiometer, as illustrated in Figure 6-21.

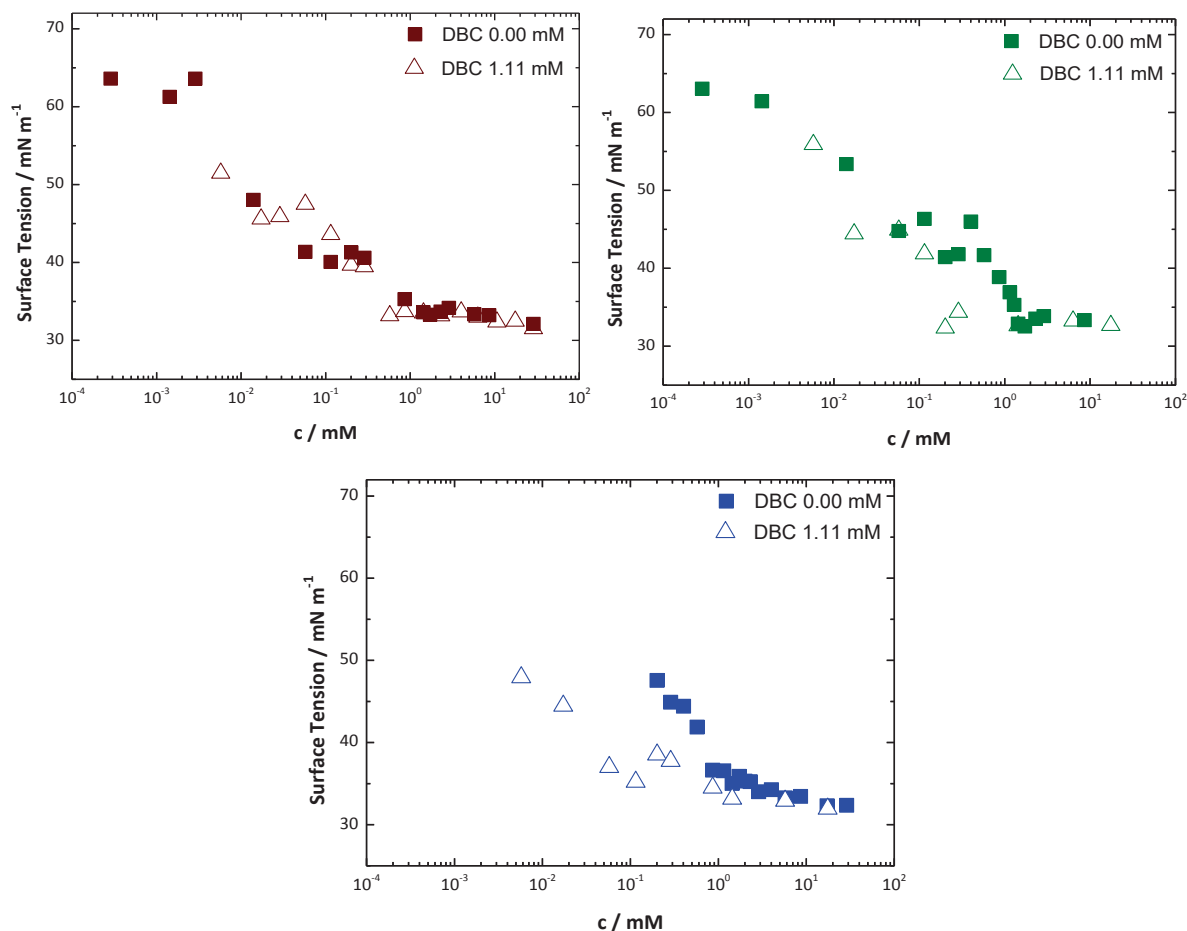


Figure 6-21 Surface tension measurements of the binary system H₂O-LAS and the ternary system H₂O-LAS-DBC with 1.11 mM DBC and varied LAS concentrations, measured with a *Du Nouy* ring tensiometer, at 298 K. The samples were prepared individually for each surfactant concentration and adjusted to an initial pH of 3 (red), 5 (green), and 7 (blue).

The cmc values were determined from the intersection point of the tangents from the concentration-dependent part (below the cmc) and from the concentration-independent part (above the cmc), where a plateau arises. The cmc values determined for the LAS binary and LAS-DBC ternary systems, are presented in Table 6-6.

Table 6-6 Cmc values of LAS-in-water system and in mixture with 1.11 mM DBC, determined with a *Du Nouy* ring tensiometer, at 298 K.

System	cmc at pH		
	3 / mM	5 / mM	7 / mM
H ₂ O-LAS	1.4	1.4	1.4
H ₂ O-LAS-DBC 1.11 mM	0.6	0.3	0.1

The cmc of the LAS-in-water system was found to be 1.4 mM at pH 7, which agrees well with the literature^[129], in which a cmc of 1.2 mM was found.

When the pH was lowered by the addition of a hydrochloric acid solution (HCl) (**2.0 M**), the cmc values did not change, although the surface tension slightly decreased with decreasing pH.

Lower cmc values were determined in the presence of DBC, independent of the pH, which could be due to the addition of electrolytes^[130], or DBC's slight surface-activity, as discussed in section 6.1.2.3 (Table 6-3).

Increasing the pH of the ternary system H₂O-LAS-DBC by adding a sodium hydroxide solution (NaOH) (**2.0 M**), led to a decrease in the LAS cmc values, which could also be an effect of electrolytes or due to DBC's slight surface-activity.

When comparing the surface tension of the LAS binary and LAS-DBC ternary systems at various pH values, it was observed that as long as the cmc was above the cmc for the LAS-in-water system, both systems had similar surface properties, regardless of pH. At pH 3, both systems also demonstrated similar surface properties below the cmc of the LAS binary system. However, at increased pH values, the differences in surface tensions of the two systems below the H₂O-LAS cmc, appeared to be more pronounced. This could be attributable to either the addition of electrolytes, such as the HCl or NaOH solutions, or alternatively, a slight interaction between the LAS and DBC molecules at the air-water interface.

It should also be considered, that slight interactions between LAS and DBC molecules at the air-water interface, could also occur at a pH of 3. Lowering the pH promotes the formation of a gel network, as outlined in Chapter 4.2.2. For a gel network to be formed, the gellant concentration must first be higher than the critical gelation concentration and, in the case of DBC, the carboxyl group has to be protonated for the formation of a gel network by hydrogen bondings^[30] (for the structure of DBC, refer to Chapter 6.1.2.3, Figure 6-16).

6.2.2. Molecular Interactions above the Critical Gelation Concentration

6.2.2.1. Phase Transition Temperature

In order to study the influence of surfactant molecules on the phase transition of DBC from the sol to the gel phase, the apparent $T_{\text{sol-gel}}$ values for different cooling rates were determined using rheological measurements.

The gellant concentration was kept constant at 6.69 mM, to ensure the same conditions as for the DBC-in-water system (Chapter 6.1.1).

The measurement of the temperature dependency of G' and G'' values of the ternary system H_2O -LAS-DBC with a LAS concentration of 7.17 mM, is shown in Figure 6-22. A surfactant concentration of 7.17 mM was chosen, because an interesting trend of G' values was found at this concentration. Namely, the G' values first decreased to the apparent $T_{\text{sol-gel}}$ value for a cooling rate of 10 K/min, and then sharply increased when the temperature was lowered further. The appearance of a minimum during the transition from the induction to the gelation stage, will be discussed in detail in Chapter 6.2.2.4.

While decreasing the temperature from 353 to 336 K, the G' values were nearly constant at 6×10^{-01} Pa. With a further decrease of the temperature to 331 K, the G' values decreased over one order of magnitude and reached a value of 3×10^{-02} Pa, before increasing sharply to $6 \times 10^{+02}$ Pa.

An apparent $T_{\text{sol-gel}}$ value for a cooling rate of 10 K/min was determined from the beginning of the increase of the G' values. The apparent transition from the sol to the gel phase, was observed at 331 K.

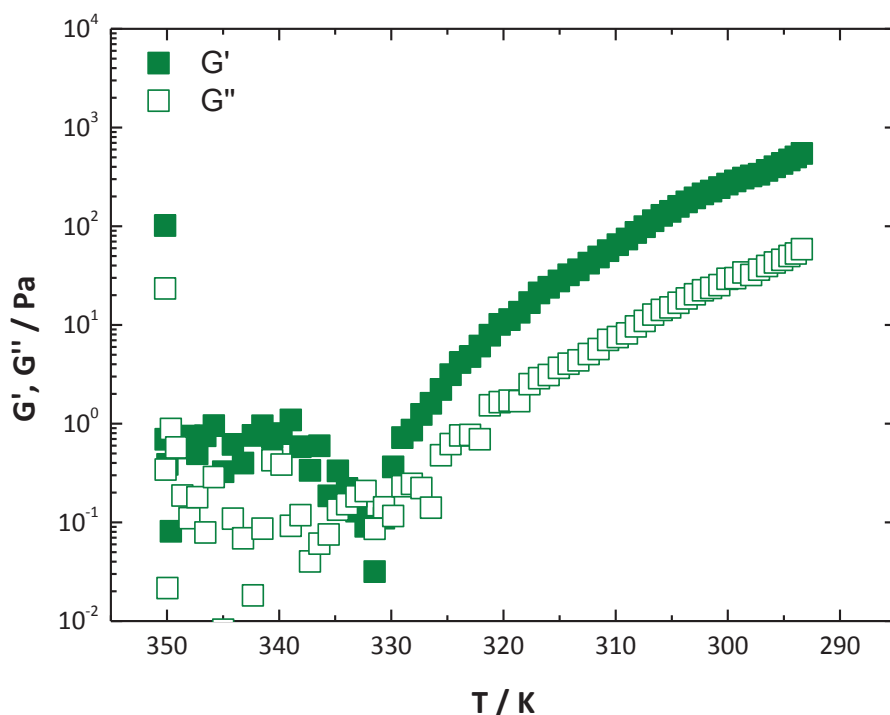


Figure 6-22 Storage modulus G' and loss modulus G'' vs. temperature of the ternary system H₂O-LAS-DBC with a surfactant concentration of 7.17 mM and a gellant concentration of 6.69 mM, measured with oscillating shear rheometry, at a constant frequency of 1 Hz, a shear strain of 0.05 %, and a cooling rate of 10 K/min, using a parallel plate geometry with a gap of 800 μm .

Different cooling rates were tested to discover the effect of LAS on the DBC gelation process. Various concentrations of LAS were added to a 6.69 mM binary system of H₂O-DBC.

The apparent $T_{\text{sol-gel}}$ values of the ternary system at cooling rates of 5 and 10 K/min, are presented in Figure 6-23.

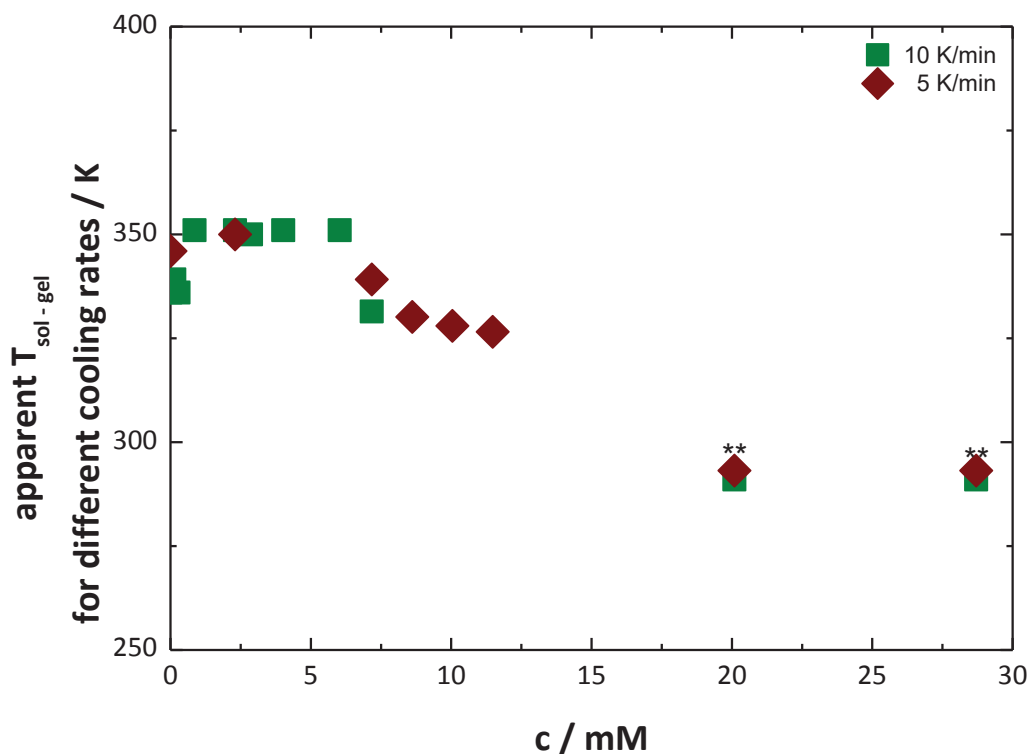


Figure 6-23 Apparent $T_{\text{sol-gel}}$ values for different cooling rates of the ternary system H_2O -LAS-DBC with a gellant concentration of 6.69 mM and varied surfactant concentrations, measured with oscillating shear rheometry, at a constant frequency of 1 Hz, a shear strain of 0.05 %, and cooling rates of 5 and 10 K/min, using a parallel plate geometry with a gap of 800 μm . Symbols marked with a double asterisk, **, indicate the temperature at which the gelation occurred by a long-term measurement.

The apparent $T_{\text{sol-gel}}$ values of the ternary system for a cooling rate of 10 K/min, could be taken as being identical below a 0.29 mM surfactant concentration. These values were recorded between 336 and 339 K. When the LAS concentration was further increased, up to 6.03 mM, the apparent $T_{\text{sol-gel}}$ value for a cooling rate of 10 K/min, increased from 336 to 351 K. Above this concentration, the values decreased from 351 to 331 K. At high surfactant concentrations of greater than 20.09 mM, the apparent $T_{\text{sol-gel}}$ value for a cooling rate of 10 K/min was 293 K. At this temperature, the gelation process was recorded by a long-term measurement, as no gelation occurred within the given timeframe of the temperature-sweep measurement.

It can be concluded that the DBC gel network formation was promoted by the addition of LAS for a LAS concentration of up to 6.03 mM, as greater $T_{\text{sol-gel}}$ values were determined than for the DBC-in-water system. At high surfactant concentrations of above 20.09 mM LAS, the $T_{\text{sol-gel}}$ values determined were lower than when LAS was absent, hence, the gel network formation was delayed.

The determination of the apparent $T_{\text{sol-gel}}$ values for a cooling rate of 5 K/min, showed a similar trend to that of a 10 K/min cooling rate. For concentrations of up to 2.30 mM LAS, the values were found to be between 346 and 350 K.

It is important to note that, for LAS concentrations of up to 1.72 mM, the transition from the sol to the gel phase could not be determined by using rheology, as the rheometer's measuring limit was 353 K.

The $T_{\text{sol-gel}}$ value was greater than 353 K; at this temperature, the gelation process was either in the last part of the gelation stage, or the quasi-equilibrium stage had been reached.

Between 7.17 to 11.48 mM LAS, the values decreased from 339 to 326 K and no gelation occurred above 20.09 mM LAS during the temperature-sweep measurement. Comparing the values with those obtained in the absence of LAS, it was found that gel network formation was promoted of up to a LAS concentration of 2.30 mM, which is slightly above the cmc of 1.4 mM, and delayed by a further increase of the concentration. The promotion was shown by higher $T_{\text{sol-gel}}$ values than for the DBC-in-water system and the delay, by lower $T_{\text{sol-gel}}$ values than for binary system H₂O-DBC.

The promotion and delay of gel network formation are clearly shown by measuring the G' values' dependency on the temperature, by cooling the sample at a rate of 5 K/min, as shown in Figure 6-24.

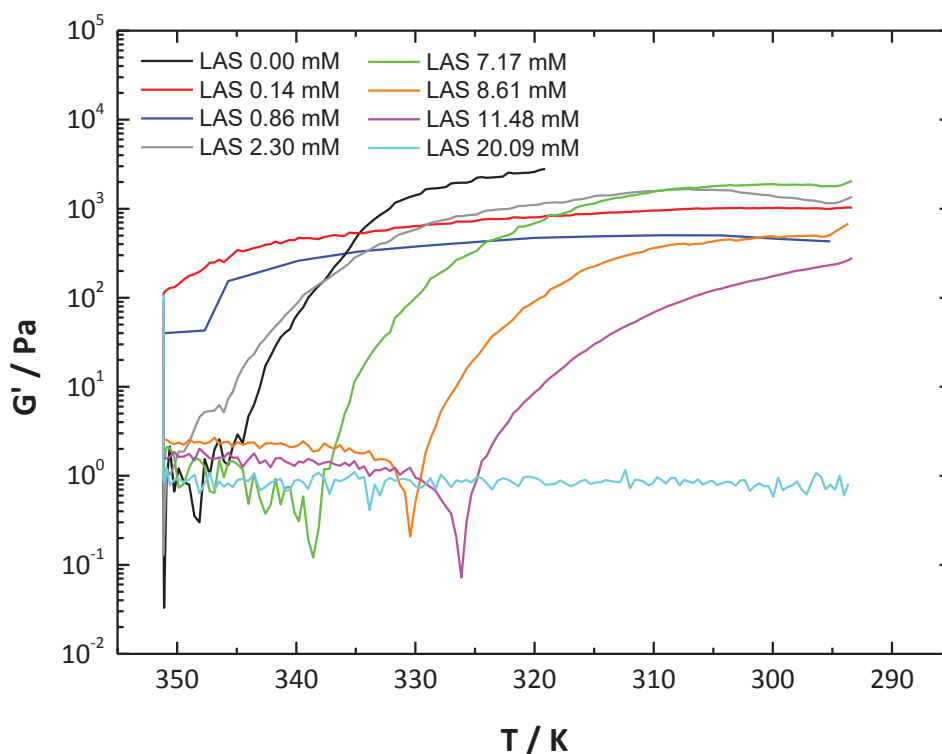


Figure 6-24 Measurement of the temperature dependency of the storage modulus G' of the ternary system H_2O -LAS-DBC with a gellant concentration of 6.69 mM and varied surfactant concentrations, measured with a parallel plate geometry and a gap of 800 μm at 293 K with oscillating shear rheometry at a constant frequency of 1 Hz, a shear strain of 0.05 %, and a cooling rate of 5 K/min.

In the absence of LAS, gel formation started at a temperature of 346 K and was completed at 331 K, with a G' value of $3 \times 10^{+03}$ Pa. However, in the presence of LAS, it was found that the gel formation was promoted by the surfactant molecules for surfactant concentrations of up to 2.30 mM, as the G' values either plateaued or began to increase at higher temperatures than in the DBC-in-water system. Even at 353 K, the G' values of the ternary gels H_2O -LAS-DBC with surfactant concentrations of 0.14 mM and 0.86 mM, were two orders of magnitudes higher than for the DBC-in-water system and the G' values reached a plateau at a temperature below 340 K.

When investigating surfactant concentrations between 7.17 and 11.48 mM, the gel formation was delayed as surfactant concentration increased, whereby it was either in progress or completed at 293 K and the G' values were in the same range as for the binary system H₂O-DBC. A further increase in the LAS concentration inhibited the gel formation within the cooling cycle from 353 to 293 K.

That the gelation process began at higher temperatures with the addition of LAS at low surfactant concentrations, rather than at high surfactant concentrations, could possibly be due to the dispersion of DBC particles being enhanced by surfactant molecules during the heating process during sample preparation. This in turn could lead to the formation of smaller aggregates, as a result of a decrease in the interfacial tension^{[38],[53],[131]} between the gellant aggregates and the water phase and facilitate the nucleation of gellant aggregates.

In order to understand the delay in gel network formation above 7.17 mM LAS with increasing surfactant concentration, the micelle distance at high surfactant concentrations was calculated using two assumptions: 1) the shape of the aggregates was spherical, which did not change with increasing gellant concentration, and 2) the aggregates were evenly distributed in a cubic lattice^[132]. Accordingly, the determination of the micelle distance was related to the distance from center to center.

The number of surfactant molecules N_S is given by^[133]:

$$N_S = (c_s - \text{cmc}) * N_A \quad \mathbf{6-5}$$

with the surfactant concentration c_s , the critical micelle concentration cmc and the *Avogadro* constant N_A .

The number of surfactant molecules for a surfactant concentration of 28.70 mM, is $1.64 \times 10^{+22}$ molecules/l.

Thus, the number of micelles, N_M , can be expressed as:

$$N_M = \frac{N_S}{N_{\text{AGG}}} \quad \mathbf{6-6}$$

with the aggregation number N_{AGG} . An aggregation number of 57 was found in the literature^[134], for LAS. Thus, the number of micelles is $2.87 \times 10^{+20}$ micelles/l.

It can be concluded that a single micelle has a volume of 3.48×10^{-24} m³/micelle.

The distance from micelle center to micelle center, is thus given by:

$$l = \sqrt[3]{V_M} - d_h \quad 6-7$$

with the distance l , volume of micelle V_M and hydrodynamic diameter of micelle d_h .

The micelles' hydrodynamic diameter was determined by using dynamic light scattering measurements. The *Brownian* motion of particles driven by the random collision of particles with the molecules of the surrounding aqueous medium, was measured and then the hydrodynamic diameter was determined from the number distribution, by using the *Mie* theory^[100].

The correlation function of the binary system H₂O-LAS with a surfactant concentration of 28.70 mM, is shown in Figure 6-25.

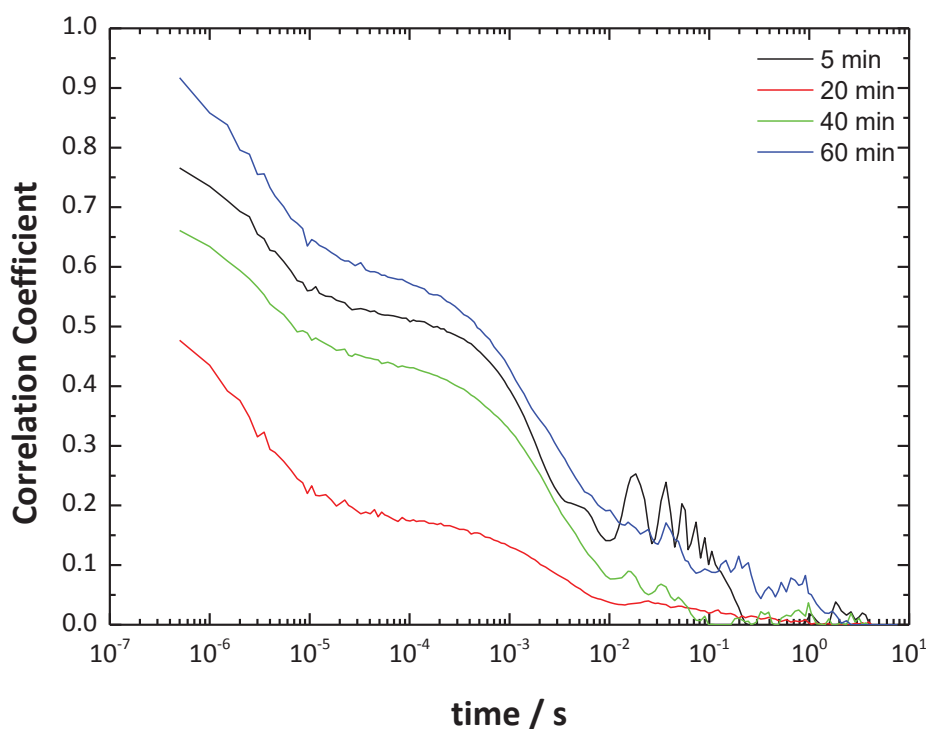


Figure 6-25 Correlation function of the binary system H₂O-LAS with a surfactant concentration of 28.70 mM, measured with Zetasizer Nano Series, at 298 K. The measurement was repeated at regular 5-minute intervals. For a clear display, the measurements were recorded after 5, 20, 40 and 60 minutes.

The curves were related to a single exponential decay function, which was characteristic of a dispersion consisting of particles with the same diameter (Chapter 4.3.2, equation 4-5).

The correlation function provides information on the diffusion coefficient by fitting the correlation function with algorithms. The hydrodynamic diameter could be obtained by using the *Stokes-Einstein* equation (Chapter 4.3.2, equation 4-2).

The intensity distribution was calculated from the information from the correlation function, which was then illustrated as a number distribution, by using the Mie theory^[100], as depicted in Figure 6-26.

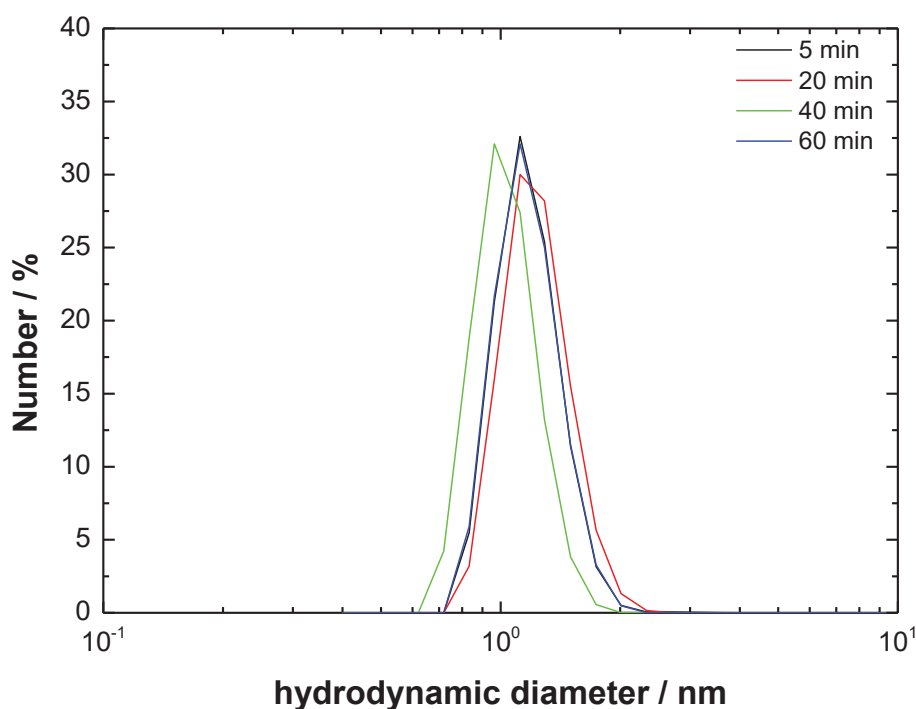


Figure 6-26 Number distribution of the binary system H₂O-LAS with a surfactant concentration of 28.70 mM, measured with Zetasizer Nano Series, at 298 K. The measurement was repeated at regular 5-minute intervals. For a clear display, the measurements were recorded after 5, 20, 40 and 60 minutes.

It was found that particles with a hydrodynamic diameter of 1 nm were present in the LAS-in-water system; their diameter did not change over time.

The hydrodynamic diameters, determined from the number distribution of the binary system H₂O-LAS with LAS concentrations of 20.09 and 28.70 mM, are presented in Table 6-7.

Table 6-7 Hydrodynamic diameter of particles in the binary system H₂O-LAS with surfactant concentrations of 20.09 and 28.70 mM, measured from the number distribution with ZetaSizer Nano Series, at 298 K. The measurement was repeated at regular 5-minute intervals.

t / min	Hydrodynamic diameter / nm	
	H ₂ O-LAS 20.09 mM	H ₂ O-LAS 28.70 mM
5	1.1	1.2
60	1.1	1.2

The hydrodynamic diameter for both surfactant concentrations was found to be 1 nm, which did not increase over time.

The diameters of LAS micelles, reported in the literature^{[135],[136]}, were found to be 1.7^[135] and 2.0 nm^[136], which were slightly larger by a factor of 2. However, this deviation could be due to the different analytical methods used to determine the micelles' diameter, or due to the use of LAS from a different supplier.

Therefore, in this work, the diameter of LAS micelles determined by dynamic light scattering will be used, rather than the values determined in the literature^{[135],[136]}.

According to equation 6-7, the center-to-center distance of micelles is 14 nm for a surfactant concentration of 28.70 mM.

Hence, a densely packed system of micelles existed at high surfactant concentrations.

It can be concluded that the delay in gel network formation could be due to the diffusion of gellant monomers being hindered by surfactant micelles. Furthermore, the gellant aggregates could be hindered sterically, due to the surfactant molecules on their surface being adsorbed in such a way that the molecules are unable to interact directly with one another. This barrier must be overcome for the aggregates to nucleate.

6.2.2.2. Optical Microscopy

The gel network's morphology, on the μm -scale, in a mixture with LAS below and above the cmc of 1.4 mM (Chapter 6.2.1.1, Table 6-6), is illustrated in Figure 6-27 and Figure 6-28.

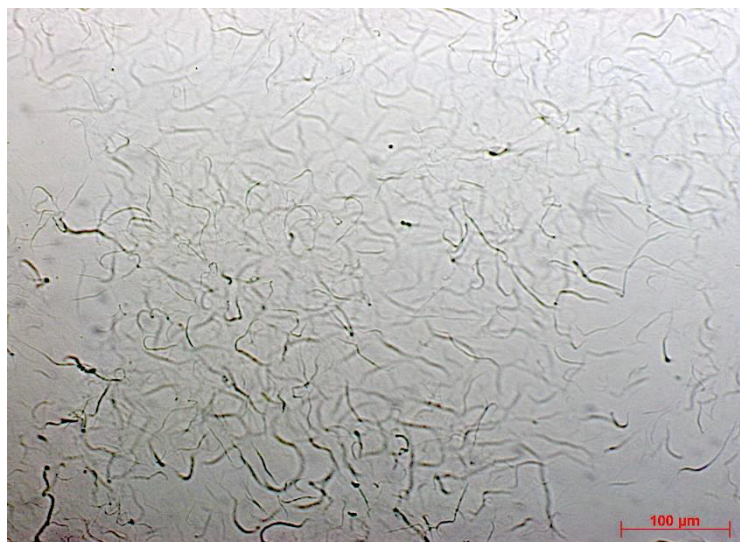


Figure 6-27 Optical microscopy image of the ternary system H_2O -LAS-DBC with a gellant concentration of 6.69 mM and a surfactant concentration of 0.29 mM. The sample was transferred onto the slide at 353 K and was allowed to cool to 298 K. The image was taken after 20 minutes (scale bar = 100 μm).



Figure 6-28 Optical microscopy image of the ternary system H_2O -LAS-DBC with a gellant concentration of 6.69 mM and a surfactant concentration of 20.09 mM. The sample was transferred onto the slide at 353 K and was allowed to cool to 298 K. The image was taken after 180 minutes (scale bar = 100 μm).

Nearly the same structures were found in the 0.29 mM LAS ternary mixture, as in the DBC-in-water system (Chapter 6.1.2.1, Figure 6-14). The short fibers with an apparent thickness between 1 and 2 μm , were randomly oriented and curved.

In the presence of 20.09 mM LAS, optical microscopy images were taken after 5, 60, and 180 minutes. The formation of a fiber-like network could be observed after 180 minutes. No structures had been formed after 5 and 60 minutes, which could be regarded as confirming the delay in gel network formation at high surfactant concentrations, observed from rheological measurements, as presented in Figure 6-24 (Chapter 6.2.2.1).

After 180 minutes, long, entangled fibers were formed, which differed from the gel network structure of the DBC binary system (Chapter 6.1.2.1, Figure 6-14), and of the DBC ternary system in mixture with 0.29 mM LAS (Figure 6-27).

Very thin fibers with an apparent fiber thickness of up to 1 μm , and thick fibers with an apparent fiber thickness of up to 5 μm , were formed. Taking the diffraction phenomena during optical microscopy measurement into account, the values for the apparent fiber thickness could also result from bundles of gel fibers.

6.2.2.3. Cryogenic-Transmission Electron Microscopy

Cryo-TEM measurements of the ternary systems of H_2O -LAS-DBC with a gellant concentration of 6.69 mM and varied surfactant concentrations, were performed to gain insights into the gel network's morphology on the nm-scale.

Cryo-TEM images of water and of the binary system of H_2O -LAS with varied surfactant concentrations, were also taken as a reference.

The cryo-TEM image of water is presented in Figure 6-29.

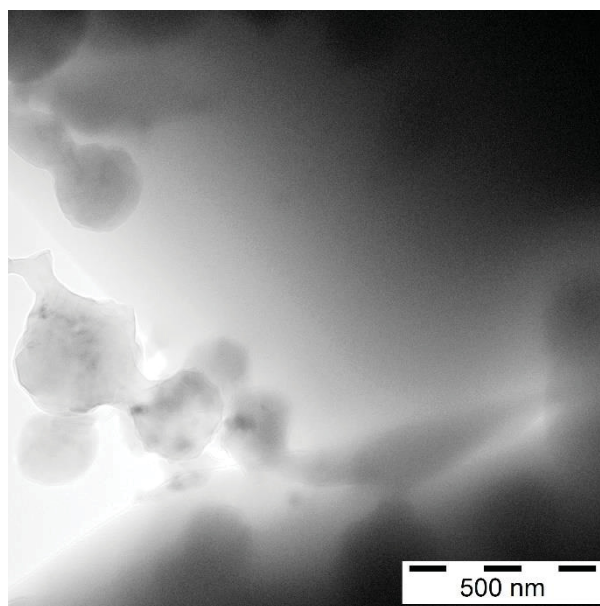


Figure 6-29 Cryo-TEM image of water.

The formation of a thin layer of water and additional ice crystals, resulting from the condensation of water from the air into particles in the liquid nitrogen, which then adhered to the copper grid during the preparation of the sample for cryo-TEM^[137], was found. The ice crystals had a typical structure of hexagonal or vitreous crystals^[137].

The cryo-TEM image of the binary system H₂O-LAS with 20.09 mM LAS, is presented in Figure 6-30.

Higher accentuated hexagonal structures, which came from the ice crystals together with deformed, spherulite-like structures with a diameter between 70 and 180 nm, were found. The diameter of these structures was determined with the “*iTEM*” imaging software for electron microscopy. The values obtained meant that the appearance of micelles could be excluded, as a diameter of 1 nm was determined with DLS measurements (Chapter 6.2.2.1, Table 6-7).

This suggests that the surfactant molecules could influence the crystallization of water, which could be shown by deformed spherulite-like structures, instead of hexagonal or vitreous crystals.

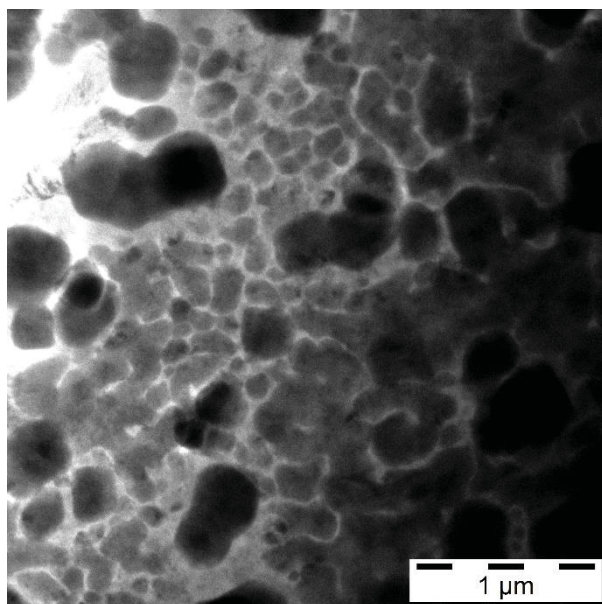


Figure 6-30 Cryo-TEM image of the binary system H₂O-LAS with a surfactant concentration of 20.09 mM.

The cryo-TEM image of the LAS-in-water system with a surfactant concentration of 28.70 mM, is presented in Figure 6-31.

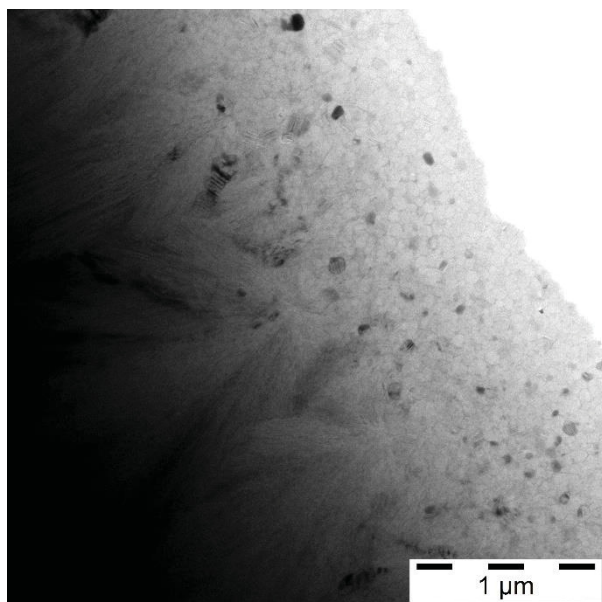


Figure 6-31 Cryo-TEM image of the binary system H₂O-LAS with a surfactant concentration of 28.70 mM.

In the presence of 28.70 mM LAS, deformed spherulite-like structures were formed with a smaller diameter, between 30 and 80 nm, than those formed in the presence of 20.09 mM LAS (Figure 6-30). The image looked like a foam structure made up of crystals.

The cryo-TEM images of DBC in a mixture with 0.29 mM, are shown in Figure 6-32.

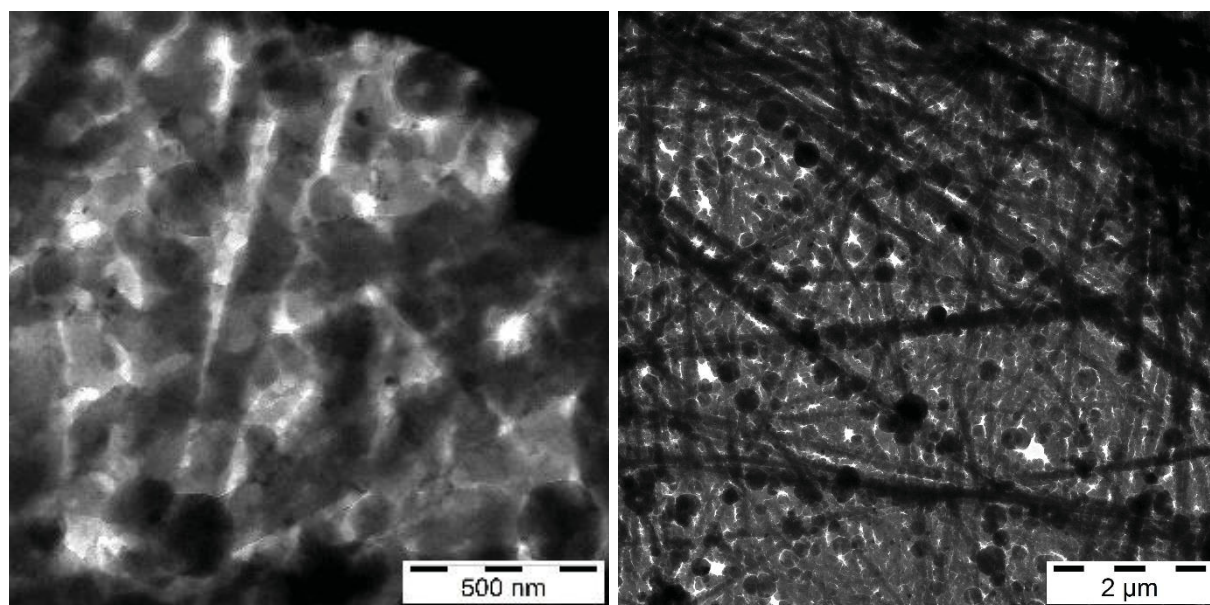


Figure 6-32 Cryo-TEM images of the ternary system H₂O-LAS-DBC with a surfactant concentration of 0.29 mM and a gellant concentration of 6.69 mM. The sample was at first allowed to cool from 363 to 298 K. After standing at 298 K for 5 minutes, the sample was prepared for cryo-TEM.

Fiber-like aggregates of spherulites and individual spherulites, which presumably grow longitudinally, were found. It could be confirmed that the spherulites were not ice crystals, as the shape of these structures appeared to be rounder than the spherulites visualized without the addition of DBC (Figure 6-30 and Figure 6-31).

The thickness of the fiber-like aggregates, which were entangled and randomly oriented, was found to be between 70 and 240 nm. The gel network structure in a mixture with 0.29 mM, looked very similar to that of DBC in the absence of LAS (Chapter 6.1.2.2, Figure 6-15) and the thickness of the visualized structures was in accordance with that of the DBC-in-water system, which were found to be between 80 and 230 nm.

When comparing the cryo-TEM image with the optical microscopy image of DBC in the presence of 0.29 mM LAS (Chapter 6.2.2.2, Figure 6-27), the apparent fiber thickness, between 1 and 2 μm , visualized by optical microscopy could presumably result from bundles of fiber-like aggregates. The thickness of the fiber-like aggregates determined from the cryo-TEM image, was between 70 and 240 nm. The data indicates that bundles of fiber-like aggregates could have been visualized by using optical microscopy.

The cryo-TEM images of DBC in a mixture with 20.09 mM, taken after 5 and 60 minutes, are presented in Figure 6-33 and Figure 6-34.

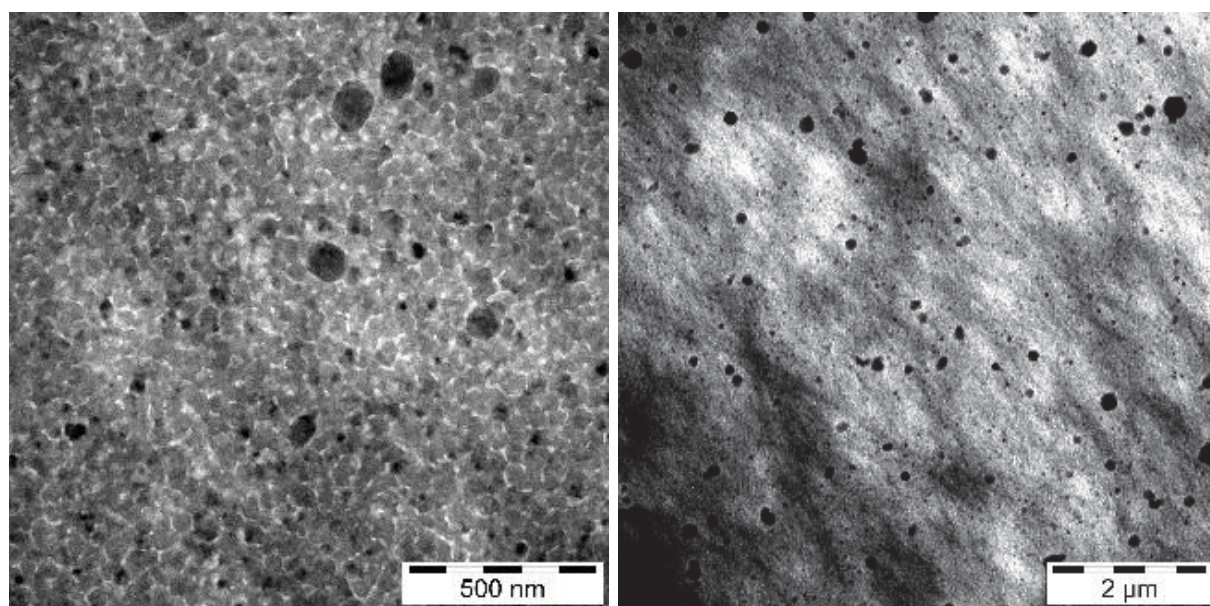


Figure 6-33 Cryo-TEM images of the ternary system H_2O -LAS-DBC with a surfactant concentration of 20.09 mM and a gellant concentration of 6.69 mM. The sample was at first allowed to cool from 363 to 298 K. After standing at 298 K for 5 minutes, the sample was prepared for cryo-TEM.

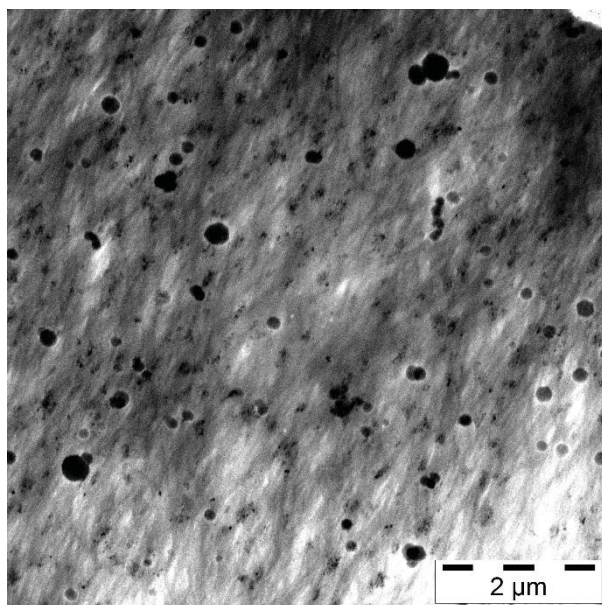


Figure 6-34 Cryo-TEM image of the ternary system H₂O-LAS-DBC with a surfactant concentration of 20.09 mM and a gellant concentration of 6.69 mM. The sample was at first allowed to cool from 363 to 298 K. After standing at 298 K for 60 minutes, the sample was prepared for cryo-TEM.

The images were taken after 5 minutes to show the structures during the induction stage and, after 60 minutes, to ensure that the formation of a gel network had been completed during the quasi-equilibrium stage.

Spherulites could be visualized after 5 minutes, which had become fiber-like structures when the image was taken after 60 minutes. However, it was not clear whether solid fibers or fiber-like aggregates had been formed. The thickness of these structures was found to be of up to 100 nm.

Deformed spherulite-like structures with a diameter between 70 and 180 nm, were found when DBC was not added. It was assumed that surfactant molecules could influence the crystallization of water, which would be shown by deformed spherulite-like structures (Figure 6-30).

It could be confirmed that the spherulites visualized in the mixture with DBC were not ice crystals, as the shape of these structures seemed to be rounder than the spherulites visualized in the absence of DBC (Figure 6-30).

The cryo-TEM images of the ternary system H₂O-LAS-DBC with 28.70 mM LAS and 6.69 mM DBC, taken after 5 and 60 minutes, are presented in Figure 6-35.

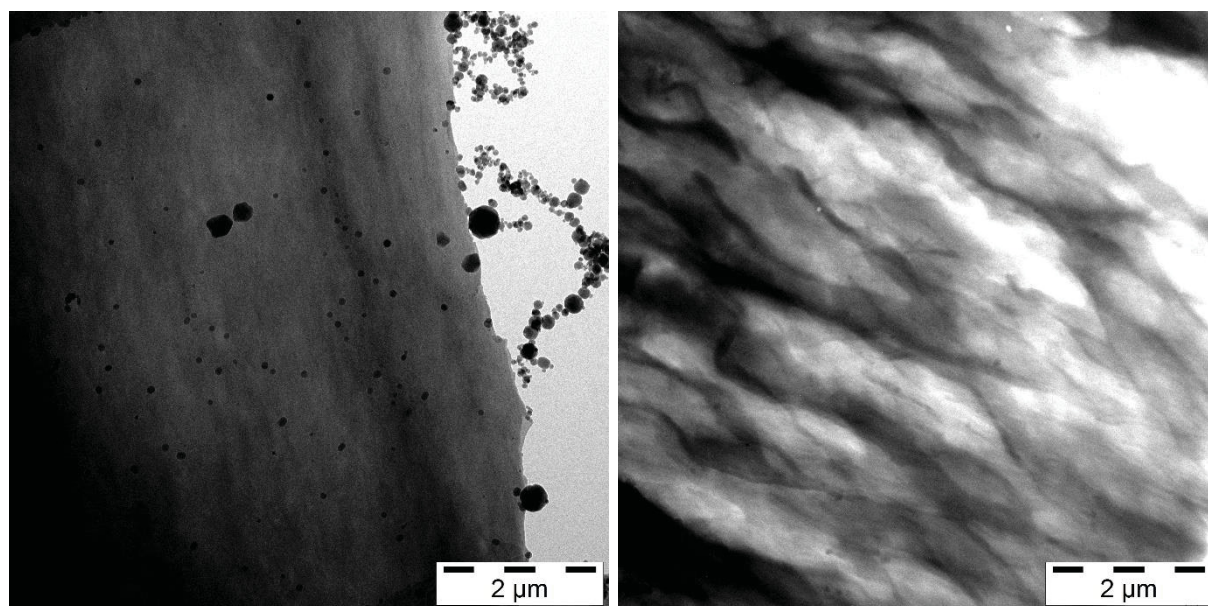


Figure 6-35 Cryo-TEM images of the ternary system H₂O-LAS-DBC with a surfactant concentration of 28.70 mM and a gellant concentration of 6.69 mM. The sample was at first allowed to cool from 363 to 298 K. After standing at 298 K for 5 (left) and 60 minutes (right), the sample was prepared for cryo-TEM.

No spherulites could be visualized in a mixture with 28.70 mM LAS after 5 minutes, which could indicate the delay of gel network formation.

After 60 minutes, fiber-like structures with a thickness of up to 100 nm had been formed, which were closely bundled with each other. From the image, it is not clear whether solid fibers, or fiber-like aggregates, were formed.

The thicknesses of the fiber-like aggregates, or solid fibers, determined from cryo-TEM images, are summarized in Table 6-8.

Table 6-8 Thicknesses of the fiber-like aggregates, or solid fibers, determined from cryo-TEM images of the ternary system H₂O-LAS-DBC with a gellant concentration of 6.69 mM and varied surfactant concentrations.

c / mM	Thicknesses of the fiber-like aggregates, or solid fibers / nm
0.00	80 - 230
0.29	70 - 280
20.09	up to 100
28.70	up to 100

It was shown that the thickness of the fiber-like aggregates, or solid fibers, became lower with increasing surfactant concentration, so that a finer gel network was formed at higher surfactant concentrations. This could be attributed to the adsorption of surfactant molecules on the surface of the gellant aggregates, leading to a decrease in the interfacial tension between the gellant aggregates and the water phase. The decrease in the interfacial tension could enable the aggregates to have a bigger surface so that a finer gel network can be formed.

Elongated, single fiber-like aggregates of spherulites with a thickness of up to 280 nm were formed at low LAS concentrations; these changed to a bundled gel network structure of either solid fibers or fiber-like aggregates, with a thickness of up to 100 nm, at high surfactant concentrations.

6.2.2.4. Kinetics of the Sol-Gel Phase Transition

The DBC gelation process was studied in a mixture with LAS, to find out how the DBC induction, gelation, and quasi-equilibrium stages would be influenced by the presence of surfactant molecules at below and above the cmc.

The evolution of the G' values for the ternary system H₂O-LAS-DBC, with a surfactant concentration of 0.29 mM and a gellant concentration of 6.69 mM, is outlined in Figure 6-36.

The sample was cooled from 353 to 293 K, at a rate of 10 K/min. The induction stage was found to last of up to 90 s and the G' values were found to be between 3×10^{-02} and 5×10^{-01} Pa. In the gelation stage, of up to 290 s, the G' values increased sharply from 1×10^{-01} to $1 \times 10^{+02}$ Pa and plateaued during the quasi-equilibrium stage.

It is important to note that the transition from the induction to the gelation stage, is correlated to the transition from the sol to the gel phase. Accordingly, promotion or delay of gel network formation can be attributed to the induction stage of the gelation process.

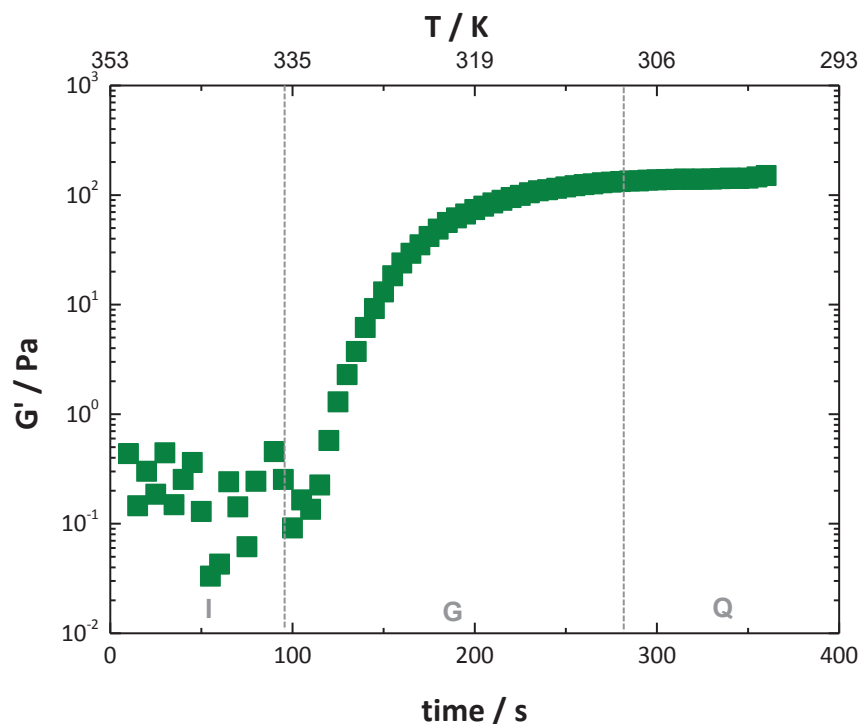


Figure 6-36 Evolution of the storage modulus G' of the ternary system H₂O-LAS-DBC with 0.29 mM LAS and 6.69 mM DBC, measured with oscillating shear rheometry, at a constant frequency of 1 Hz, a shear strain of 0.05 %, and a cooling rate of 10 K/min, using a parallel plate geometry with a gap of 800 μ m (I- Induction stage, G - Gelation stage, Q - Quasi-equilibrium stage).

For the application of the *Dickinson* equation proposed by *Huang et al.*^[13], the following parameters were taken from the temperature-sweep measurement:

Table 6-9 Parameters taken from the kinetic data of the ternary system H₂O-LAS-DBC with 0.29 mM LAS and 6.69 mM DBC for applying the *Dickinson* equation, according to equation 6-1 (t_g – gelation time at $G'(0)$, $G'(0)$ - average values of G' in the induction stage, $G'(\infty)$ - average values of G' in the quasi-equilibrium stage). The error bars give the standard deviation for the average $G'(0)$ and $G'(\infty)$ values determined for this surfactant concentration.

Parameter	Value
t_g	90 s
$G'(0)$	$1 \times 10^{-01} \text{ Pa} \pm 1 \times 10^{-01} \text{ Pa}$
$G'(\infty)$	$1 \times 10^{+02} \text{ Pa} \pm 3 \times 10^{+02} \text{ Pa}$

The fractal analysis of the kinetic data in terms of the *Dickinson* equation, is outlined in Figure 6-37.

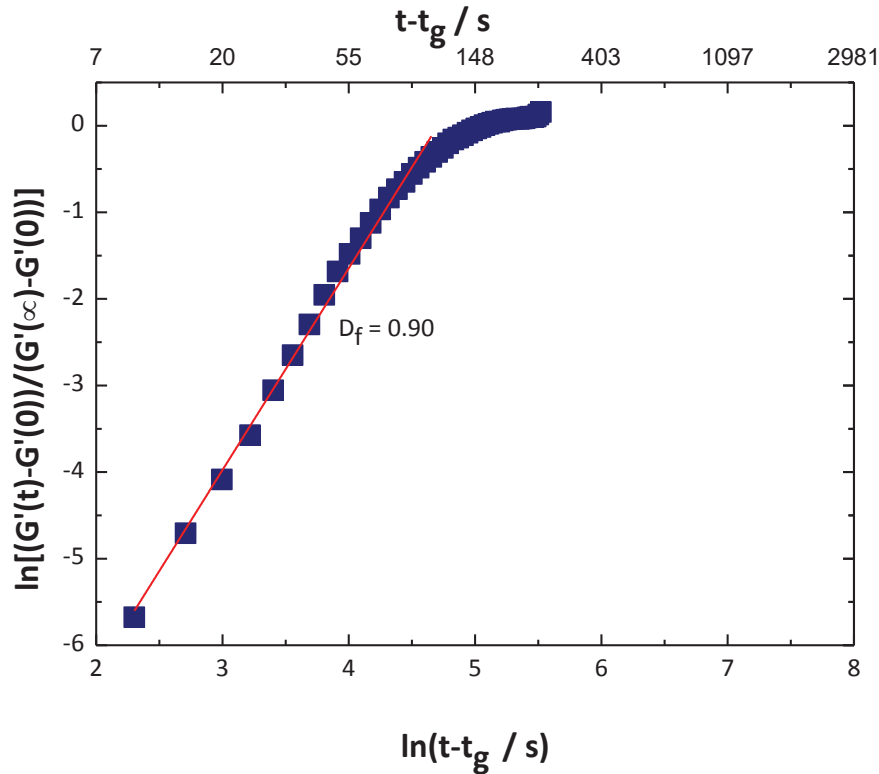


Figure 6-37 Fractal analysis of the kinetic data in terms of the *Dickinson* equation, according to equation 6-1, of the ternary system H₂O-LAS-DBC with a surfactant concentration of 0.29 mM and a gellant concentration of 6.69 mM, measured with oscillating shear rheometry at a constant frequency of 1 Hz, a shear strain of 0.05 %, and a cooling rate of 10 K/min, using a parallel plate geometry with a gap of 800 μ m.

A D_f value of 0.90 was determined which, according to *Huang et al.*^[13], indicates a linear (open) network structure mechanism.

During the study of the morphology of the gel network with optical microscopy measurements (Chapter 6.2.2.2, Figure 6-27), the formation of short, randomly oriented and curved fibers was discovered. *Huang et al.*'s^[13] assignment to a linear (open) network structure, including entanglement of fibers, did not appear to be appropriate for the optical microscopy image of the ternary system studied in this work. However, the formation of fiber-like aggregates, which seemed to be entangled with one another, was discovered in the cryo-TEM image (Chapter 6.2.2.3, Figure 6-32).

The proposed formation of a linear (open) network structure, correlates better with the cryo-TEM than with the optical microscopy measurement.

The fractal analysis of the kinetic data, in terms of the *Dickinson* equation proposed by *Huang et al.*^[13], for the ternary system H₂O-LAS-DBC with 6.69 mM DBC and varied surfactant concentrations, is summarized in Table 6-10 for a cooling rate of 10 K/min.

Table 6-10 Rheological data applied from temperature-sweep measurements of the ternary system H₂O-LAS-DBC with 6.69 mM DBC and varied LAS concentrations, measured at a cooling rate of 10 K/min ($T_{\text{sol-gel}}$ - apparent sol-gel transition temperature for a cooling rate of 10 K/min, $G'(0)$ - average values of G' in the induction stage, $G'(\infty)$ - average values of G' in the quasi-equilibrium stage, t_g - gelation time at $G'(0)$ and t_{gelation} - difference of the gelation time at $G'(\infty)$ and $G'(0)$. Symbols marked with a double asterisk, **, indicate the temperature at which the gelation occurred by a long-term measurement). The error bars give the standard deviation for the average $G'(0)$ and $G'(\infty)$ values determined for each surfactant concentration.

c / mM	$T_{\text{sol-gel}}$ / K	t_g / s	$G'(0)$ / Pa	$G'(\infty)$ / Pa	D_f	t_{gelation} / s
00.00	336	90	$8 \times 10^{+00} \pm 8 \times 10^{-01}$	$5 \times 10^{+02} \pm 2 \times 10^{+02}$	0.92	108
0.14	339	70	$9 \times 10^{-02} \pm 5 \times 10^{-02}$	$2 \times 10^{+02} \pm 1 \times 10^{+02}$	0.83	200
0.29	336	90	$1 \times 10^{-01} \pm 8 \times 10^{-02}$	$1 \times 10^{+02} \pm 2 \times 10^{+02}$	0.90	200
0.86	351	5	$5 \times 10^{+00} \pm 5 \times 10^{-01}$	$1 \times 10^{+03} \pm 3 \times 10^{+02}$	0.85	108
2.30	351	5	$9 \times 10^{-01} \pm 2 \times 10^{-01}$	$7 \times 10^{+02} \pm 4 \times 10^{+02}$	1.08	221
2.87	350	5	$3 \times 10^{+00} \pm 4 \times 10^{-01}$	$4 \times 10^{+02} \pm 5 \times 10^{+01}$	1.09	245
4.02	351	5	$1 \times 10^{+00} \pm 3 \times 10^{-01}$	$8 \times 10^{+02} \pm 2 \times 10^{+02}$	0.66	235
6.03	351	5	$2 \times 10^{+00} \pm 5 \times 10^{-02}$	$5 \times 10^{+02} \pm 3 \times 10^{+02}$	0.70	260
7.17	331	120	$3 \times 10^{-02} \pm 1 \times 10^{-02}$	$6 \times 10^{+02} \pm 1 \times 10^{+02}$	0.81	265
14.35	293**	-	$2 \times 10^{+00} \pm 1 \times 10^{+00}$	$2 \times 10^{+00} \pm 1 \times 10^{+00}$	-	-
20.09	293**	-	$5 \times 10^{-01} \pm 4 \times 10^{-01}$	$5 \times 10^{-01} \pm 1 \times 10^{-01}$	-	-
28.70	293**	-	$6 \times 10^{-01} \pm 5 \times 10^{-01}$	$6 \times 10^{-01} \pm 1 \times 10^{-01}$	-	-

As previously mentioned, the addition of LAS to the 6.69 mM H₂O-DBC binary system promoted gel network formation of up to a surfactant concentration of 6.03 mM, as the transition from the sol to the gel phase, $T_{\text{sol-gel}}$, was observed at higher values than in the absence of LAS (Chapter 6.2.2.1, Figure 6-23). In addition, lower t_g values were found in the mixture with LAS than in the DBC-in-water system, indicating the promotion of gel network formation. Below 6.03 mM LAS, the apparent $T_{\text{sol-gel}}$ values for a cooling rate of 10 K/min, increased from 336 to 351 K and the t_g values decreased from 90 to 5 s. Above 7.17 mM LAS, the DBC gelation was delayed, as shown by the $T_{\text{sol-gel}}$ values which were lower than for the DBC-in-water system.

It is important to note that, as mentioned in Chapter 3.1, the term “*promotion*” was also used in the literature (Chapter 3.1), whereby it was attributed to the completed gel network structure, i.e. to the quasi-equilibrium stage. In this work, the term is used to describe the behavior during the induction stage.

$G'(0)$ values of between 3×10^{-02} and $8 \times 10^{+00}$ Pa were found and the $G'(\infty)$ values ranged from $1 \times 10^{+02}$ to $1 \times 10^{+03}$ Pa, for a surfactant concentration of up to 7.17 mM. More scattering of the $G'(0)$, rather than the $G'(\infty)$ values was found, which could presumably be attributed to the randomly driven aggregation of the gellant monomers within the induction stage, leading to different $G'(0)$ values.

No gelation occurred for concentration above 14.35 mM LAS within the given timeframe. The G' values were independent of the temperature and ranged from 5×10^{-01} to $2 \times 10^{+00}$ Pa.

No clear trend in the t_{gelation} values for the addition of LAS of up to 7.17 mM into the DBC-in-water system, could be found. The values found were between 108 and 265 s. Fitting the kinetic data, in terms of the *Dickinson* equation, provided D_f values of up to 1.1, which will be later discussed.

The kinetics of gel network formation of DBC-in-LAS systems were also studied by cooling the sample at a rate of 5 K/min, as presented in Table 6-11.

Table 6-11 Rheological data applied from temperature-sweep measurements of the ternary system H₂O-LAS-DBC with 6.69 mM DBC and varied LAS concentrations, measured at a cooling rate of 5 K/min ($T_{\text{sol-gel}}$ - apparent sol-gel transition temperature for a cooling rate of 5 K/min, $G'(0)$ - average values of G' in the induction stage, $G'(\infty)$ - average values of G' in the quasi-equilibrium stage, t_g - gelation time at $G'(0)$ and t_{gelation} - difference of the gelation time at $G'(\infty)$ and $G'(0)$. Symbols marked with a double asterisk, **, indicate the temperature at which the gelation occurred by a long-term measurement). The error bars give the standard deviation for the average $G'(0)$ and $G'(\infty)$ values determined for each surfactant concentration.

c / mM	$T_{\text{sol-gel}}$ / K	t_g / s	$G'(0)$ / Pa	$G'(\infty)$ / Pa	D_f	t_{gelation} / s
00.00	346	85	$1 \times 10^{+00} \pm 2 \times 10^{-01}$	$3 \times 10^{+03} \pm 3 \times 10^{+02}$	0.79	288
0.14	> 353	-	$8 \times 10^{+01} \pm 3 \times 10^{+01}$	$4 \times 10^{+03} \pm 1 \times 10^{+03}$	-	-
0.86	> 353	-	$4 \times 10^{+01} \pm 1 \times 10^{+01}$	$5 \times 10^{+02} \pm 1 \times 10^{+02}$	-	-
1.72	> 353	-	$1 \times 10^{+02} \pm 8 \times 10^{+01}$	$5 \times 10^{+02} \pm 1 \times 10^{+02}$	-	-
2.30	351	5	$1 \times 10^{-01} \pm 8 \times 10^{-02}$	$1 \times 10^{+03} \pm 5 \times 10^{+02}$	0.75	221
7.17	339	170	$1 \times 10^{-01} \pm 6 \times 10^{-02}$	$1 \times 10^{+03} \pm 4 \times 10^{+02}$	0.86	324
8.61	330	265	$2 \times 10^{-01} \pm 1 \times 10^{-01}$	$8 \times 10^{+02} \pm 2 \times 10^{+02}$	0.98	288
10.04	328	285	$3 \times 10^{-01} \pm 1 \times 10^{-01}$	$7 \times 10^{+02} \pm 3 \times 10^{+02}$	0.82	410
11.48	326	315	$7 \times 10^{-02} \pm 5 \times 10^{-02}$	$4 \times 10^{+02} \pm 2 \times 10^{+02}$	1.06	410
20.09	293**	-	$1 \times 10^{-02} \pm 3 \times 10^{-01}$	$1 \times 10^{-02} \pm 3 \times 10^{-02}$	-	-
28.70	293**	-	$8 \times 10^{-01} \pm 8 \times 10^{-01}$	$8 \times 10^{-01} \pm 5 \times 10^{-01}$	-	-

The addition of LAS to the 6.69 mM H₂O-DBC binary system, promoted the formation of a gel network for surfactant concentrations of up to 2.30 mM, as shown by the fact that the $T_{\text{sol-gel}}$ values were higher and the t_g values lower, than those found in the DBC-in-water system.

It is important to note that for a LAS concentration of up to 1.72 mM, the transition from the sol to the gel phase could not be determined by using rheology because the rheometer's measuring limit was 353 K.

The $T_{\text{sol-gel}}$ value was greater than 353 K; at this temperature, either the gelation process was in the last part of the gelation stage, or the quasi-equilibrium stage had been reached, which was shown by the small difference in the $G'(0)$ and $G'(\infty)$ values. The G' values increased by one order of magnitude and the three stages of the gelation process could not be monitored.

In mixtures with LAS, ranging from 2.30 to 11.48 mM, the gelation process could be monitored during the temperature-sweep measurement, which could also be obtained from the difference in the $G'(0)$ and $G'(\infty)$ values of up to four orders of magnitudes. The $G'(0)$ values identified were between 7×10^{-02} and 3×10^{-01} Pa, and the $G'(\infty)$ values were between $4 \times 10^{+02}$ and $1 \times 10^{+03}$ Pa.

For concentrations above 7.17 mM LAS, the gelation time, t_g , increased from 170 to 315 s with increasing surfactant concentration. It can be concluded that the DBC gel network formation was delayed, as higher t_g values were found in mixtures with LAS surfactant concentrations above 7.17 mM, than in the DBC-in-water system.

No clear trend for the duration of the gelation process, t_{gelation} , could be found. The values ranged between 216 and 410 s.

D_f values of up to 1.1 were found by applying the *Dickinson* equation, according to equation 6-1, which will be discussed later.

For the ternary system of H₂O-LAS-DBC with 28.70 mM LAS and 6.69 mM DBC, no gelation occurred within the given timeframe, during the temperature-sweep measurement, as illustrated in Figure 6-38.

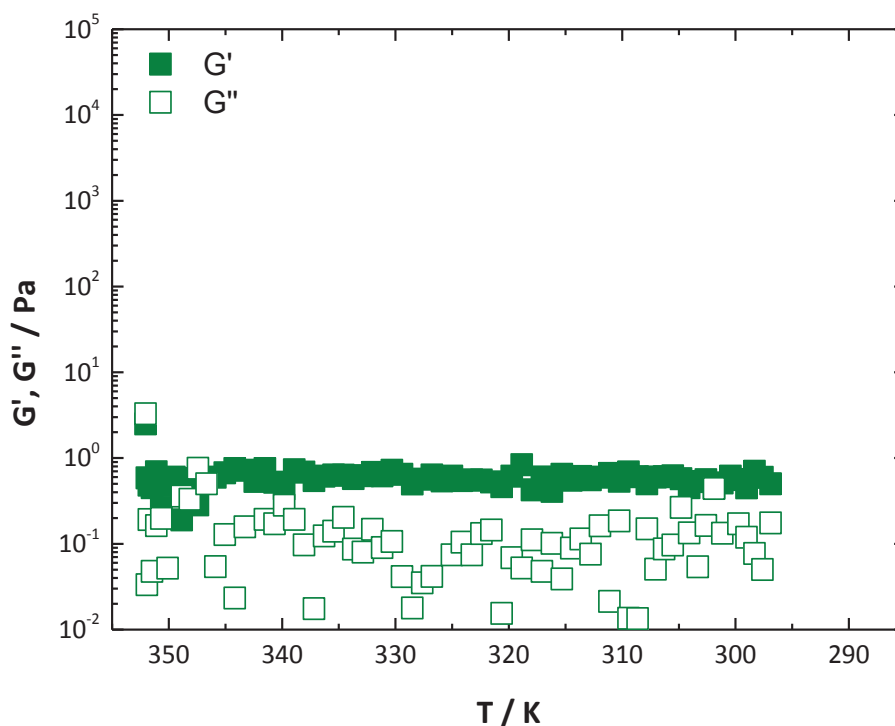


Figure 6-38 Storage modulus G' and loss modulus G'' vs. temperature of the ternary system H₂O-LAS-DBC with a surfactant concentration of 28.70 mM and a gellant concentration of 6.69 mM, measured with oscillating shear rheometry, at a constant frequency of 1 Hz, a shear strain of 0.05 %, and a cooling rate of 10 K/min, using a parallel plate geometry with a gap of 800 μ m.

The G' values were independent of the temperature and were determined at 8×10^{-1} Pa. In order to study the gelation process in the induction, gelation, and quasi-equilibrium stages, the evolution of G' values at 293 K, was studied.

The combination of the temperature-sweep and time-sweep measurements, and the application of the *Dickinson* equation, according to equation 6-1, to the ternary system H₂O-LAS-DBC with 28.70 mM LAS and 6.69 mM DBC, are outlined in Figure 6-39.

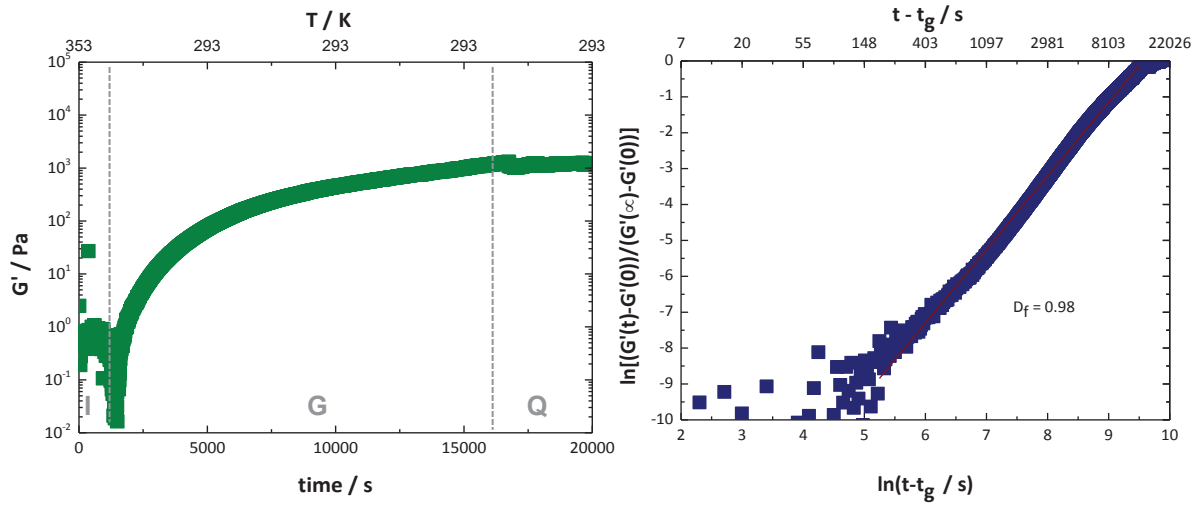


Figure 6-39 Storage modulus G' vs. time (left) and fractal analysis of the kinetic data in terms of the *Dickinson* equation, according to equation 6-1 (right), of the ternary system H₂O-LAS-DBC with 28.70 mM LAS and 6.69 mM DBC, measured with oscillating shear rheometry, at a constant strain of 0.05 %, frequency of 1 Hz, and a cooling rate of 10 K/min, using a parallel plate geometry with a gap of 800 μ m (I - Induction stage, G - Gelation stage, Q - Quasi-equilibrium stage).

G' values of between 2×10^{-01} and $1 \times 10^{+00}$ Pa were found during the induction stage, before reaching the gelation time, t_g , of 1405 s. During the transition from the induction to the gelation stage at 1405 s, the G' values decreased to 1×10^{-02} Pa and then increased sharply to $1 \times 10^{+03}$ Pa during the gelation stage, until the quasi-equilibrium stage was reached at 15661 s.

A D_f value of 0.98 was determined by applying the *Dickinson* equation according to equation 6-1, which correlates with the formation of a linear (open) network structure.

The fractal analysis of the kinetic data, in terms of the *Dickinson* equation of the ternary system H₂O-LAS-DBC for LAS concentrations above 20.09 mM and a gellant concentration of 6.69 mM, is summarized in Table 6-12.

Table 6-12 Fractal analysis of the kinetic data of the ternary system H₂O-LAS-DBC with 6.69 mM DBC and varied LAS concentrations, acquired by time-sweep measurements, in terms of the *Dickinson* equation, according to equation 6-1, at 293 K. The prepared samples were transferred into the rheometer at 353 K and were cooled to 293 K at a rate of 10 K/min (T - measuring temperature, G'(0) - average values of G' in the induction stage, G'(∞) - average values of G' in the quasi-equilibrium stage, t_g - gelation time at G'(0) and t_{gelation} - difference of the gelation time at G'(∞) and G'(0)). The error bars give the standard deviation for the average G'(0) and G'(∞) values determined for each surfactant concentration.

c / mM	T _{sol-gel} / K	t _g / s	G'(0) / Pa	G'(∞) / Pa	D _f	t _{gelation} / s
20.09	293	505	8 x 10 ⁻⁰³ ± 4 x 10 ⁻⁰²	3 x 10 ⁺⁰² ± 1 x 10 ⁺⁰²	0.84	7452
28.70	293	1405	1 x 10 ⁻⁰² ± 3 x 10 ⁻⁰²	1 x 10 ⁺⁰³ ± 3 x 10 ⁺⁰²	0.98	14256

D_f values of up to 1.0 were found. The gelation time, t_g, increased with increasing surfactant concentrations, from 505 to 1405 s, and was greater than that of the DBC-in-water system (Table 6-10). According to this, the DBC gel network formation was delayed. The G'(0) values found were between 8 x 10⁻⁰³ and 1 x 10⁻⁰² Pa, taken from the minimum of G' value during the transition from the induction to the gelation stage, and the G'(∞) values ranged between 3 x 10⁺⁰² and 1 x 10⁺⁰³ Pa.

By comparing the t_g values with those of the ternary system H₂O-LAS-DBC with surfactant concentrations of above 7.17 mM (Table 6-10), it was found that the DBC gel network formation was further delayed by an increase in the LAS concentration, as the t_g values were higher than those of the DBC-in-water system. Within the observed concentration range of between 7.17 and 28.70 mM, the delay of gel network formation was more pronounced at high surfactant concentrations than at low surfactant concentrations.

As previously mentioned, the $G'(0)$ values were taken from the minimum of G' value during the transition from the induction to the gelation stage. The appearance of a minimum is shown in Figure 6-40.

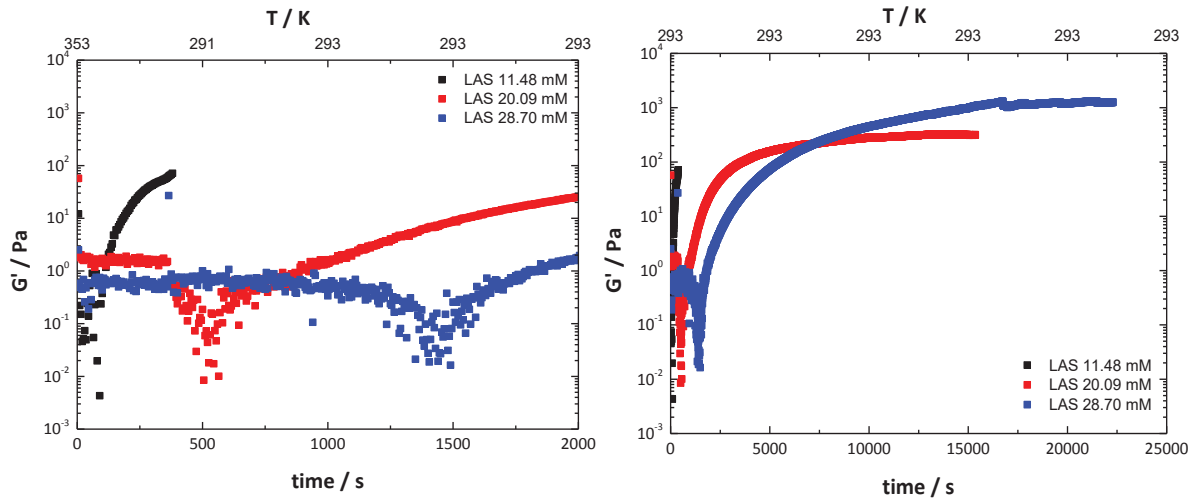


Figure 6-40 Storage modulus G' vs. time (right) and the extract from the diagram (left) of the ternary system H_2O -LAS-DBC with 6.69 mM DBC and varied LAS concentrations, for the illustration of the minimum during the gelation process. The data were taken from temperature-sweep measurement for a surfactant concentration of 11.48 mM LAS, and from the combination of temperature-sweep and time-sweep measurements, for LAS concentrations above 20.09 mM. The samples were cooled from 353 to 293 K at a rate of 10 K/min (below the minimum of G' - induction stage, above the minimum of G' - gelation stage).

The minimum of G' value was found at the gelation time, t_g , at which the transition from the induction to the gelation stage occurred. The delay in gel network formation with increasing of the surfactant concentrations, is clearly shown, as the minimum was found at higher t_g values.

The possibility has been discussed that the delay could be due to the gellant aggregates being hindered sterically, due to the adsorption of surfactant molecules on their surface so that the molecules were unable to interact directly with one another. This barrier must be overcome for the aggregates to nucleate.

The appearance of a minimum might be due to following: The concentration of gellant monomers is reduced during the aggregation process, which could lead to a momentary minimum of G' value. As a result of the generation of large aggregates with high G' values, the G' value increases rapidly, and a minimum appears during the gelation process.

The appearance of a minimum during the gelation process could also be explained by a kinetic model, according to equation:



with the gellant monomers A, the gellant aggregates with elasticity B and gellant aggregates with more elasticity C.

Under the assumption that the equilibrium process between A and B is slower than that between B and C, the appearance of minimum of G' value could be because B is dissipated by C until it is loaded from A. Consequently, the G' values decrease until a quasi-stationary state is reached. Then, B is constant and the G' values increase with the formation of larger aggregates.

To gain a deeper understanding of the influence of surfactant molecules on the kinetics of DBC, the gelation stage of the gelation process was investigated. To maintain the same conditions, the gelation time, t_g , was taken as 5 s for each LAS concentration studied.

The log-linear and linear-linear plots of G' against time, for the ternary system H_2O -LAS-DBC with varied LAS concentrations and 6.69 mM DBC, are shown in Figure 6-41 and Figure 6-42.

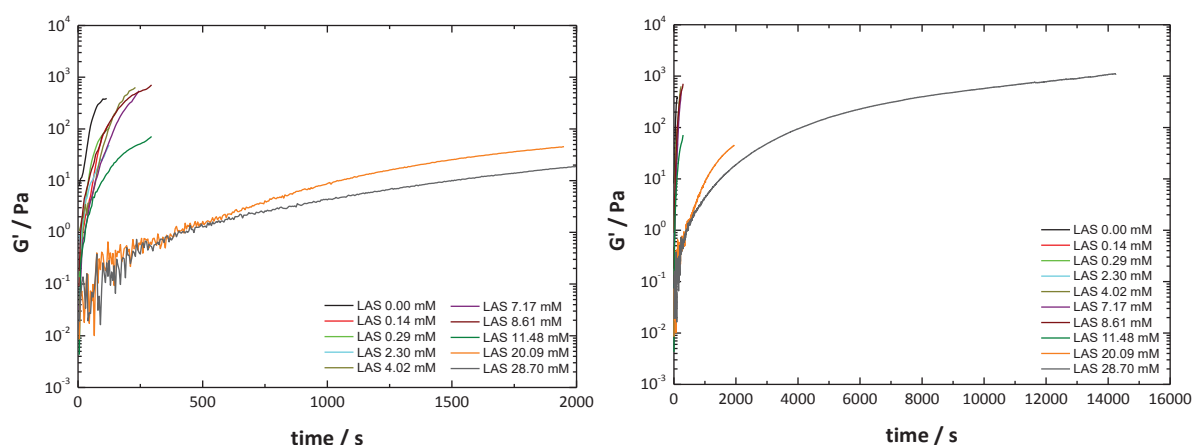


Figure 6-41 Log-linear plot of the storage modulus G' vs. time (right) and the extract from the diagram (left) during the gelation stage of the ternary system H_2O -LAS-DBC with a gellant concentration of 6.69 mM and varied surfactant concentrations, measured with oscillating shear rheometry, at a constant strain of 0.05 %, frequency of 1 Hz, and a cooling rate of 10 K/min, using a parallel plate geometry, with a gap of 800 μm .

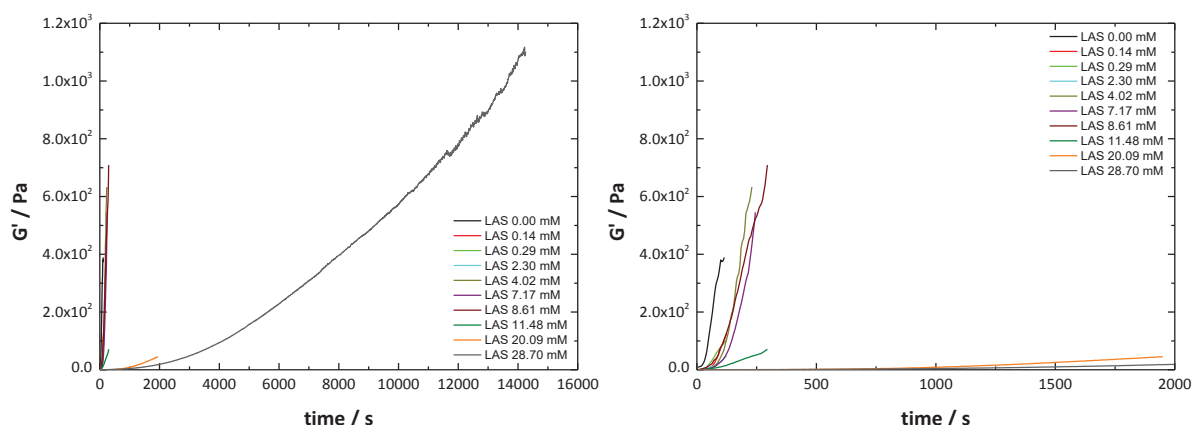


Figure 6-42 Linear-linear plot of the storage modulus G' vs. time (right) and the extract from the diagram (left) during the gelation stage of the ternary system H_2O -LAS-DBC with a gellant concentration of 6.69 mM and varied surfactant concentrations, measured with oscillating shear rheometry, at a constant strain of 0.05 %, frequency of 1 Hz, and a cooling rate of 10 K/min, using a parallel plate geometry, with a gap of 800 μm .

The samples were cooled at a rate of 10 K/min in order to study the influence of LAS molecules on the kinetics of DBC gel network formation, both below and above the cmc. As was shown by the temperature-sweep measurements, the induction stage was influenced by surfactant molecules. When cooling the sample at a rate of 5 K/min, the DBC gel network formation was promoted for concentrations of up to 2.30 mM LAS, and delayed for those above 7.17 mM LAS (Chapter 6.2.2.1, Figure 6-24).

Due to fast gelation below the cmc, rheology could not be used to study the gelation process with its three stages, the induction, gelation, and quasi-equilibrium stages.

However, due to the superposition of the temperature drop and the kinetic behavior by fast cooling (Chapter 6.1.1, Figure 6-13), the complete gelation process could be investigated by using rheology, even at low surfactant concentrations.

It was found that the DBC gelation rate was strongly influenced in mixtures with LAS. The increase in the surfactant concentration was attributed to slower gelation rates. Even the addition of small amounts of LAS, caused the G' values to increase more slowly than in the absence of LAS.

Without the addition of LAS, the G' values increased from $8 \times 10^{+00}$ to $5 \times 10^{+02}$ Pa, within 108 s. Below the cmc, the values for mixtures with 0.14 mM LAS, increased from 9×10^{-02} to $2 \times 10^{+02}$ Pa within 200 s. Above the cmc, in the presence of 28.70 mM LAS, it was possible to observe an increase of the G' values from 1×10^{-02} to $1 \times 10^{+03}$ Pa within 14256 s.

The slower gelation rates were more pronounced at concentrations above 20.09 mM LAS, than at lower concentrations.

To analyze the effect of LAS on the DBC gelation rate, the time at which a G' value of $5 \times 10^{+01}$ Pa was achieved by DBC in the absence and presence of LAS, $t-t_g$, was determined from Figure 6-41. This value is the lowest G' value that was obtained for all the surfactant concentrations studied.

This analysis was also performed to study the effect of surfactant molecules on the gelation rate of DBC, by cooling the sample at a rate of 5 K/min. At this cooling rate, the lowest G' value observed for all the surfactant concentrations, was $3 \times 10^{+02}$ Pa.

The $t-t_g$ values for different cooling rates against the LAS concentrations, are outlined in Table 6-13.

Table 6-13 Rheological data applied from the analysis of the kinetic data of the ternary system H₂O-LAS-DBC with a gellant concentration of 6.69 mM and varied surfactant concentrations, measured at cooling rates of 5 and 10 K/min. For the determination of the $t-t_g$ values, the time was taken at which the same G' value was obtained for all surfactant concentrations (t_g - gelation time, fixed G' value for a cooling rate of 5 K/min – $3 \times 10^{+02}$ Pa and fixed G' value for a cooling rate of 10 K/min – $5 \times 10^{+01}$ Pa).

c / mM	t-t _g for a cooling rate of ... / s	
	5 K/min	10 K/min
00.00	110	30
0.14	-	85
0.29	-	70
7.17	140	115
11.48	1610	240
20.09	4255	1950
28.70	17265	3045

When studying the gelation stage of the gelation process by cooling the sample at a rate of 5 K/min, the G' value of $3 \times 10^{+02}$ Pa was obtained after 110 s, in the absence of LAS. When LAS was added to the DBC-in-water system at a surfactant concentration of above 7.17 mM, this G' value was obtained later.

The t_{-t_g} values increased from 110 to 17265 s. For a LAS concentration above 11.48 mM, the difference in the t_{-t_g} values, compared with the DBC-in-water system, became more pronounced than for surfactant concentrations below this level.

The slower DBC gelation rate with increasing surfactant concentration, was also found by cooling the sample at a rate of 10 K/min. The difference in the t_{-t_g} values determined in the absence and presence of LAS, becomes higher above 7.17 mM LAS than below this concentration. The DBC-in-water system's t_{-t_g} value was observed to be 30 s, and of up to 85 s in mixtures with LAS between 0.14 and 0.29 mM and of up to 3045 s for concentrations above 7.17 mM.

By comparing the t_{-t_g} values obtained for both cooling rates, it can be concluded that the decrease in the gelation rate in the presence of LAS, was more pronounced at high surfactant concentrations than at low surfactant concentrations. In addition, the DBC gelation rate in mixtures with LAS, was reduced more by cooling at a rate of 5 than at 10 K/min.

The data indicates that the slower gelation rate of DBC with the addition of surfactant molecules, could be attributable to strong DBC-LAS interactions, such as complex formation or surfactant molecules being adsorbed on the surface of the gellant aggregates.

By using cryo-TEM measurements, it was found that the morphology of DBC changed from a rough (fiber thickness of up to 280 nm) to a fine network structure (fiber thickness of up to 100 nm).

This could be related to the adsorption of surfactant molecules on the surface of the gellant aggregates, leading to a decrease in the interfacial tension between the gellant aggregates and the water phase, so that a finer gel network could be formed.

This hypothesis is schematically illustrated in Figure 6-43.

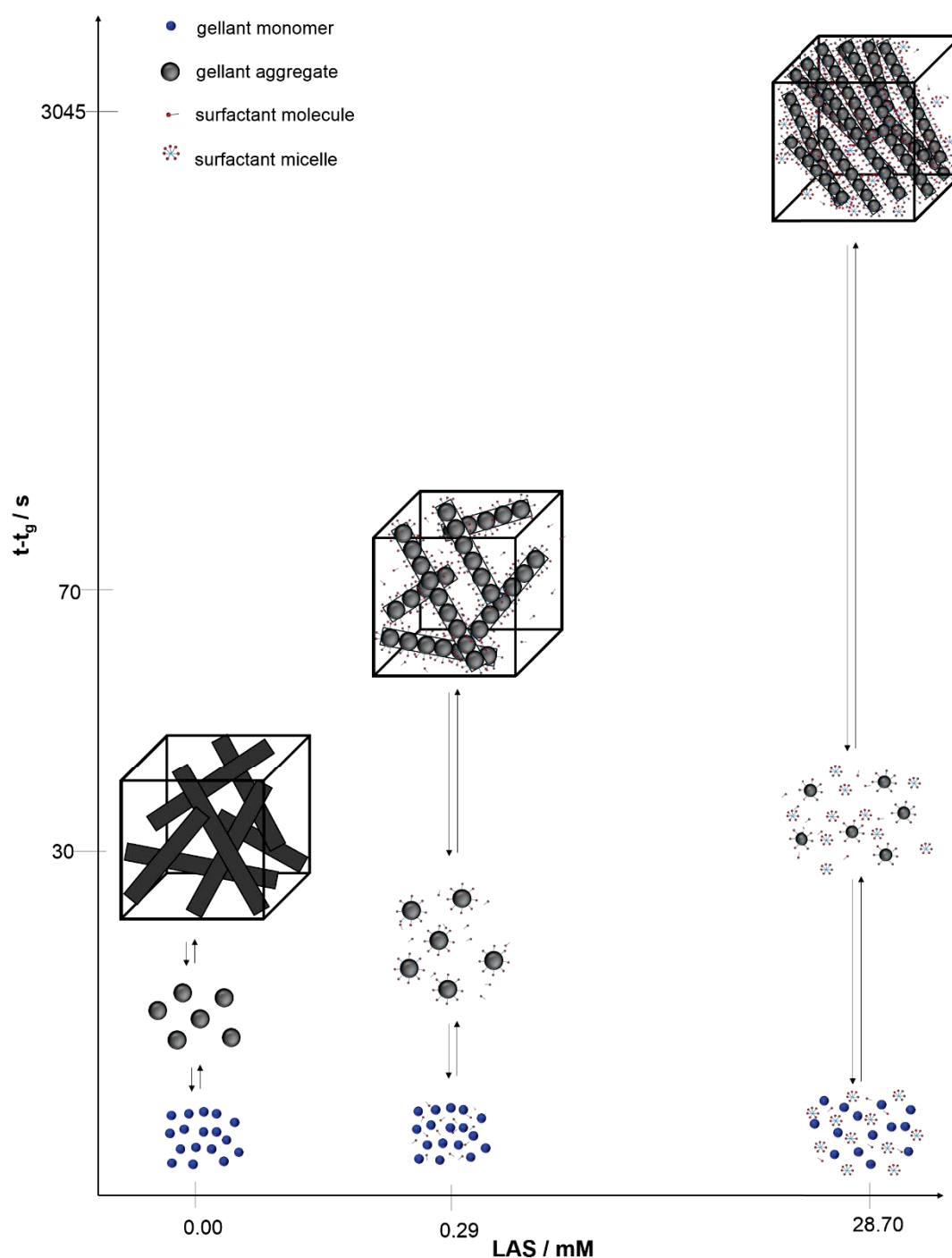


Figure 6-43 Schematic illustration of the gel network formation of the ternary system H_2O - LAS - DBC with 6.69 mM DBC and varied LAS concentration. The $t-t_g$ values were taken from the analysis of the kinetic data, measured at a cooling rate of 10 K/min. For the determination of the $t-t_g$ values, the time was taken at which the same G' value was obtained for all surfactant concentrations (t_g - gelation time, G' value for a cooling rate of 10 K/min – $5 \times 10^{+01}$ Pa). The gelation rate is decreased with the increase of LAS concentration which could be related to the adsorption of surfactant molecules on the surface of the gellant aggregates, leading to a decrease in the interfacial tension between the gellant aggregates and the water phase, so that a finer gel network could be formed.

When comparing the results obtained with the findings from applying the *Dickinson* equation, it was found that the influence of surfactant molecules on the gelation stage could be understood better by determining the $t-t_g$ values for a fixed G' value, than by using fractal analysis of the kinetic data in terms of the *Dickinson* equation, as similar D_f values were found in the presence of LAS, which would mean that the DBC gelation rate was not influenced by surfactant molecules.

However, this is due to the standardized *Dickinson* equation by the ratio of $G'(t)-G'(0)$ and $G'(\infty)-G'(0)$. To use the *Dickinson* equation to monitor the real influence of LAS on the gelation stage of the gelation process, the $G'(0)$ and $G'(\infty)$ values should not deviate from each other if the LAS concentration increases. Then, the real effect of surfactant molecules on the gelation stage, with different D_f values, could be studied. However, the $G'(0)$ and $G'(\infty)$ values showed high scattering with an increase in the surfactant concentration, leading to similar D_f values due to the standardized *Dickinson* equation.

The $G'(0)$ and $G'(\infty)$ values for the ternary system H_2O -LAS-DBC with 6.69 mM and varied surfactant concentrations, are shown in Figure 6-44 and Figure 6-45.

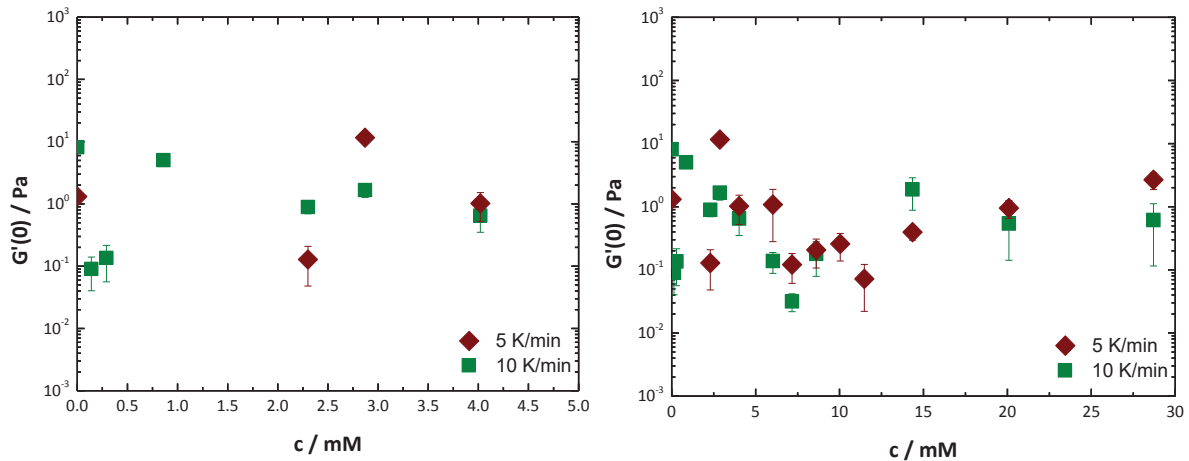


Figure 6-44 Storage modulus in the induction stage $G'(0)$ (right) and the extract from the diagram at lower surfactant concentrations (left) of the ternary system H_2O -LAS-DBC with a gellant concentration of 6.69 mM, as a function of LAS concentration, measured at 293 K with oscillating shear rheometry at a frequency of 1 Hz, and a strain of 0.05 %, using a parallel plate geometry with a gap of 800 μm . The prepared sample was transferred into the rheometer at 353 K and was cooled to 293 K at rates of 5 and 10 K/min. The error bars give the standard deviation for the average $G'(0)$ values determined for each surfactant concentration.

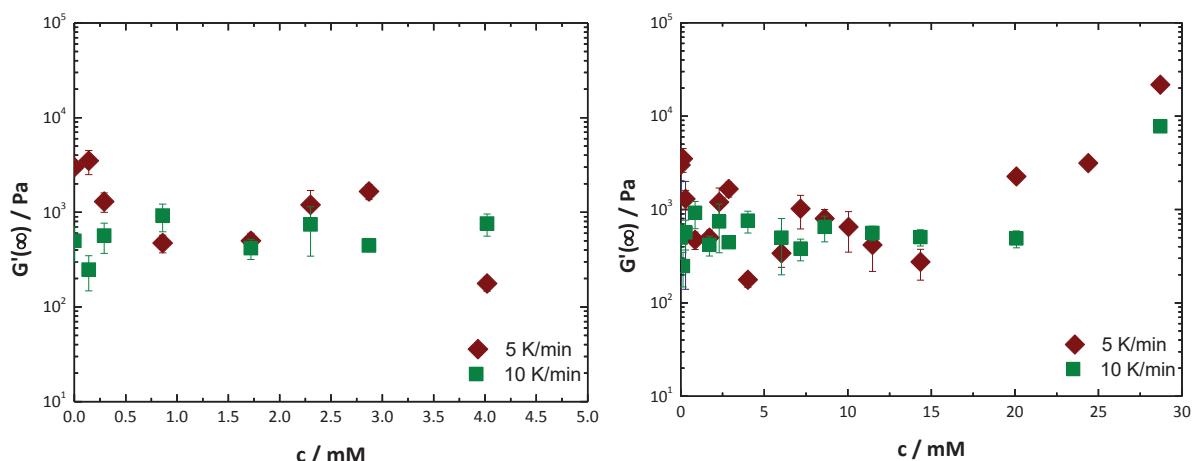


Figure 6-45 Storage modulus in the quasi-equilibrium stage $G'(\infty)$ (right) and the extract from the diagram at lower surfactant concentrations (left) of the ternary system H₂O-LAS-DBC with a gellant concentration of 6.69 mM, as a function of surfactant concentration, measured at 293 K with oscillating shear rheometry at a frequency of 1 Hz, and a strain of 0.05 %, using a parallel plate geometry with a gap of 800 μ m. The prepared sample was transferred into the rheometer at 353 K and was cooled to 293 K at rates of 5 and 10 K/min. The error bars give the standard deviation for the average $G'(\infty)$ values determined for each surfactant concentration.

For LAS concentrations of up to 28.70 mM, the $G'(0)$ values ranged between 3×10^{-02} and $8 \times 10^{+00}$ Pa by cooling at a rate of 10 K/min, and between 7×10^{-02} and $1 \times 10^{+01}$ Pa by cooling at a rate of 5 K/min. No clear trend for $G'(0)$ values with an increase in the surfactant concentration, could be found. This suggests that the wide scattering of the $G'(0)$ values could be attributed to the randomly driven aggregation of gellant monomers during the induction stage, which would lead to different $G'(0)$ values.

The G' values for the quasi-equilibrium stage, $G'(\infty)$, were less scattered than the $G'(0)$ values.

When cooling the sample at the rate of 10 K/min, the $G'(\infty)$ values of between $3 \times 10^{+02}$ and $1 \times 10^{+03}$ Pa were obtained for a LAS concentration of up to 14.35 mM. When the surfactant concentration was increased, the $G'(\infty)$ values ranged between $1 \times 10^{+03}$ and $8 \times 10^{+03}$ Pa.

A similar trend was found for a lower cooling rate as for fast cooling. The $G'(\infty)$ values increased slightly at high surfactant concentrations. For LAS concentrations of up to 14.35 mM, the $G'(\infty)$ ranged between $2 \times 10^{+02}$ and $4 \times 10^{+03}$ Pa and, above this concentration, $G'(\infty)$ values of between $4 \times 10^{+03}$ and $2 \times 10^{+04}$ Pa were found.

The slight increase in the $G'(\infty)$ values at high surfactant concentrations, could indicate for the formation of a finer gel network structure (Chapter 6.1.2.4), which seems to be confirmed as the DBC's morphology changed from elongated, single fiber-like aggregates with a thickness of up to 280 nm, to a bundled gel network structure made up of either solid fibers or fiber-like aggregates with a thickness of up to 100 nm.

To summarize the key findings on the properties of the gelling agent DBC in mixtures with LAS, it was found that molecular interactions between DBC and LAS molecules presumably occurred below the critical gelation concentration, as the LAS's surface tension and cmc were lowered by the addition of small amounts of DBC.

The gelation process was studied by using rheology. It was found that the addition of surfactant molecules to the DBC-in-water system, strongly influenced the induction and gelation stages of DBC and, to a lesser extent, the quasi-equilibrium stage. The transition from the induction to the gelation stage, was promoted at low surfactant concentrations and delayed at high surfactant concentrations.

The promotion of gel network formation was demonstrated by higher $T_{\text{sol-gel}}$ values and lower t_g values than for the binary system H₂O-DBC.

It is believed that the promotion of gel network formation was due to the enhanced dispersion of DBC particles by surfactant molecules during the heating process in sample preparation. This could lead to the formation of smaller aggregates by decreasing the interfacial tension^{[38],[53],[131]} between the gellant aggregates and the water phase, which could facilitate the gellant aggregates' nucleation process.

The delay in gel network formation was demonstrated by lower $T_{\text{sol-gel}}$ values and higher t_g values than for the DBC-in-water system. The delay could be attributed to the diffusion of gellant monomers being hindered by surfactant micelles, as the existence of a densely packed micelle system was assumed from various calculations.

Furthermore, the delay in gel network formation could be attributed to the steric hindrance of gellant aggregates due to LAS molecules being adsorbed on the surface of gellant aggregates so that the molecules are unable to interact directly with one another. This barrier must be overcome for the aggregates' nucleation.

The influence of LAS on the gelation stage was clearly shown by the $t-t_g$ values for a fixed G' value, rather than applying the standardized *Dickinson* equation, which led to similar D_f values.

By determining the $t-t_g$ values for a fixed G' value, the decrease in the gelation rate from an increase of the LAS concentration, could be found. The slower gelation rate was more pronounced at high surfactant concentrations than at low concentrations, for both the cooling rates studied. It was believed, based on the cryo-TEM images, that a finer gel network structure was formed when the LAS concentration was increased, and that the formation of a fine gel network structure took longer than a rough gel network structure when the morphological transition occurs within the same system.

The formation of a fine network structure could be due to the adsorption of surfactant molecules on the surface of the gellant aggregates, leading to a decrease in the interfacial tension between the aggregates and the water phase, so that a finer gel network could be formed.

The $G'(\infty)$ values during the quasi-equilibrium stage, were found to be slightly greater at high surfactant concentrations than at low surfactant concentrations, which could be attributable to the formation of a finer gel network structure due to the addition of LAS.

From the findings, it could be concluded that when the gel network formation is promoted at low LAS concentrations, i.e. when the induction stage starts at a lower t_g value than in the DBC-in-water system, then the $G'(\infty)$ values and the gel network's morphology were not greatly influenced by an increase in LAS concentration.

In contrast, when the gel network formation is delayed at high LAS concentrations, the $G'(\infty)$ values were found to be greater than for the binary system H₂O-DBC and the gel network was made up of finer, fiber-like aggregates or solid fibers.

By including the findings from the study of the gelation stage, it was found that the lower the gelation rate, the finer the resulting gel network structure, as the thickness of the fiber-like aggregates or solid fibers, decreased from 280 to 100 nm when the LAS concentration was increased.

6.3. Study of the Gelation Behavior of DBC in the Presence of C₁₂₋₁₈E₇

6.3.1. Molecular Interactions below the Critical Gelation Concentration

6.3.1.1. Surface Tension Measurements

The effect of gellant molecules on the cmc and surface tension of C₁₂₋₁₈E₇ (Dehydol LT7) was studied using 1.11 mM DBC, to prevent any DBC gelation during the measurements.

The determination of the cmc of C₁₂₋₁₈E₇ in the absence and presence of DBC at pH 5, is illustrated in Figure 6-46.

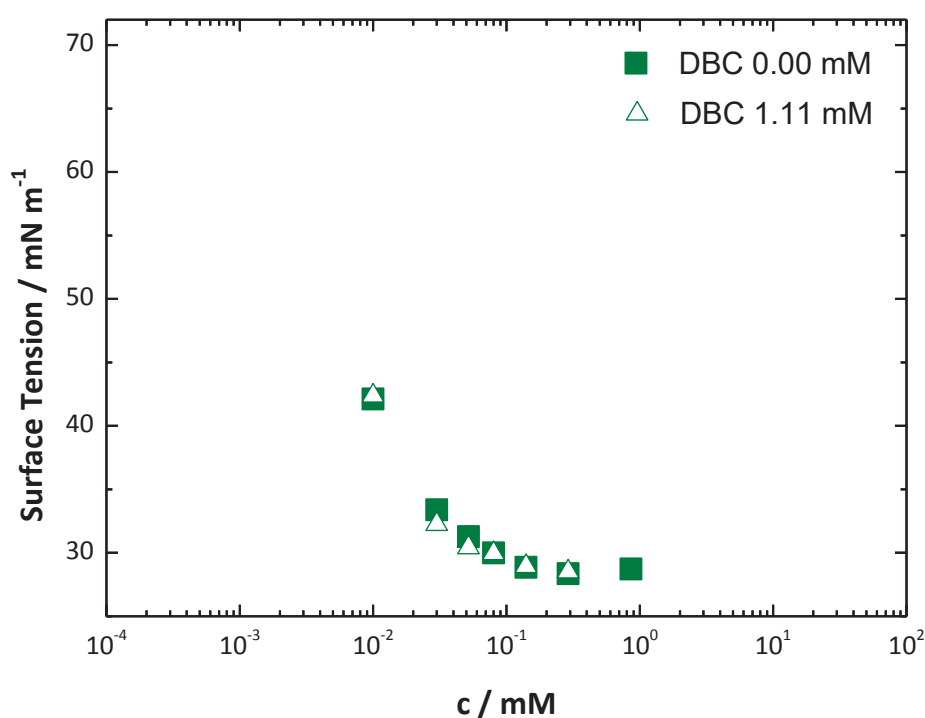


Figure 6-46 Surface tension of the ternary system H₂O-C₁₂₋₁₈E₇-DBC with a gellant concentration of 0.00 and 1.11 mM and varied surfactant concentrations, measured with a *De Nouy* ring tensiometer, at 298 K. The samples were prepared individually for each surfactant concentration and adjusted to an initial pH of 5. The values correspond to the first measured value, when the ring get in contact with the surface of the liquid.

To completely prevent gel network formation, the tests were performed at pH 5 because, as has already been discussed, DBC gel formation could be promoted at pH 3 (Chapter 6.2.1.1).

The cmc values determined for C₁₂₋₁₈E₇-in-water system and in a mixture with 1.11 mM DBC, are presented in Table 6-14.

Table 6-14 Cmc values of the H₂O-C₁₂₋₁₈E₇ binary system and H₂O-C₁₂₋₁₈E₇-DBC ternary system with 1.11 mM DBC, determined with a *Du Nouy* ring tensiometer, at 298 K and pH 5.

System	cmc / mM
H ₂ O-C ₁₂₋₁₈ E ₇	0.1
H ₂ O-C ₁₂₋₁₈ E ₇ -DBC 1.11 mM	0.1

The cmc of C₁₂₋₁₈E₇-in-water system was observed to be 0.1 mM and did not change in a mixture with DBC. In addition, the surface tension of the binary system H₂O-C₁₂₋₁₈E₇ did not change in a mixture with DBC. DBC-in-water system's slight surface-activity was discussed in Chapter 6.1.2.3, as the water's surface tension was lowered from 68.3 to 55.5 mN/m, by the addition of 1.11 mM DBC at pH 5 (Table 6-3). According to the results obtained in the presence of C₁₂₋₁₈E₇, it seems that DBC did not show any surface-activity, as the surface tension was not changed by the addition of the gelling agent.

In the literature^{[26],[34],[93]}, it was found that the cmc of non-ionic surfactants was independent of the presence of low molecular weight gellants (LMWGs), showing that no molecular interactions occurred between the gellant and the surfactant molecules. However, bearing in mind that the non-ionic surfactant is very surface-active, the slight surface-activity of small amounts of DBC could be superposed by the presence of C₁₂₋₁₈E₇ molecules. Thus, the possibility of an interaction between DBC and C₁₂₋₁₈E₇ molecules at the air-water interface, should not be ignored.

6.3.2. Molecular Interactions above the Critical Gelation Concentration

6.3.2.1. Phase Transition Temperature

The measurement of the temperature dependency of G' and G'' values for the ternary system $\text{H}_2\text{O}-\text{C}_{12-18}\text{E}_7\text{-DBC}$, with 6.69 mM DBC and a surfactant concentration of 0.08 mM, is outlined in Figure 6-47.

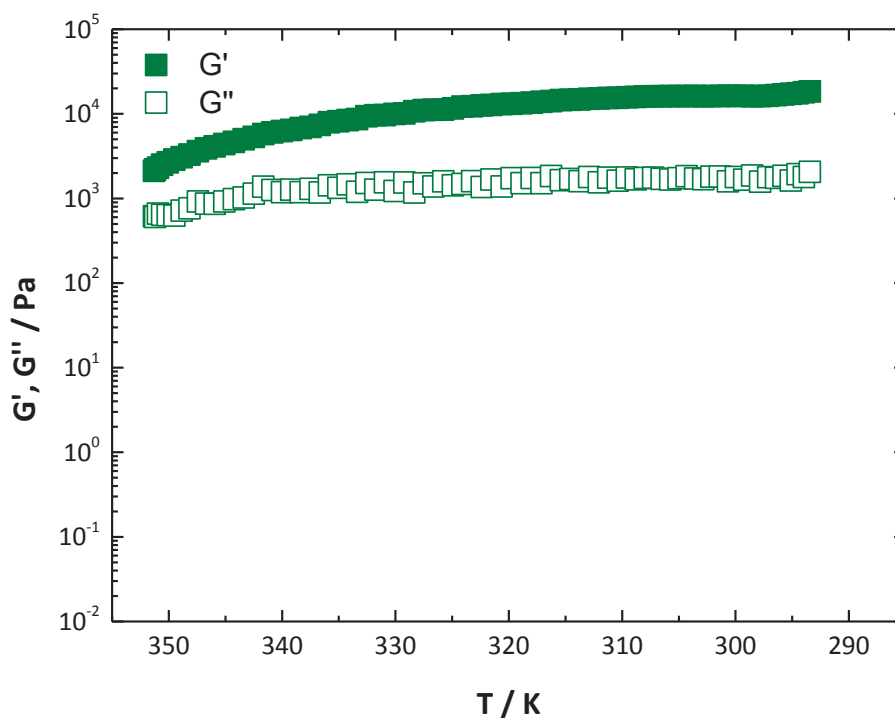


Figure 6-47 Storage modulus G' and loss modulus G'' vs. temperature of the ternary system $\text{H}_2\text{O}-\text{C}_{12-18}\text{E}_7\text{-DBC}$ with a surfactant concentration of 0.08 mM and a gellant concentration of 6.69 mM, measured with oscillating shear rheometry at a constant frequency of 1 Hz, a shear strain of 0.05 %, and a cooling rate of 10 K/min, using a parallel plate geometry, with a gap of 800 μm .

By lowering the temperature from 353 to 330 K at a rate of 10 K/min, the G' values were increased from $2 \times 10^{+03}$ to $1 \times 10^{+04}$ Pa. With a further decrease in the temperature, the G' values increased to $2 \times 10^{+04}$ Pa. The G' value of $2 \times 10^{+03}$ Pa, at 353 K, indicated that a gel network had been formed, so that the apparent $T_{\text{sol-gel}}$ value for a cooling rate of 10 K/min, was higher than 353 K but could not be determined using rheological measurements because the rheometer's measuring limit is 353 K to prevent any effects from evaporation during the measurements.

In the absence of $C_{12-18}E_7$, an apparent $T_{\text{sol-gel}}$ value was determined for a cooling rate of 10 K/min of 336 K, by rheological measurement (Chapter 6.1.1, Figure 6-12).

Hence, the apparent $T_{\text{sol-gel}}$ values for a cooling rate of 10 K/min were greater than 353 K due to the addition of $C_{12-18}E_7$ molecules, so that the DBC gel network formation was promoted, which is clearly shown in Figure 6-48.

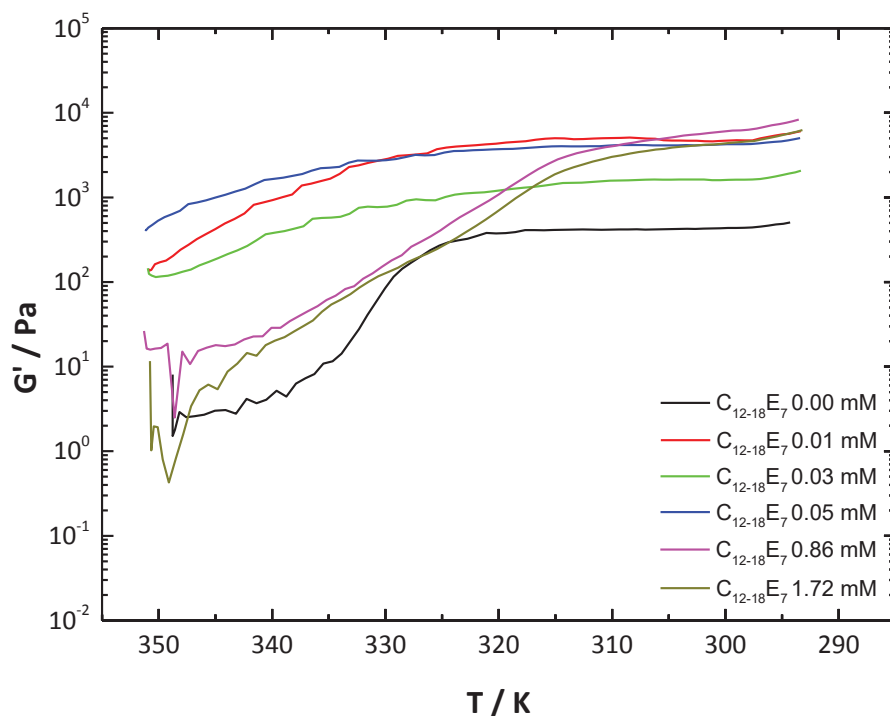


Figure 6-48 Measurement of the temperature dependency of the storage modulus G' of the ternary system H_2O - $C_{12-18}E_7$ -DBC with a gellant concentration of 6.69 mM and varied surfactant concentrations, measured with a parallel plate geometry, and a gap of 800 μm , at 293 K with oscillating shear rheometry at a constant frequency of 1 Hz, a shear strain of 0.05 %, and a cooling rate of 10 K/min.

For $C_{12-18}E_7$ concentrations of up to 0.05 mM, which is below the cmc of 0.1 mM (Chapter 6.3.1.1, Table 6-14), it can be seen that, gel formation even occurred at a temperature of 353 K, as the G' values ranged from $1 \times 10^{+02}$ to $5 \times 10^{+02}$ Pa, hence, the temperature at the transition from the sol to the gel phase, was greater than 353 K, which was the rheometer's measuring limit to prevent any effects of evaporation.

The gelation process started at 349 K at surfactant concentrations above 0.86 mM, and at 336 K in the absence of surfactant.

As the $T_{\text{sol-gel}}$ values were greater in the mixture with $C_{12-18}E_7$, it can be concluded that the DBC gel network formation was promoted within the low surfactant concentration range of up to 1.72 mM.

However, the promotion of gel formation was more pronounced at surfactant concentrations below 0.05 mM, as the transition from the induction to the gelation stage occurred at higher temperatures than at concentrations higher than this.

The promotion of gel network formation could presumably be because of the better dispersion of DBC particles by C₁₂₋₁₈E₇ molecules during the heating process in sample preparation. This could lead to smaller aggregates being formed by the decrease in interfacial tension^{[38],[53],[131]} between the gellant aggregates and the water phase, and facilitate the nucleation of the aggregates.

The G' values of DBC in the presence of the non-ionic surfactant, were greater than those of the DBC-in-water system, which could indicate the formation of a finer gel network structure than the binary gel H₂O-DBC.

In a mixture with C₁₂₋₁₈E₇, the G' values of between $2 \times 10^{+03}$ and $1 \times 10^{+04}$ Pa were observed in the quasi-equilibrium stage, when the gel network formation had been completed.

In the absence of C₁₂₋₁₈E₇, the G' value was found to be $5 \times 10^{+02}$ Pa.

When cooling the sample at a rate of 5 K/min, the transition from the sol to the gel phase could not be studied using rheology, due to fast gelation. As the rheometer's measuring limit was 353 K, it can be concluded that the transition temperature was higher than 353 K, i.e. higher than for the DBC-in-water system. This shows that DBC gel network formation was even promoted at a lower cooling rate.

It is important to mention that by the adding C₁₂₋₁₈E₇ molecules to the DBC-in-water system, slightly turbid solutions were formed at a surfactant concentration of above 1.72 mM at 401 K, which was found to be the dissolution temperature of DBC.

The appearance of a turbid solution of non-ionic surfactant systems upon heating, was mentioned in Chapter 4.1. A phase separation, into a surfactant-rich and a surfactant-poor liquid phase, occurred upon heating the aqueous surfactant solution due to dehydration of the non-ionic surfactant's polar head-group, leading to enhanced micelle-micelle interaction^{[65],[66]}. And from an application perspective, the phase boundary to the two-phase region^[67] was defined as the cloud point, which was determined as a surfactant concentration of 1 wt-%^[68].

In the literature^[138], the cloud point of C₁₂₋₁₈E₇ was found to be 321 K. This value correlates to a molar concentration of 19.61 mM, assuming that the density of the non-ionic surfactant is the same as water, which is 1 g/m³ at a normal pressure of 1.01 bar^[139].

The appearance of a turbid solution at a surfactant concentration of above 1.72 mM, was only observed in the presence of DBC. Without the addition of the gelling agent, a clear solution was formed, at this surfactant concentration, at 401 K. As the surfactant concentration is much lower than 19.61 mM, it is clear that the surfactant concentration of 1.72 mM did not exceed the phase boundary into the two-phase region. Accordingly, the appearance of a turbid solution following the addition of 6.69 mM DBC, does not seem to be attributable to the transition into the two-phase region. However, this could be a result of strong interactions between DBC and C₁₂₋₁₈E₇ molecules, leading to the formation of aggregates that are large enough to scatter light and produce a turbid solution.

Therefore, the influence of the non-ionic surfactant on the gelation properties of DBC was only studied of up to a C₁₂₋₁₈E₇ concentration of 1.72 mM.

6.3.2.2. Rheological Study

The rheological properties of DBC in the presence of C₁₂₋₁₈E₇ were studied. The effect of surfactant molecules on the $G'(\infty)$ values for a constant gellant concentration of 6.69 mM, was investigated as outlined in Figure 6-49.

Without the addition of C₁₂₋₁₈E₇, a $G'(\infty)$ value of $5 \times 10^{+02}$ Pa was determined. In a mixture with C₁₂₋₁₈E₇ and a concentration of up to 1.72 mM, the values increased from $5 \times 10^{+02}$ to a range between $5 \times 10^{+03}$ and $2 \times 10^{+04}$ Pa. As the values were greater than those of the DBC-in-water system, it can be assumed that a finer gel network was formed in a mixture with the non-ionic surfactant, than in the absence of the surfactant molecule.

It was found that DBC gel network formation was promoted by the addition of the non-ionic surfactant C₁₂₋₁₈E₇ within the studied concentration range of up to 1.72 mM, as the transition from the induction to the gelation stage was observed at higher $T_{\text{sol-gel}}$ values than in the absence of the surfactant. The promotion of gel network formation was more pronounced at C₁₂₋₁₈E₇ concentrations of up to 0.05 mM, than at higher concentrations.

In addition, the $G'(\infty)$ values were found to be higher than those of the binary system H₂O-DBC, which could indicate the formation of a finer gel network in the presence of the non-ionic surfactant, than the DBC-in-water system.

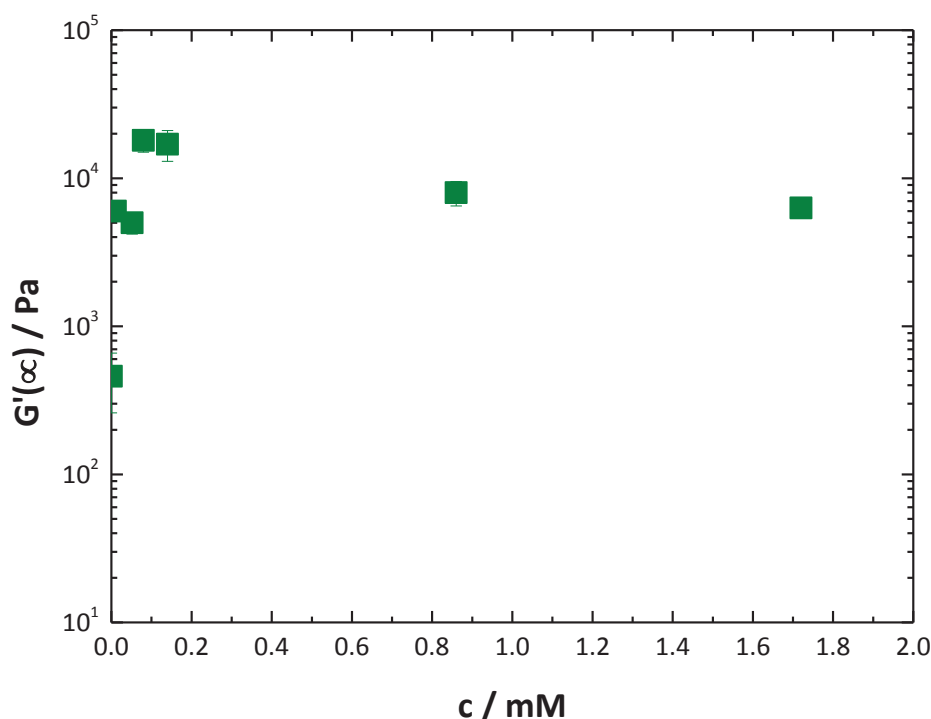


Figure 6-49 Storage modulus in the quasi-equilibrium stage $G'(\infty)$ of the ternary system H₂O-C₁₂₋₁₈E₇-DBC with 6.69 mM DBC as a function of surfactant concentration, measured at 293 K with oscillating shear rheometry, at a frequency of 1 Hz, and a strain of 0.05 %, using a parallel plate geometry with a gap of 800 μm . The prepared sample was transferred into the rheometer at 353 K and was cooled to 293 K at a rate of 10 K/min. The error bars give the standard deviation for the average $G'(\infty)$ values determined for each surfactant concentration.

6.4. Comparison of the Gelation Behavior of DBC in the Presence of LAS and C₁₂₋₁₈E₇

The influence of two different types of surfactants in mixtures with DBC, below and above the critical gelation concentration, were compared with one another.

As the kinetics on the DBC gelation process could not be studied in mixtures with C₁₂₋₁₈E₇ molecules due to fast gelation, the effects of LAS and C₁₂₋₁₈E₇ molecules on the induction and quasi-equilibrium stages of DBC gelation were compared.

For concentrations below the critical gelation concentration, it was found that the addition of 1.11 mM DBC influenced the cmc and surface tension of the LAS-in-water system. In contrast, the cmc and surface tension of the binary system H₂O-C₁₂₋₁₈E₇ did not change in the presence of DBC.

The reduction in cmc and the surface tension with the addition of DBC at pH 5 (Chapter 6.2.1.1, Table 6-6), was believed to be due to the addition of electrolytes, such as HCl or NaOH solutions, DBC's slight surface-activity (Chapter 6.1.2.3, Table 6-3), or, alternatively, a slight interaction between the LAS and DBC molecules at the air-water interface.

Even though no indication of molecular interactions between DBC and C₁₂₋₁₈E₇ molecules was found using surface tension measurements, it was assumed that the possible interactions between the molecules at the air-water phase could be superposed by highly surface-active C₁₂₋₁₈E₇ molecules, as the surface tension of the water was lowered from 68 to 28 mN/m.

For concentrations above the critical gelation concentration, it was found that a gel network was formed in mixtures with LAS and C₁₂₋₁₈E₇. Interestingly, a gel network was formed in the presence of LAS, of up to a concentration of 28.70 mM LAS. However, in the presence of C₁₂₋₁₈E₇, the gel network formation was limited to a concentration of up to 1.72 mM. Above this concentration, turbid solutions were formed at the water's dissolution temperature and phase separation or crystallization occurred upon cooling, rather than gel formation.

As the non-ionic surfactant is a more hydrophobic compound than the ionic surfactant, the interactions between DBC and C₁₂₋₁₈E₇ molecules could, presumably, be stronger than those between DBC and LAS molecules, as DBC tends to be a hydrophobic compound. As such, the strong interactions with the surfactant molecules seems to promote crystallization above a certain ratio of DBC and C₁₂₋₁₈E₇ molecules, rather than DBC gel formation.

The gelation process was influenced by the presence of LAS and C₁₂₋₁₈E₇ molecules above the critical gelation concentration.

The induction stage of the gelation process was found to be promoted by the addition of surfactant molecules to the 6.69 mM DBC-in-water system, as the transition from the sol to the gel phase occurred at higher temperatures than that of the binary gel H₂O-DBC.

When cooling the sample at a rate of 10 K/min, the formation of a gel network was promoted at LAS concentrations of up to 6.03 mM (Chapter 6.2.2.4, Table 6-10) and by a C₁₂₋₁₈E₇ concentration of up to 1.72 mM (Chapter 6.3.2.1, Figure 6-48).

As the C₁₂₋₁₈E₇ concentration was limited to a maximum of 1.72 mM, it was not clear from a comparison of the transition values in the presence of the non-ionic and ionic surfactant of up to this concentration, whether one of the surfactants had promoted the gel network formation more, or whether their actions were identical as the apparent $T_{\text{sol-gel}}$ values for a cooling rate of 10 K/min were greater than 353 K for both ternary systems of H₂O-LAS-DBC and H₂O-C₁₂₋₁₈E₇-DBC, so that they could not be determined by rheological measurements due to the rheometer's measuring limit.

Different influences from surfactant molecules were found when the gel network formation was completed.

The $G'(\infty)$ values of the ternary systems H₂O-LAS-DBC and H₂O-C₁₂₋₁₈E₇-DBC, with varied surfactant concentrations and 6.69 mM DBC in the quasi-equilibrium stage, are summarized in Figure 6-50.

By adding C₁₂₋₁₈E₇ to the DBC-in-water system, greater $G'(\infty)$ values were found than for the binary system H₂O-DBC.

In the absence of $C_{12-18}E_7$, the G' value was found to be $5 \times 10^{+02}$ Pa. In mixtures with $C_{12-18}E_7$, of up to a concentration of 1.72 mM, the $G'(\infty)$ values ranged between $5 \times 10^{+03}$ and $2 \times 10^{+04}$ Pa, which could indicate the formation of a finer gel network than that formed in the DBC-in-water system.

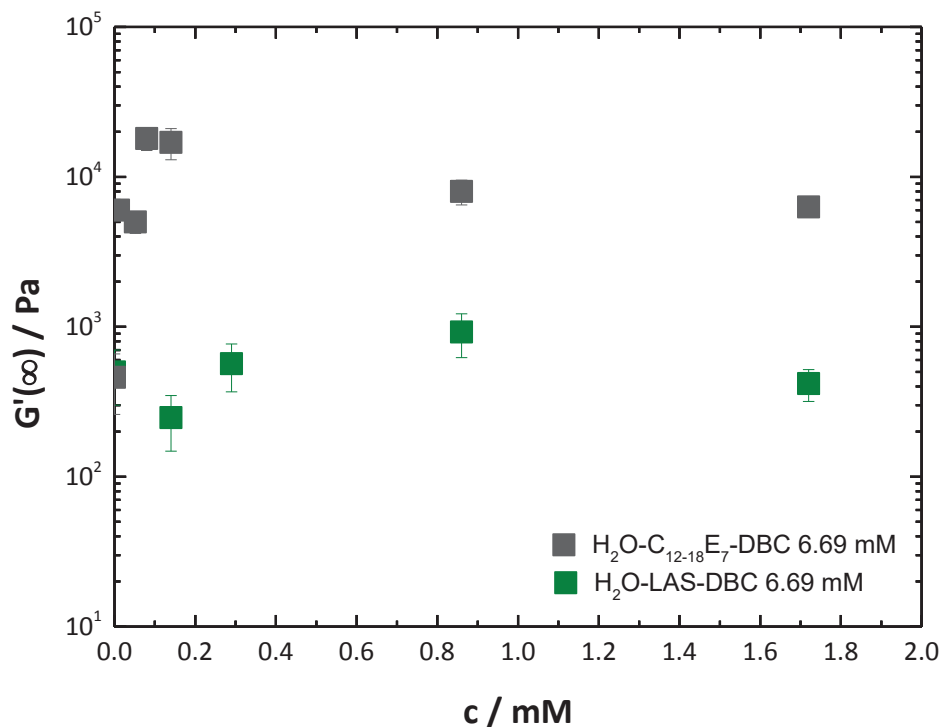


Figure 6-50 Storage modulus in the quasi-equilibrium stage $G'(\infty)$ vs. surfactant concentration of the ternary systems $H_2O-C_{12-18}E_7$ -DBC and H_2O -LAS-DBC with 6.69 mM DBC, measured at 293 K with oscillating shear rheometry, at a frequency of 1 Hz, and a strain of 0.05 %, using a parallel plate geometry, with a gap of 800 μ m. The prepared sample was transferred into the rheometer at 353 K and was cooled to 293 K at a rate of 10 K/min. The error bars give the standard deviation for the average $G'(\infty)$ values determined for each surfactant concentration.

In the presence of LAS, the $G'(\infty)$ values were found to range between $3 \times 10^{+02}$ and $1 \times 10^{+03}$ Pa and when compared with the binary system H_2O -DBC, the values could be taken as being similar, within the error limit.

The $G'(\infty)$ values of DBC were up by one order of magnitude higher in the presence of $C_{12-18}E_7$ than in mixtures with LAS, which could indicate that a finer gel network was formed by the ternary system $H_2O-C_{12-18}E_7$ -DBC, than by H_2O -LAS-DBC (Chapter 6.1.2.4).

The non-ionic surfactant was found to be more surface-active than the ionic surfactant, as the water's surface tension was reduced from 68 to 28 mN/m in the presence of C₁₂₋₁₈E₇ (Chapter 6.3.1.1, Figure 6-46) and from 68 to 33 mN/m in a mixture with LAS (Chapter 6.2.1.1, Figure 6-21). Presumably, the interfacial tension between the gellant aggregates and the water phase, could be lowered more during the induction stage by the adsorption of C₁₂₋₁₈E₇ molecules on the surface of the hydrophobic aggregates than by the adsorption of LAS molecules. This could produce the formation of a finer gel network, with greater $G'(\infty)$ values, in the presence of C₁₂₋₁₈E₇ than in a mixture with LAS.

To summarize, the gel network formation was promoted in mixtures with C₁₂₋₁₈E₇ and LAS molecules within the low surfactant concentration range of up to 1.72 mM, as greater $T_{\text{sol-gel}}$ values were determined for the mixtures with surfactant molecules, than for the binary system H₂O-DBC. In the quasi-equilibrium stage, higher $G'(\infty)$ values were found for the DBC-in-C₁₂₋₁₈E₇ system, than for the DBC-in-LAS system, which could indicate a finer gel network structure for DBC in mixtures with C₁₂₋₁₈E₇, than in the presence of LAS.

6.5. Study of the Gelation Behavior of L-Tyr-L-Tyr in the Presence of LAS

From a scientific perspective, it is interesting to study the gelation properties of two different LMWGs in mixtures with surfactants, to obtain a further insight into the influence of surfactant molecules on their gelation behavior.

The gelation properties of a second LMWG of the same substance class as DBC, were characterized in water and in the presence of LAS, to discover whether the results obtained for DBC could be also attributed to L-Tyr-L-Tyr or whether it would act differently, due to the chemical structure of L-Tyr-L-Tyr being different to that of DBC, as shown in Figure 6-51.

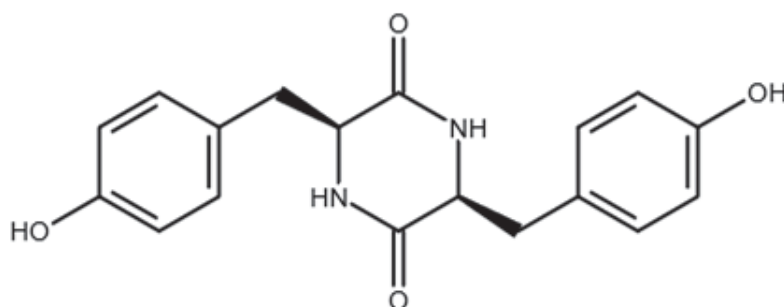


Figure 6-51 Chemical structure of L-Tyr-L-Tyr.

Both LMWGs belong to the amino acid derivative substance group, and they consist of two aromatic phenyl groups. L-Tyr-L-Tyr has two amido groups in a cyclic structure, instead of an open-chain structure as in DBC. In addition, the cyclic dipeptide containing the lipophilic amino acid L-tyrosine, is a more hydrophobic compound than DBC, which consists of hydrophilic cysteine units (for the structure of DBC, refer to Chapter 6.1.2.3, Figure 6-16).

Furthermore, L-Tyr-L-Tyr consists of two hydroxyl groups and DBC consists of two carboxyl groups, so that L-Tyr-L-Tyr favors gelation in neutral and DBC in acidic environments, which was also shown by the surface tension measurements, as the water's pH decreased from 7 to 3.5 in mixtures with DBC. To ensure the same conditions for the characterization of the LMWGs' gelation properties, the pH of the L-Tyr-L-Tyr hydrogels was adjusted to pH 3.5 by the addition of a hydrochloric acid solution (**2.0 M**).

6.5.1. Gelation Behavior of L-Tyr-L-Tyr in a Water System

The measurement of the temperature dependency of the G' and G'' values of the 6.69 mM binary system of H₂O-L-Tyr-L-Tyr, is shown in Figure 6-52.

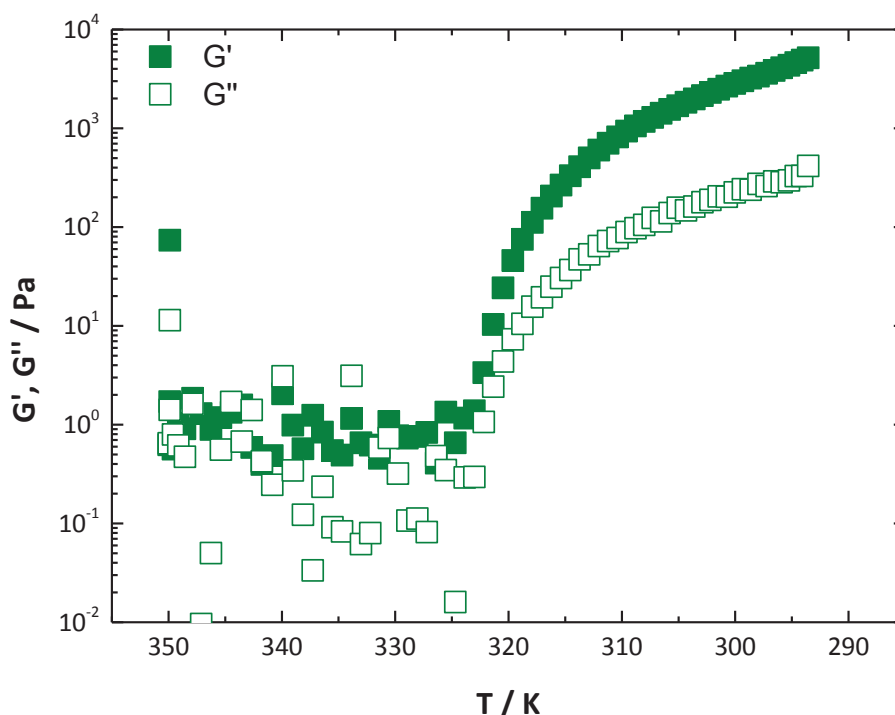


Figure 6-52 Storage modulus G' and loss modulus G'' vs. temperature of the 6.69 mM binary system of H₂O-L-Tyr-L-Tyr, measured with oscillating shear rheometry, at a constant frequency of 1 Hz, a shear strain of 0.05 %, and a cooling rate of 10 K/min, using a parallel plate geometry, with a gap of 800 μm .

When cooling at a rate of 10 K/min, the G' values were independent of the temperature, of up to 324 K. The values were found to be $1 \times 10^{+00}$ Pa. Up to this temperature, the G'' values showed high scattering upon cooling.

When the temperature was lowered further to 293 K, the G' values were over one order of magnitude higher than the G'' values, hence the elastic behavior was dominant over the viscous behavior. The G' values increased from $1 \times 10^{+00}$ to $8 \times 10^{+03}$ Pa, and the G'' values from 3×10^{-01} to $4 \times 10^{+02}$ Pa. The start of the increase in G' values was taken as the apparent $T_{\text{sol-gel}}$ value for a cooling rate of 10 K/min, which was observed to be 324 K.

The temperature-sweep of the L-Tyr-L-Tyr-in-water system was repeated six times; each time, either a strong deviation of the transition temperature was found, such as between 298 and 313 K, or phase separation occurred instead of gel formation.

Imaging measurements of the 6.69 mM binary system of H₂O-L-Tyr-L-Tyr were performed in order to identify the reason for the irreproducible measurements, as presented in Figure 6-53.

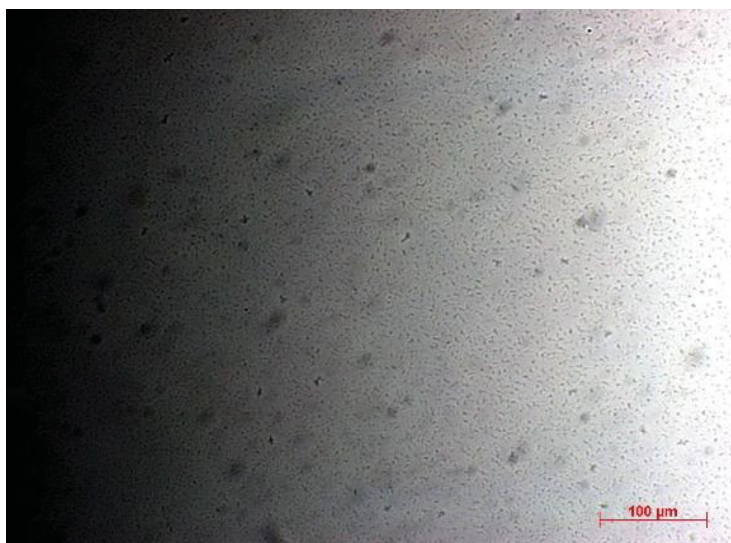


Figure 6-53 Optical microscopy image of the binary system H₂O-L-Tyr-L-Tyr with a gellant concentration of 6.69 mM. The sample was transferred onto the slide at 353 K and was allowed to cool to 298 K. The image was taken after 20 minutes (scale bar = 100 μm).

Spherulites with a diameter between 2 and 4 μm can be seen. The spherulites become slightly larger with time while no formation of fiber-like structures could be seen, even after 180 minutes.

It can be concluded that the gelation behavior of L-Tyr-L-Tyr-in-water system was randomly driven, and therefore the results obtained from the rheological and imaging measurements should be considered to be those of a single experiment.

6.5.2. Molecular Interactions in Mixture with LAS

As the L-Tyr-L-Tyr-in-water system's gelation ability was randomly driven, it was studied in mixtures with surfactant molecules, to see whether the reproducibility of the gel network formation could be improved.

6.5.2.1. Phase Transition Temperature

The apparent $T_{\text{sol-gel}}$ value for a cooling rate of 10 K/min of the ternary system H₂O-LAS-L-Tyr-L-Tyr with surfactant concentrations of 7.17 mM and 6.69 mM L-Tyr-L-Tyr, was determined by temperature-sweep measurement, as presented in Figure 6-54.

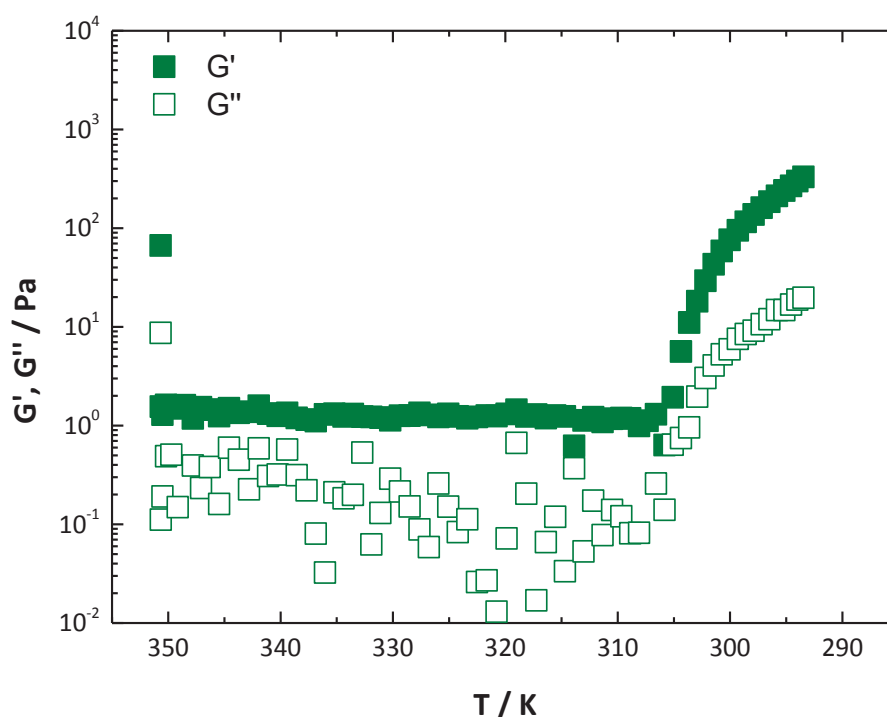


Figure 6-54 Storage modulus G' and loss modulus G'' vs. temperature of the ternary system H₂O-LAS-L-Tyr-L-Tyr with a surfactant concentration of 7.17 mM and a gellant concentration of 6.69 mM, measured with oscillating shear rheometry, at a constant frequency of 1 Hz, a shear strain of 0.05 %, and a cooling rate of 10 K/min, using a parallel plate geometry, with a gap of 800 μm .

A surfactant concentration of 7.17 mM was chosen to ensure the same conditions as for the ternary system of H₂O-LAS-DBC (Chapter 6.2.2.1, Figure 6-22).

When the temperature was lowered from 353 to 306 K, the G' values were independent of the temperature and were observed at $2 \times 10^{+00}$ Pa. The G'' values showed high scattering and ranged between 1×10^{-02} and $1 \times 10^{+00}$ Pa. The G' values decreased slightly at 306 K, from $2 \times 10^{+00}$ to 8×10^{-01} Pa. Above this temperature, the G' values were over one order of magnitude higher than the G'' values and increased sharply, from 8×10^{-01} to $3 \times 10^{+02}$ Pa. The G'' values were increased to $2 \times 10^{+01}$ Pa by cooling to 293 K. The transition from the sol to the gel phase was recorded at 306 K, as the G' values increased sharply below this temperature.

The measurement was reproducible; therefore, it can be concluded that the addition of surfactant molecules promotes the gelation behavior of L-Tyr-L-Tyr.

This could be attributable to the possible enhancement of the dispersion of the gelling agent in water by the addition of surfactant molecules, as they could adsorb on the gellant aggregates' surface leading to a decrease in the interfacial tension between the aggregates and the water phase, thus promoting the nucleation process, which leads to reproducible measurements.

In order to study the effect of further surfactant concentrations on the phase transition behavior of L-Tyr-L-Tyr, the apparent $T_{\text{sol-gel}}$ values for different cooling rates of the ternary system H₂O-LAS-L-Tyr-L-Tyr with 6.69 mM L-Tyr-L-Tyr, and varied LAS concentrations, were determined by temperature-sweep measurements, as shown in Figure 6-55.

For LAS concentrations of up to 14.35 mM and cooling at a rate of 5 K/min, the transition from the sol to the gel phase was observed between 302 and 307 K. At higher concentrations, the values slightly decreased to 293 K, which is the temperature at which the gelation process was investigated using long-term measurement, as no gelation occurred within the given timeframe when cooling at a rate of 5 K/min.

By rapidly cooling at 10 K/min, the transition temperature for mixtures with LAS of up to 28.70 mM, ranged from 295 to 312 K.

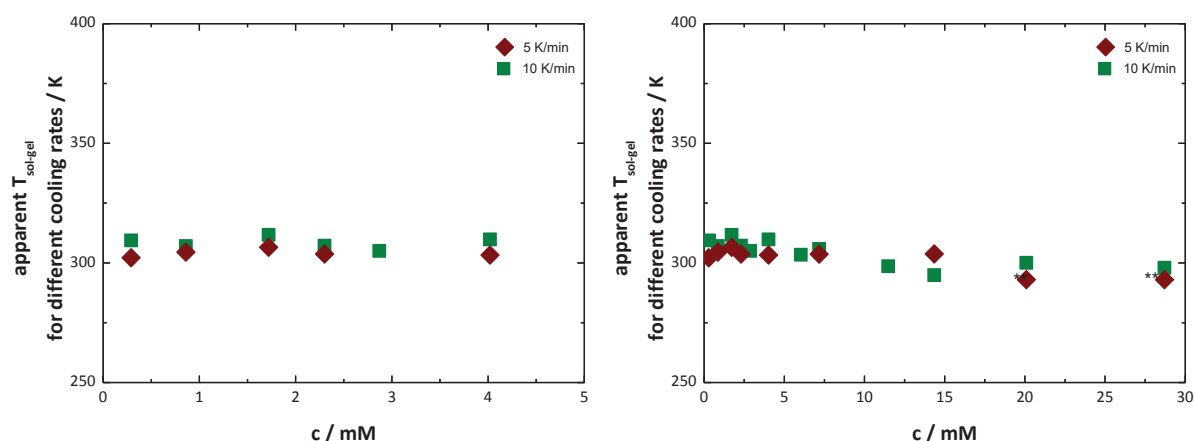


Figure 6-55 Apparent $T_{\text{sol-gel}}$ values for different cooling rates (right) and the extract from the diagram at lower surfactant concentrations (left) of the ternary system H_2O -LAS-L-Tyr-L-Tyr with 6.69 mM L-Tyr-L-Tyr and varied LAS concentrations, measured with oscillating shear rheometry, at a constant frequency of 1 Hz, a shear strain of 0.05 %, and cooling rates of 5 and 10 K/min, using a parallel plate geometry, with a gap of 800 μm . Symbols marked with a double asterisk, **, indicate the temperature at which the gelation occurred by a long-term measurement.

The apparent $T_{\text{sol-gel}}$ values determined for different cooling rates, could be taken as being similar for concentrations of up to 14.35 mM LAS; above this concentration, the values were lower due to cooling at rate of 5 K/min rather than 10 K/min. It can be concluded that for a surfactant concentration of up to 14.35 mM, the gelation process of L-Tyr-L-Tyr in a mixture with LAS, was not influenced by the cooling rate, while at high surfactant concentrations, the gel network formation was slightly delayed by slow cooling, as the beginning of the gelation process was found to be 293 K, which was lower than in the presence of 0.29 mM LAS. As L-Tyr-L-Tyr-in-water's transition temperature was not reproducible, the $T_{\text{sol-gel}}$ value for mixtures with 0.29 mM LAS, could be taken as a reference by comparing the values with one another to find out whether a promotion or delay of gel network formation occurred.

That L-Tyr-L-Tyr gel network formation is delayed, at high surfactant concentrations, by cooling at a rate of 5 K/min, is clearly shown in Figure 6-56.

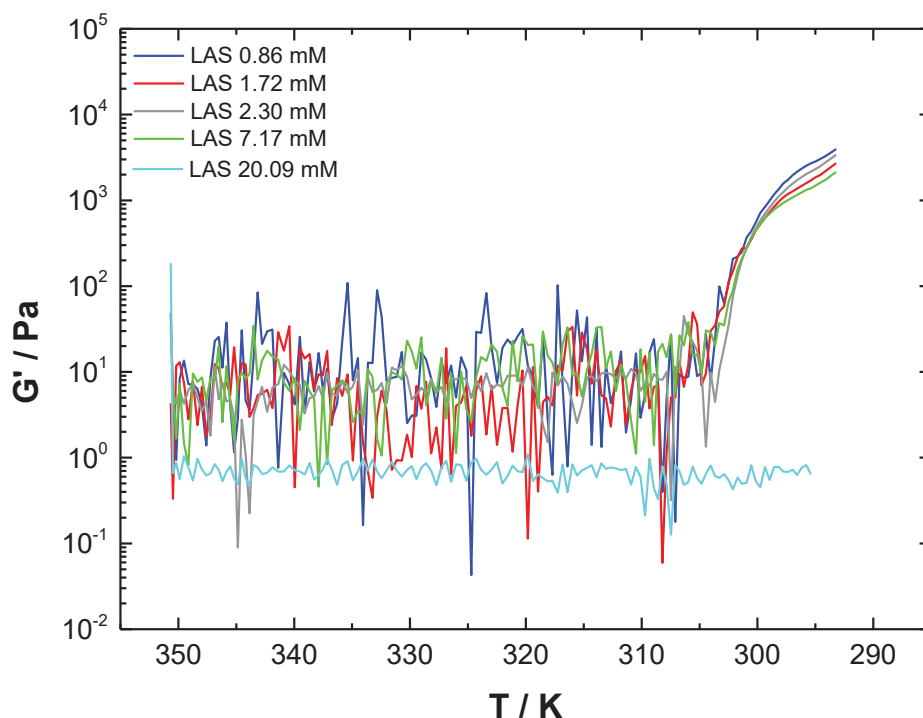


Figure 6-56 Measurement of the temperature dependency of the storage modulus G' of the ternary system H_2O -LAS-L-Tyr-L-Tyr with a gellant concentration of 6.69 mM and varied surfactant concentrations, measured with a parallel plate geometry, and a gap of 800 μm , at 293 K with oscillating shear rheometry, at a constant frequency of 1 Hz, a shear strain of 0.05 %, and a cooling rate of 5 K/min.

When the temperature was lowered from 353 to 304 K, the G' values showed high scattering of up to a LAS concentration of 7.17 mM. The values ranged between 4×10^{-02} and $1 \times 10^{+02}$ Pa. Between 304 to 293 K, the G' values increased sharply from $9 \times 10^{+00}$ to a range between $2 \times 10^{+03}$ and $4 \times 10^{+03}$ Pa.

At a high surfactant concentration, 20.09 mM LAS, the G' values were independent of the temperature and were found to be 8×10^{-01} Pa. No gelation occurred in the temperature-sweep measurement during the given timeframe, and compared with the ternary system in a mixture with 0.29 mM LAS, it was found that the gel formation of L-Tyr-L-Tyr was delayed.

6.5.2.2. Microscopic Images

Optical microscopy and cryo-TEM measurements were performed to gain insights into the morphology of L-Tyr-L-Tyr in a mixture with LAS.

The gel network structure of the ternary system H₂O-LAS-L-Tyr-L-Tyr, with a surfactant concentration of 0.29 mM and a gellant concentration of 6.69 mM on the μm -scale, was investigated by using optical microscopy, as shown in Figure 6-57.



Figure 6-57 Optical microscopy image of the ternary system H₂O-LAS-L-Tyr-L-Tyr with a gellant concentration of 6.69 mM and a surfactant concentration of 0.29 mM. The sample was transferred onto the slide at 353 K and was allowed to cool to 298 K. The image was taken after 20 minutes (scale bar = 100 μm).

The image was taken after 20 minutes to ensure that the gel network formation was completed.

It was possible to see rhomboids, trapezoids, rhombuses and triangles, which were either connected to each other or separate, and between 18 and 26 μm in width. It seems that each structure consists of spherulites with a diameter of between 10 and 22 μm , as shown by the higher contrast at the center of the structure, which becomes lower away from the center^[140].

When the surfactant concentration was increased further, the measurement was performed after 180 minutes, as the gel network formation was delayed at high surfactant concentration (Chapter 6.5.2.1, Figure 6-56).

The optical microscopy image of the ternary system H_2O -LAS-L-Tyr-L-Tyr, with a surfactant concentration of 20.09 mM and a gellant concentration of 6.69 mM, is shown in Figure 6-58.

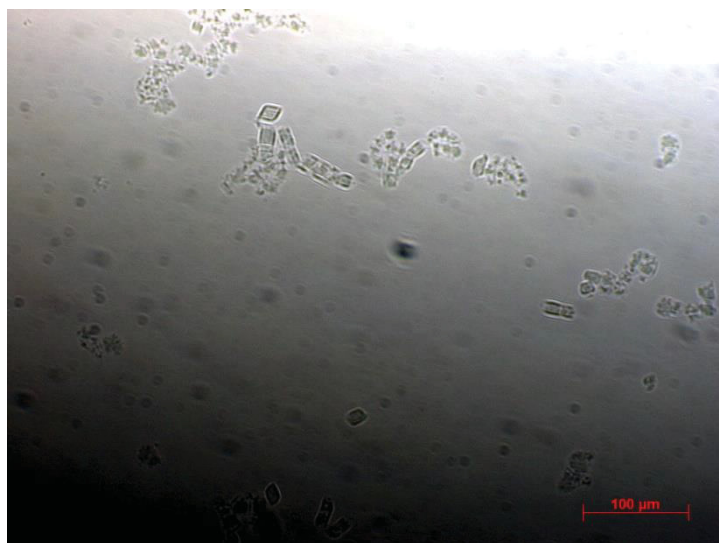


Figure 6-58 Optical microscopy image of the ternary system H_2O -LAS-L-Tyr-L-Tyr with a gellant concentration of 6.69 mM and a surfactant concentration of 20.09 mM. The sample was transferred onto the slide at 353 K and was allowed to cool to 298 K. The image was taken after 180 minutes (scale bar = 100 μm).

It was possible to see rhomboids of between 8 and 17 μm in width, which were either connected to each other or separate. They appeared to be filled with spherulites, indicated by the higher contrast in the center of the structure than outside it^[140].

Due to diffraction phenomena^[115] during the measurements, it could be said that the widths determined for the rhomboids correlate to those determined from the irregular structures which were formed in the presence of 0.29 mM LAS (Figure 6-57).

It can be concluded from the optical microscopy images, that the visualized structures did not change when the LAS concentration was increased.

Cryo-TEM measurements were performed to visualize the structures on the nm-scale. The cryo-TEM images of 6.69 mM L-Tyr-L-Tyr in the presence of 0.29 mM LAS, taken after 5 and 45 minutes, are shown in Figure 6-59 and Figure 6-60.

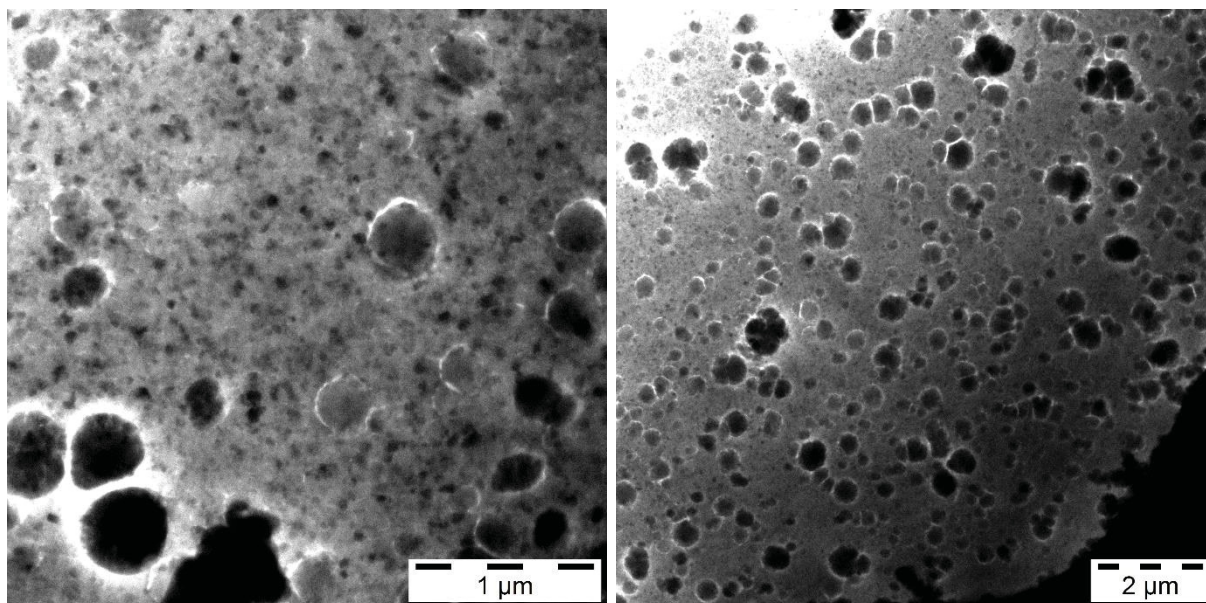


Figure 6-59 Cryo-TEM images of the ternary system H₂O-LAS-L-Tyr-L-Tyr with a surfactant concentration of 0.29 mM and a gellant concentration of 6.69 mM. The sample was at first allowed to cool from 363 to 298 K. After standing at 298 K for 5 minutes, the sample was prepared for cryo-TEM.

Deformed spherulite-like structures with a diameter of between 50 and 600 nm, could be visualized. In addition, ice crystals were also found as a result of water from the air condensing into particles in the liquid nitrogen^[137]. This suggests that surfactant molecules could influence the crystallization of water and therefore, that the deformed spherulite-like structures could be ice crystals, as mentioned in Chapter 6.2.2.3.

The cryo-TEM image taken after 45 minutes, is presented in Figure 6-60.

It is possible to see the formation of either solid fibers or densely-packed fiber-like aggregates. The structures are curved and seem to correlate with each other. The visualized structures were found to be up to 60 nm thick.

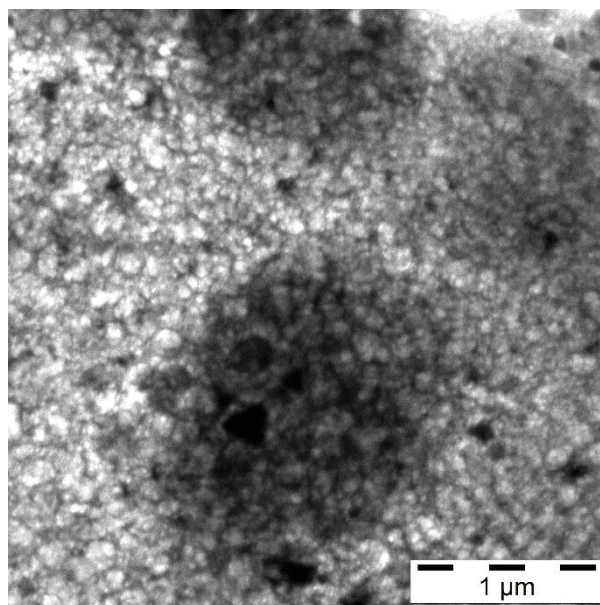


Figure 6-60 Cryo-TEM image of the ternary system H₂O-LAS-L-Tyr-L-Tyr with a surfactant concentration of 0.29 mM and a gellant concentration of 6.69 mM. The sample was at first allowed to cool from 363 to 298 K. After standing at 298 K for 45 minutes, the sample was prepared for cryo-TEM.

In order to study the influence of LAS molecules at high surfactant concentrations, on the morphology of the L-Tyr-L-Tyr gel network, cryo-TEM images of the ternary system H₂O-LAS-L-Tyr-L-Tyr with 20.09 mM LAS and 6.69 mM L-Tyr-L-Tyr, were taken after 5 and 45 minutes, as shown in Figure 6-61 and in Figure 6-62.

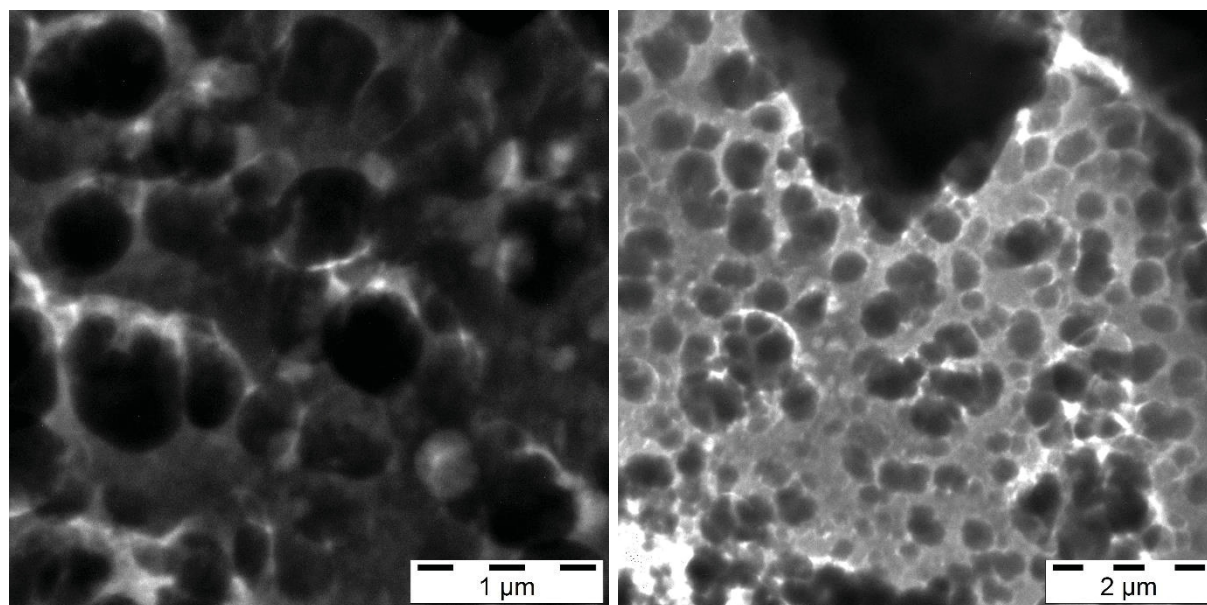


Figure 6-61 Cryo-TEM images of the ternary system H₂O-LAS-L-Tyr-L-Tyr with a surfactant concentration of 20.09 mM and a gellant concentration of 6.69 mM. The sample was at first allowed to cool from 363 to 298 K. After standing at 298 K for 5 minutes, the sample was prepared for cryo-TEM.

After 5 minutes, it is possible to see the formation of deformed spherulite-like structures with diameters of between 200 and 500 nm, which could presumably be ice crystals. In the absence of L-Tyr-L-Tyr, deformed structures with a diameter of between 70 and 180 nm were found (Chapter 6.2.2.3, Figure 6-30). It can be concluded that the presence of L-Tyr-L-Tyr has a strong influence on the crystallization of water.

The cryo-TEM image of this ternary system, taken after 45 minutes, is presented in Figure 6-62.

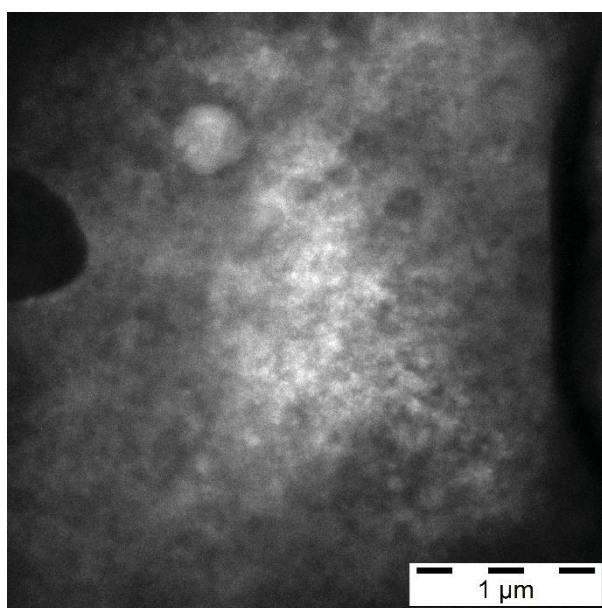


Figure 6-62 Cryo-TEM image of the ternary system H₂O-LAS-L-Tyr-L-Tyr with a surfactant concentration of 20.09 mM and a gellant concentration of 6.69 mM. The sample was at first allowed to cool from 363 to 298 K. After standing at 298 K for 45 minutes, the sample was prepared for cryo-TEM.

The formation of a dense network structure consisting of either solid fibers or fiber-like aggregates, can be seen. The thickness of these structures was found to be up to 60 nm.

Even though the nature of the structures forming the gel network is unclear, the morphology of the gel network did not change with increasing LAS concentrations. A fine gel network structure with a fiber thickness of up to 60 nm, was visualized in mixtures with LAS molecules below and above the cmc.

6.5.2.3. Kinetics of the Sol-Gel Phase Transition

The influence of surfactant molecules on the L-Tyr-L-Tyr gelation process was studied by using rheology.

The measurement of the dependency of the G' values on the temperature and time following the addition of 28.70 mM LAS into the 6.69 mM binary system of H₂O-L-Tyr-L-Tyr, is illustrated in Figure 6-63.

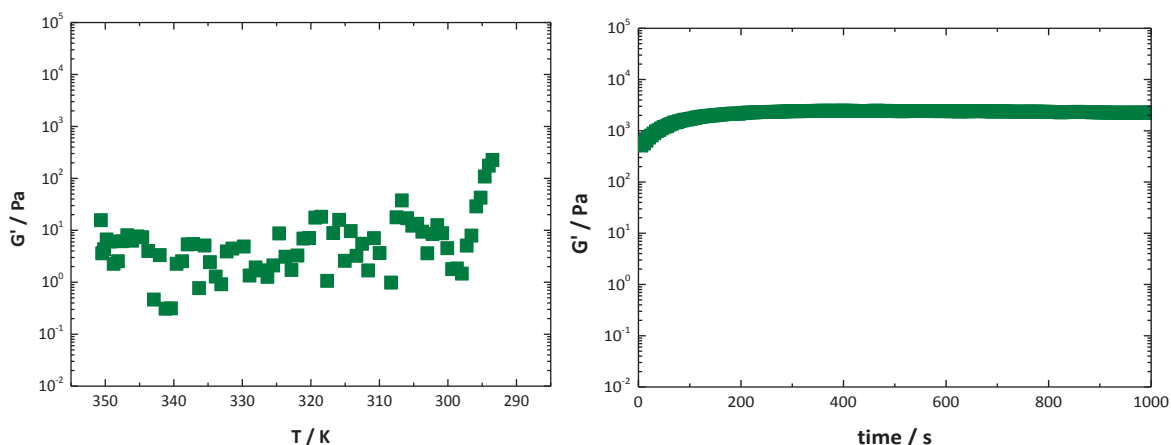


Figure 6-63 Storage modulus G' vs. temperature (left) and storage modulus G' vs. time at a temperature of 293 K (right) of the ternary system H₂O-LAS-L-Tyr-L-Tyr with a surfactant concentration of 28.70 mM and a gellant concentration of 6.69 mM, measured with oscillating shear rheometry, at a constant frequency of 1 Hz, a shear strain of 0.05 %, and a cooling rate of 10 K/min, using a parallel plate geometry, with a gap of 800 μ m.

When the sample was cooled from 353 to 298 K, at a rate of 10 K/min, the G' values were scattered between 3×10^{-01} and $4 \times 10^{+01}$ Pa. The G' values increased from $1 \times 10^{+00}$ to $2 \times 10^{+02}$ Pa between 298 and 293 K. The point when the G' value began to increase was taken as the apparent $T_{\text{sol-gel}}$ value, for a cooling rate of 10 K/min.

Gel formation was not completed within the given timeframe at 293 K, as the G' values did not show a plateau. Therefore, the evolution of the G' values was studied at 293 K, to ensure that the gel network formation was completed. At this temperature, the G' values increased slightly, from $7 \times 10^{+02}$ to $2 \times 10^{+03}$ Pa, and plateaued after 115 s.

To illustrate the three stages of the gelation process, the data taken from the temperature and time-sweep measurements were combined and fitted in terms of the *Dickinson* equation (equation 6-1), as presented in Figure 6-64.

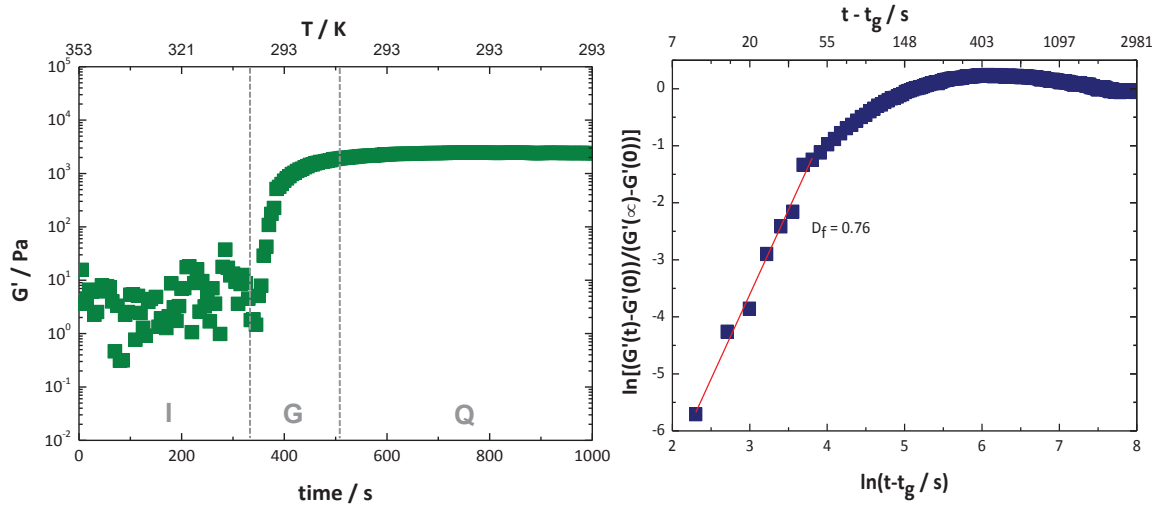


Figure 6-64 Combination of temperature-sweep and time-sweep measurements (left) and the fractal analysis of the kinetic data in terms of the *Dickinson* equation, according to equation 6-1 (right), of the ternary system H₂O-LAS-L-Tyr-L-Tyr with 28.70 mM LAS and 6.69 mM L-Tyr-L-Tyr, measured with oscillating shear rheometry, at a constant frequency of 1 Hz, a shear strain of 0.05 %, and a cooling rate of 10 K/min, using a parallel plate geometry, with a gap of 800 μ m (I - Induction stage, G - Gelation stage, Q - Quasi-equilibrium stage).

The G' values ranged between 3×10^{-01} and $4 \times 10^{+01}$ Pa, during the induction stage of up to 345 s. During the gelation stage, between 345 and 555 s, the G' values increased from $1 \times 10^{+00}$ to $2 \times 10^{+03}$ Pa and plateaued in the quasi-equilibrium stage, when the gel network formation had been completed after 555 s.

For the fractal analysis of the kinetic data in terms of the *Dickinson* equation, the following parameters were taken from the rheological measurements:

Table 6-15 Parameters taken from the kinetic data of the ternary system H₂O-LAS-L-Tyr-L-Tyr with a surfactant concentration of 28.70 mM and 6.69 mM L-Tyr-L-Tyr for applying the *Dickinson* equation, according to equation 6-1 (t_g – gelation time at $G'(0)$, $G'(0)$ - average values of G' in the induction stage, $G'(\infty)$ - average values of G' in the quasi-equilibrium stage). The error bars give the standard deviation for the average $G'(0)$ and $G'(\infty)$ values determined for this surfactant concentration.

Parameter	Value
t_g	345 s
$G'(0)$	$1 \times 10^{+00}$ Pa \pm $1 \times 10^{+00}$ Pa
$G'(\infty)$	$2 \times 10^{+03}$ Pa \pm $4 \times 10^{+02}$ Pa

The application of the *Dickinson* equation provided a D_f value of 0.76, which, according to *Huang et al.*^[13], would be related to the formation of a linear (open) network structure. This would describe a network structure made up of entangled fibers.

By using imaging measurements (Chapter 6.5.2.2), it was found that irregular structures of rhomboids, trapezoids, rhombuses and triangles consisting of spherulites could be visualized by using optical microscopy, and the formation of a densely packed network structure of either solid fibers or fiber-like aggregates, was visualized by using cryo-TEM.

The determined D_f value's assignment to an entangled network structure, seems to be more appropriate for the cryo-TEM finding, rather than the optical microscopy measurements.

The D_f values for further surfactant concentrations with samples cooled at a rate of 10 K/min, are summarized in Table 6-16.

The apparent $T_{\text{sol-gel}}$ values for a cooling rate of 10 K/min, mark the beginning of the gelation process and are related to the transition from the induction to the gelation stage, at t_g .

No clear trend in the $T_{\text{sol-gel}}$ and t_g values for the addition of LAS into the L-Tyr-L-Tyr-in-water system, could be found. The $T_{\text{sol-gel}}$ values ranged between 295 and 312 K, and the t_g values between 250 and 360 s.

The $G'(0)$ values found were between 1×10^{-02} and $3 \times 10^{+00}$ Pa, and the $G'(\infty)$ values between $7 \times 10^{+02}$ and $5 \times 10^{+03}$ Pa.

Application of the *Dickinson* equation produced D_f values of up to 1.1, which did not show a clear trend with an increase in LAS concentration.

Table 6-16 Fractal analysis of the kinetic data of the ternary system H₂O-LAS-L-Tyr-L-Tyr with 6.69 mM L-Tyr-L-Tyr and varied surfactant concentrations, acquired by dynamic rheological measurements, in terms of the *Dickinson* equation, according to equation 6-1. The prepared samples were transferred into the rheometer at 353 K and were cooled to 293 K at a rate of 10 K/min ($T_{\text{sol-gel}}$ - apparent sol-gel transition temperature for a cooling rate of 10 K/min, $G'(0)$ - average values of G' in the induction stage, $G'(\infty)$ - average values of G' in the quasi-equilibrium stage, t_g - gelation time at $G'(0)$ and t_{gelation} - difference of the gelation time at $G'(\infty)$ and $G'(0)$). The error bars give the standard deviation for the average $G'(0)$ and $G'(\infty)$ values determined for each surfactant concentration.

c / mM	$T_{\text{sol-gel}} /$ K	$t_g /$ s	$G'(0) /$ Pa	$G'(\infty) /$ Pa	D_f	$t_{\text{gelation}} /$ s
0.29	309	265	$8 \times 10^{-01} \pm 3 \times 10^{-01}$	$3 \times 10^{+03} \pm 5 \times 10^{+02}$	0.97	320
0.86	307	280	$2 \times 10^{+00} \pm 8 \times 10^{-01}$	$2 \times 10^{+03} \pm 4 \times 10^{+02}$	0.96	285
1.72	312	250	$2 \times 10^{-01} \pm 5 \times 10^{-02}$	$4 \times 10^{+03} \pm 8 \times 10^{+02}$	0.94	320
2.30	307	270	$1 \times 10^{-02} \pm 2 \times 10^{-01}$	$2 \times 10^{+03} \pm 6 \times 10^{+02}$	0.96	390
2.87	305	270	$3 \times 10^{+00} \pm 1 \times 10^{+00}$	$5 \times 10^{+03} \pm 5 \times 10^{+02}$	1.06	245
4.02	310	265	$2 \times 10^{-02} \pm 1 \times 10^{-02}$	$4 \times 10^{+03} \pm 6 \times 10^{+02}$	1.12	245
7.17	306	290	$6 \times 10^{-01} \pm 3 \times 10^{-01}$	$1 \times 10^{+03} \pm 8 \times 10^{+02}$	1.02	500
14.35	295	360	$9 \times 10^{-02} \pm 5 \times 10^{-02}$	$7 \times 10^{+02} \pm 1 \times 10^{+02}$	1.05	280
20.09	300	325	$2 \times 10^{-01} \pm 1 \times 10^{-01}$	$1 \times 10^{+03} \pm 2 \times 10^{+02}$	1.07	390
28.70	298	345	$1 \times 10^{+00} \pm 1 \times 10^{+00}$	$2 \times 10^{+03} \pm 4 \times 10^{+02}$	0.76	210

From the results, it can be concluded that when cooling the sample at a rate of 10 K/min, no delay in L-Tyr-L-Tyr gel network formation could be found at high LAS concentrations, compared to cooling at a rate of 5 K/min (Chapter 6.5.2.1, Figure 6-56). Interestingly, a minimum of G' value was found during the transition from the induction to the gelation stage, which is shown in Figure 6-65.

For LAS concentrations of up to 4.02 mM, the transition from the induction to the gelation stage was observed between 265 and 270 s and the minimum of G' value at t_g was found between 1×10^{-02} and 8×10^{-01} Pa.

At high surfactant concentrations, above 20.09 mM LAS, the minimum was found between 325 and 345 s, with G' values in a range between 2×10^{-01} and $1 \times 10^{+00}$ Pa.

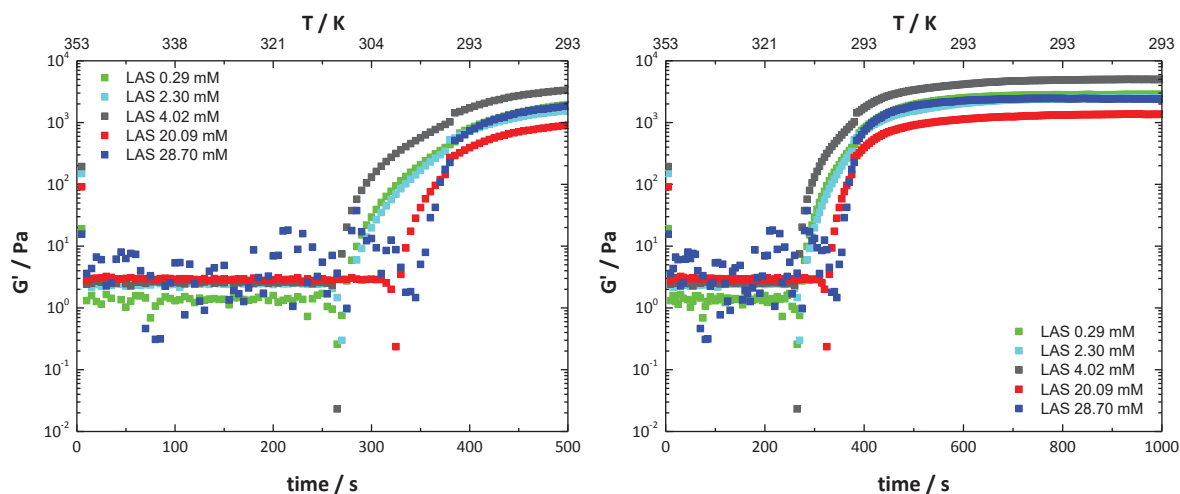


Figure 6-65 Storage modulus G' vs. time (right) and the extract from the diagram (left) of the ternary system H_2O -LAS-L-Tyr-L-Tyr with 6.69 mM L-Tyr-L-Tyr and varied surfactant concentrations. The data were taken from the combination of temperature-sweep and time-sweep measurements. The samples were cooled from 353 to 293 K at a rate of 10 K/min (below the minimum of G' - induction stage, above the minimum of G' - gelation stage).

The minimum of G' value could be due to the following reason: The concentration of gellant monomers is reduced during the aggregation process, which could lead to a momentary minimum of G' value. As a result of the generation of large aggregates with high G' values, the G' value increases rapidly and a minimum appears during the gelation process.

The gelation process in mixtures with LAS was also studied for a cooling rate of 5 K/min, to find out, whether a clear trend could be found for D_f values.

The data used to apply the *Dickinson* equation, are summarized in Table 6-17.

Table 6-17 Fractal analysis of the kinetic data of the ternary system H₂O-LAS-L-Tyr-L-Tyr with 6.69 mM L-Tyr-L-Tyr and varied surfactant concentrations, acquired by dynamic rheological measurements, in terms of the *Dickinson* equation, according to equation 6-1. The prepared samples were transferred into the rheometer at 353 K and were cooled to 293 K at a rate of 5 K/min ($T_{\text{sol-gel}}$ - apparent sol-gel transition temperature for a cooling rate of 5 K/min, $G'(0)$ - average values of G' in the induction stage, $G'(\infty)$ - average values of G' in the quasi-equilibrium stage, t_g - gelation time at $G'(0)$ and t_{gelation} - difference of the gelation time at $G'(\infty)$ and $G'(0)$. The error bars give the standard deviation for the average $G'(0)$ and $G'(\infty)$ values determined for each surfactant concentration.

c / mM	$T_{\text{sol-gel}}$ / K	t_g / s	$G'(0)$ / Pa	$G'(\infty)$ / Pa	D_f	t_{gelation} / s
0.29	302	610	$2 \times 10^{+01} \pm 3 \times 10^{+00}$	$1 \times 10^{+03} \pm 3 \times 10^{+02}$	0.97	320
0.86	305	580	$8 \times 10^{+00} \pm 2 \times 10^{+00}$	$1 \times 10^{+04} \pm 1 \times 10^{+03}$	1.02	250
1.72	307	550	$7 \times 10^{+00} \pm 2 \times 10^{+00}$	$8 \times 10^{+03} \pm 1 \times 10^{+03}$	0.82	280
2.30	304	590	$1 \times 10^{+01} \pm 3 \times 10^{+00}$	$1 \times 10^{+04} \pm 8 \times 10^{+02}$	1.08	320
4.02	303	605	$9 \times 10^{+00} \pm 3 \times 10^{+00}$	$3 \times 10^{+03} \pm 6 \times 10^{+02}$	1.18	345
7.17	304	585	$3 \times 10^{+01} \pm 8 \times 10^{+00}$	$5 \times 10^{+03} \pm 2 \times 10^{+03}$	1.13	175
14.35	304	590	$9 \times 10^{-02} \pm 3 \times 10^{-02}$	$4 \times 10^{+03} \pm 2 \times 10^{+03}$	1.11	320

The $T_{\text{sol-gel}}$ values for LAS concentrations of up to 14.35 mM, were found between 302 and 307 K and the t_g values between 550 and 610 s. A clear trend for these values could not be found.

The $G'(0)$ values during the induction stage ranged from 9×10^{-02} to $3 \times 10^{+01}$ Pa, and the $G'(\infty)$ values during the quasi-equilibrium stage, were found between $1 \times 10^{+03}$ and $1 \times 10^{+04}$ Pa.

The gelation stage of the gelation process was completed at between 175 and 345 s and D_f values of up to 1.2 were found, which, according to *Huang et al.*^[13], indicates the formation of a linear (open) network structure. This would describe a network structure made up of entangled fibers.

As the effect of LAS molecules on the kinetics of gel network formation could not be determined by applying the *Dickinson* equation, the gelation stage of the gelation process was investigated using log-linear and linear-linear plots of the G' values against time.

To ensure the same conditions, the gelation time, t_g , at which the transition from the induction to the gelation stage occurred, was taken as 5 s for each surfactant concentration studied.

The log-linear and linear-linear plots of the evolution of G' values for cooling at a rate of 10 K/min, are presented in Figure 6-66.

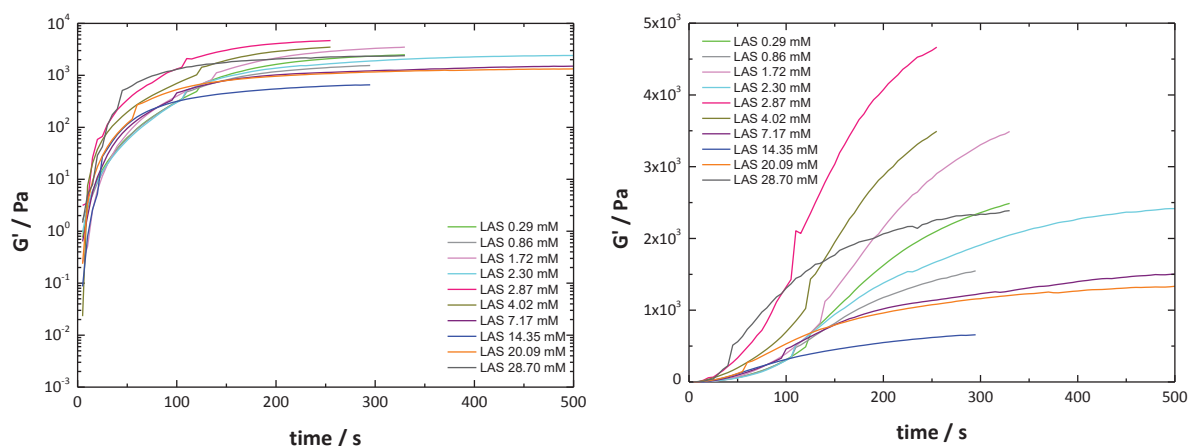


Figure 6-66 Log-linear (left) and linear-linear plots (right) of the storage modulus G' vs. time during the gelation stage of the ternary system H_2O -LAS-L-Tyr-L-Tyr with 6.69 mM L-Tyr-L-Tyr and varied surfactant concentrations, measured with oscillating shear rheometry, at a constant strain of 0.05 %, frequency of 1 Hz, and a cooling rate of 10 K/min, using a parallel plate geometry, with a gap of 800 μm .

The G' values increased with the time during the gelation stage. At the beginning of the gelation stage, $t = 0$, the G' values ranged from 2×10^{-02} to $1 \times 10^{+00}$ Pa for a LAS concentration of up to 28.70 mM and, with increasing time, the values plateaued between $7 \times 10^{+02}$ and $5 \times 10^{+03}$ Pa.

In the linear-linear plot, it can clearly be seen that the increase in G' values occurred at different rates when the LAS concentration was varied. However, no clear trend for the influence of the LAS concentration on the gelation rate, could be found.

The lowest G' value which was obtained for all the LAS concentrations studied, was $7 \times 10^{+02}$ Pa. To obtain a deeper understanding of the influence of surfactant molecules on the gelation rate, the t_{-t_g} values were taken when a G' value of $7 \times 10^{+02}$ Pa was achieved.

This was also done for a 5 K/min cooling rate. The lowest G' value to be found was $8 \times 10^{+02}$ Pa.

The values are summarized in Table 6-18.

Table 6-18 Rheological data applied from the analysis of the kinetic data of the ternary system H₂O-LAS-L-Tyr-L-Tyr with a gellant concentration of 6.69 mM and varied surfactant concentrations, measured at cooling rates of 5 and 10 K/min. For the determination of the t_{-t_g} values, the time was taken at which the same G' value was obtained for all surfactant concentrations (t_g - gelation time at $G'(0)$, fixed G' value for a cooling rate of 5 K/min – $8 \times 10^{+02}$ Pa and fixed G' value by cooling at a rate of 10 K/min – $7 \times 10^{+02}$ Pa).

c / mM	t _{-t_g} for a cooling rate of ... / s	
	5 K/min	10 K/min
0.29	215	120
0.86	60	125
1.72	95	120
2.30	55	120
2.87	305	65
4.02	105	90
7.17	50	120
14.35	225	275
20.09	-	115
28.70	-	50

When cooling the sample at a rate of 5 K/min, a G' value of $8 \times 10^{+02}$ Pa was reached between 50 and 305 s, for a LAS concentration of up to 14.35 mM. At a cooling rate of 10 K/min, a G' value of $7 \times 10^{+02}$ Pa was achieved, between 50 and 275 s, for surfactant concentrations of up to 28.70 mM.

A clear trend for the influence of varied LAS concentrations on the gelation rate within the gelation stage could not be found for either cooling rate.

In order to find out whether the quasi-equilibrium stage of the gelation process is influenced by the addition of LAS molecules to the L-Tyr-L-Tyr-in-water system, the $G'(\infty)$ values were plotted against the surfactant concentration, as shown in Figure 6-67.

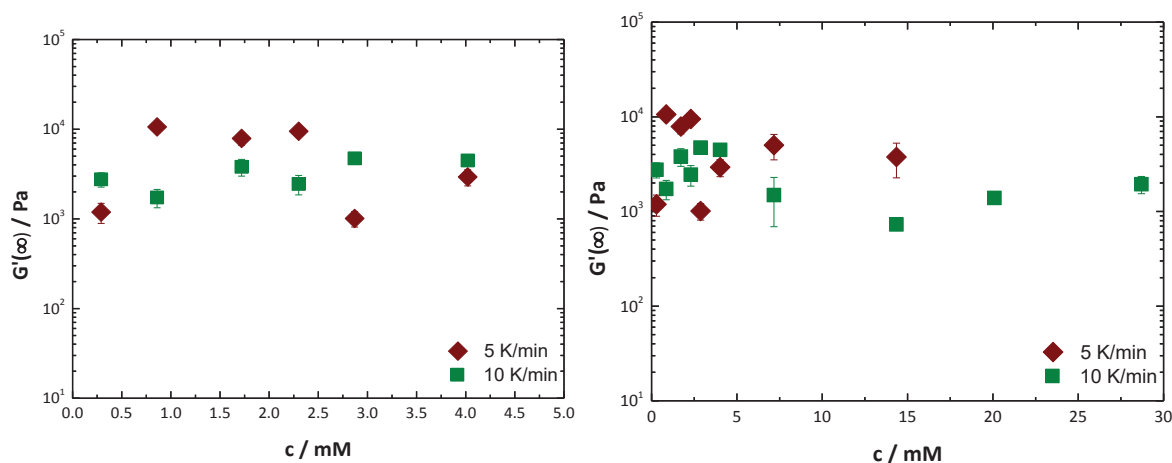


Figure 6-67 Storage modulus in the quasi-equilibrium stage $G'(\infty)$ (right) and the extract from the diagram at lower surfactant concentrations (left) of the ternary system H_2O -LAS-L-Tyr-L-Tyr with 6.69 mM L-Tyr-L-Tyr as a function of LAS concentration, measured at 293 K with oscillating shear rheometry, at a frequency of 1 Hz, and a strain of 0.05 %, using a parallel plate geometry, with a gap of 800 μm . The prepared sample was transferred into the rheometer at 353 K and was cooled to 293 K with 5 and 10 K/min. The error bars give the standard deviation for the average $G'(\infty)$ values determined for each surfactant concentration.

When cooling at a rate of 5 K/min, the $G'(\infty)$ values ranged from $1 \times 10^{+03}$ to $1 \times 10^{+04}$ Pa for a surfactant concentration of up to 14.35 mM and no correlation between $G'(\infty)$ values and an increase in the LAS concentration could be found.

For LAS concentrations of up to 28.70 mM, the values were in a range between $7 \times 10^{+02}$ and $5 \times 10^{+03}$ Pa for a fast cooling rate, 10 K/min, and as with the lower cooling rate, there was no correlation with the increase in surfactant concentration.

The $G'(\infty)$ values found were slightly greater when cooling at a rate of 5 K/min, than at 10 K/min, however due to high scattering, the values should be regarded with caution.

To summarize the key findings on the gelation properties of L-Tyr-L-Tyr, it was found that reproducible gel networks were only formed in mixtures with LAS molecules.

The three stages of the gelation process, the induction, gelation, and quasi-equilibrium stages were investigated in the presence of LAS.

In the induction stage, the transitions from the sol to the gel phase, or from the induction to the gelation stage, were delayed by high surfactant concentrations with cooling at a rate of 5 K/min. No delay in gel formation was observed with fast cooling, of 10 K/min. From these studies of the effect of LAS molecules on the gelation stage, it was shown that the gelation rate found was within similar $t-t_g$ ranges at different cooling rates. No clear correlation was found between the increase in the LAS concentration and the gelation rate.

When the gel network formation was completed during the quasi-equilibrium stage, slightly higher $G'(\infty)$ values were obtained by cooling the sample at a rate of 5 K/min, rather than 10 K/min. The values showed high scattering and varied between $1 \times 10^{+03}$ and $1 \times 10^{+04}$ Pa for slow cooling, and between $7 \times 10^{+02}$ and $5 \times 10^{+03}$ Pa for fast cooling. No clear trend was found for the $G'(\infty)$ values, which correlates with the cryo-TEM images in which the formation of a fine gel network structure made up of either solid fibers or fiber-like aggregates, with a thickness of up to 60 nm, was found. The morphology did not change with an increase in the LAS concentration.

It could be concluded that if the induction and gelation stages are not highly influenced by surfactant molecules, then a similar behavior can also be observed in the quasi-equilibrium stage, when the gel network formation is completed.

6.6. Comparison of the Gelation Behavior of DBC vs. L-Tyr-L-Tyr

The gelation processes of DBC-in-water and L-Tyr-L-Tyr-in-water systems, in the presence of LAS above the critical gelation concentration, were compared with one another to identify the differences or similarities between the two gelling agents.

The gel network formation was studied at pH 3.5 and under the same measurement conditions. When comparing the studies of the DBC-in-water and L-Tyr-L-Tyr-in-water systems, it was found that DBC was able to form reproducible gel networks in a water system. Alternatively, the gelation behavior of the L-Tyr-L-Tyr-in-water system was randomly driven, so that either a gel was formed, or the solution was precipitated, by cooling the sample.

This suggests that because DBC is a more hydrophilic compound than L-Tyr-L-Tyr, as it consists of hydrophilic cysteine units rather than hydrophobic tyrosine units, DBC could be dissolved in water by heating better than L-Tyr-L-Tyr, providing reproducible gelation. Moreover, L-Tyr-L-Tyr seems to disperse in water rather than completely dissolving, which could be the reason for its random gelation behavior (for the structure of DBC, refer to Chapter 6.1.2.3, Figure 6-16 and for that of L-Tyr-L-Tyr, refer to Chapter 6.5, Figure 6-51).

When mixed with LAS, both gelling agents formed reproducible gel networks; the three stages of the gelation process were studied by using rheology and the gels' morphology was visualized using optical and cryo-TEM microscopy.

To determine the apparent $T_{\text{sol-gel}}$ values for different cooling rates, the transition from the sol to the gel phase was investigated, which is taken as the transition from the induction to the gelation stage.

The phase transition temperatures for the ternary systems H_2O -LAS-DBC and H_2O -LAS-L-Tyr-L-Tyr, with a gellant concentration of 6.69 mM and varied surfactant concentrations, determined at a cooling rate of 10 K/min, are summarized in Figure 6-68.

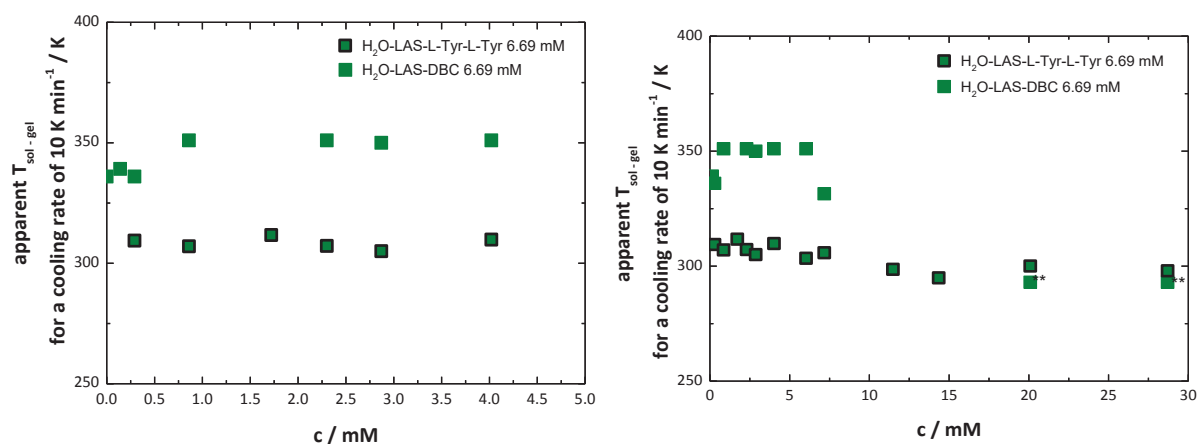


Figure 6-68 Apparent $T_{\text{sol-gel}}$ values for a cooling rate of 10 K/min (right) and the extract from the diagram at lower surfactant concentrations (left) of the ternary systems H_2O -LAS-DBC and H_2O -LAS-L-Tyr-L-Tyr with a gellant concentration of 6.69 mM and varied surfactant concentrations, measured with oscillating shear rheometry, at a constant frequency of 1 Hz, and a shear strain of 0.05 %, using a parallel plate geometry, with a gap of 800 μm . Symbols marked with a double asterisk, **, indicate the temperature at which the gelation occurred by a long-term measurement.

For LAS concentrations of up to 7.17 mM, the apparent $T_{\text{sol-gel}}$ values for the DBC-in-LAS system, at a cooling rate of 10 K/min, were higher than those of the L-Tyr-L-Tyr-in-LAS system. The values were between 331 and 351 K for DBC, and between 297 and 311 K for L-Tyr-L-Tyr. The differences between the $T_{\text{sol-gel}}$ values for the two ternary systems became lower at higher concentrations. For the DBC-in-LAS system, the apparent $T_{\text{sol-gel}}$ value at a cooling rate of 10 K/min, was 293 K, which was the temperature at which the gelation process was monitored by a long-term measurement, as no gelation occurred during the temperature-sweep measurement by cooling from 353 to 293 K. For the ternary system H₂O-LAS-L-Tyr-L-Tyr, the values ranged from 298 to 300 K.

To summarize, for LAS concentrations of up to 7.17 mM the transition from the sol to the gel phase occurred at higher temperatures in the DBC-in-LAS system, than in the L-Tyr-L-Tyr-in-LAS system. However, the opposite behavior was found at high surfactant concentrations, as the transition from the sol to the gel phase occurred at a lower temperature for DBC, than in the L-Tyr-L-Tyr ternary system.

In addition, the DBC gel network formation was delayed. No delay was found when cooling L-Tyr-L-Tyr in a mixture with LAS at high surfactant concentrations, at a rate of 10 K/min.

However, when cooled slowly, at 5 K/min, the delay was also observed for the ternary system H₂O-LAS-L-Tyr-L-Tyr at a surfactant concentration of 20.09 mM, which is shown clearly in Figure 6-69.

It was found that for LAS concentrations of up to 7.17 mM, the DBC gelation process started at least below a temperature of 338 K, however the gelation process of L-Tyr-L-Tyr started at a temperature below 304 K. At this temperature, the DBC gelation process was completed and the G' values ranged from $4 \times 10^{+02}$ to $2 \times 10^{+03}$ Pa.

Above this concentration, no gel network formation occurred within the given timeframe for both gelling agents, and G' values of $1 \times 10^{+00}$ Pa were determined.

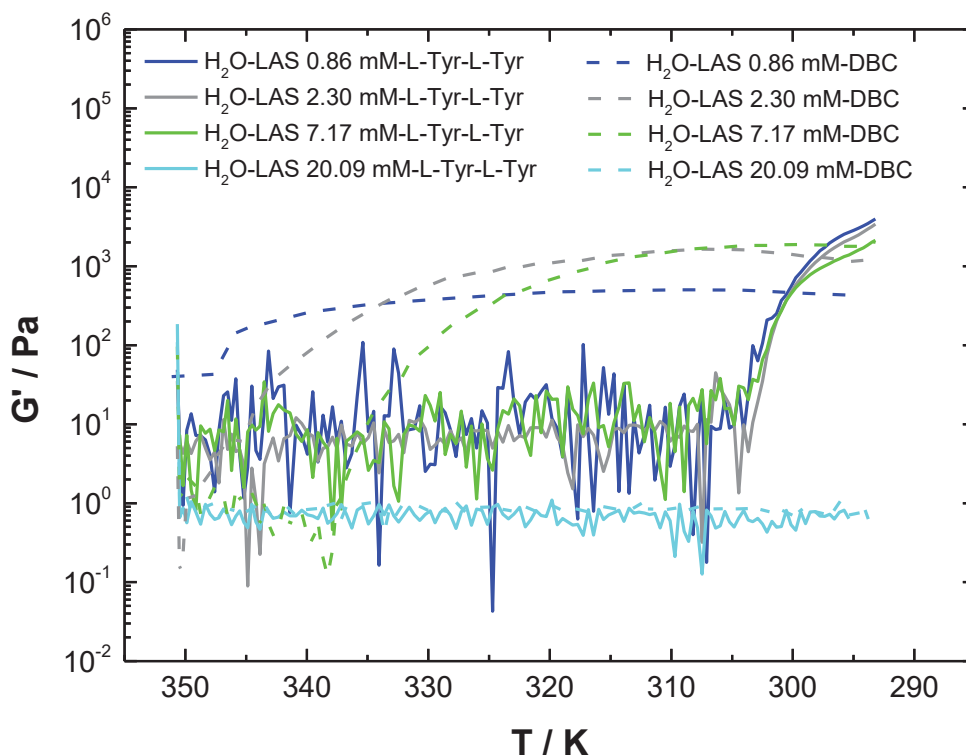


Figure 6-69 Measurement of the temperature dependency of the storage modulus G' of the ternary systems H_2O -LAS-DBC and H_2O -LAS-L-Tyr-L-Tyr with a gellant concentration of 6.69 mM and varied surfactant concentrations, measured with a parallel plate geometry, and a gap of 800 μm at 293 K with oscillating shear rheometry at a constant frequency of 1 Hz, a shear strain of 0.05 %, and a cooling rate of 5 K/min.

The gelation stage of the gelation process was studied by applying the *Dickinson* equation, according to equation 6-1, and by determining the $t-t_g$ values for the lowest G' value to be achieved by all the LAS concentrations studied.

Surprisingly, a minimum of G' value was found for both ternary systems, during the transition from the induction to the gelation stage, as depicted in Figure 6-70.

It was found that the minimum of G' value for the DBC-in-LAS system was more obvious than that of the L-Tyr-L-Tyr-in-LAS system.

The minimum of G' values for the DBC ternary system were found between 8×10^{-03} and 2×10^{-02} Pa, and those of the L-Tyr-L-Tyr ternary system ranged between 2×10^{-01} and $1 \times 10^{+00}$ Pa.

This suggests that the L-Tyr-L-Tyr gel network is made up of solid fibers, rather than fiber-like aggregates. During the transition from the induction to the gelation stage, the decrease in the concentration of individual gellant monomers could have been more superposed by the formation of short fibers, rather than aggregates, so that the minimum of G' value for the ternary system H₂O-LAS-L-Tyr-L-Tyr is less pronounced than that of the DBC-in-LAS system.

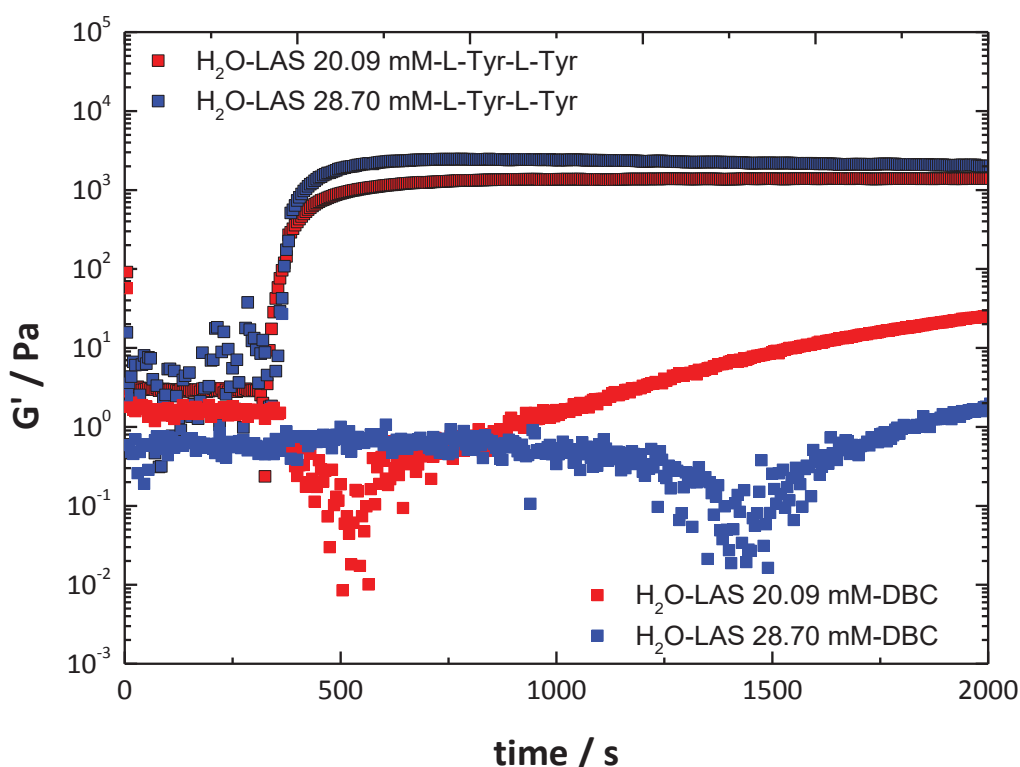


Figure 6-70 Storage modulus G' vs. time of the ternary systems H₂O-LAS-DBC and H₂O-LAS-L-Tyr-L-Tyr with a gellant concentration of 6.69 mM and varied surfactant concentrations for the illustration of the minimum during the gelation process. The data were taken from the combination of temperature-sweep and time-sweep measurements. The samples were cooled from 353 to 293 K at a rate of 10 K/min (below the minimum of G' - induction stage, above the minimum of G' - gelation stage).

The analysis of the kinetic data, in terms of the *Dickinson* equation, of the ternary systems H₂O-LAS-DBC and H₂O-LAS-L-Tyr-L-Tyr with a gellant concentration of 6.69 mM and varied surfactant concentrations, are summarized in Table 6-19.

Table 6-19 Fractal analysis of the kinetic data of the ternary systems H₂O-LAS-DBC and H₂O-LAS-L-Tyr-L-Tyr with a gellant concentration of 6.69 mM and varied surfactant concentrations, acquired by temperature and time-sweep measurements, in terms of the *Dickinson* equation, according to equation 6-1. The prepared samples were transferred into the rheometer at 353 K and were cooled to 293 K at a rate of 10 K/min ($T_{\text{sol-gel}}$ - apparent sol-gel transition temperature for a cooling rate of 10 K/min, t_g - gelation time at $G'(0)$ and t_{gelation} - difference of the gelation time at $G'(\infty)$ and $G'(0)$. Symbols marked with a double asterisk, **, indicate the temperature at which the gelation occurred by a long-term measurement at a constant temperature).

c / mM	$T_{\text{sol-gel}}$ / K		t_g / s		t_{gelation} / s		D_f	
	DBC	L-Tyr-L-Tyr	DBC	L-Tyr-L-Tyr	DBC	L-Tyr-L-Tyr	DBC	L-Tyr-L-Tyr
0.29	336	309	90	265	200	320	0.90	0.97
2.30	351	307	5	270	221	390	1.08	0.96
7.17	331	306	120	290	265	500	0.81	1.02
20.09	293**	300	505	325	7452	390	0.84	1.07

For surfactant concentrations of up to 7.17 mM, the transition from the sol to the gel phase of the ternary system H₂O-LAS-DBC occurred at higher temperatures than in the L-Tyr-L-Tyr-in-LAS system.

When LAS was added to the DBC-in-water system, at LAS concentrations of up to 7.17 mM, the gelation time, t_g , ranged between 5 and 120 s, and between 265 and 290 s for the ternary system H₂O-LAS-L-Tyr-L-Tyr.

Above this concentration, the transition from the induction to the gelation stage of the DBC-in-LAS system occurred at higher t_g values than in the L-Tyr-L-Tyr-in-LAS system. Furthermore, DBC gel network formation was delayed at high LAS concentrations, as shown by the apparent $T_{\text{sol-gel}}$ value of 293 K at a cooling rate of 10 K/min.

It can be concluded that at low surfactant concentrations, the DBC ternary system's gelation process started faster than that of the L-Tyr-L-Tyr ternary system, and at high LAS concentrations, the transition from the induction to the gelation stage occurred earlier in the ternary system H₂O-LAS-L-Tyr-L-Tyr, than in the DBC-in-LAS system.

For LAS concentrations of up to 7.17 mM, the transition from the gelation to the quasi-equilibrium stage occurred faster in the DBC-in-LAS system than in the L-Tyr-L-Tyr-in-LAS system, as shown by the lower t_{gelation} values for the DBC-in-LAS system, compared to the L-Tyr-L-Tyr ternary system. The opposite behavior was found at high LAS concentrations.

By applying the *Dickinson* equation, D_f values of up to 1.1 were found for both gelling agents, which would indicate a linear (open) network structure. Determining the D_f value did not show a clear trend for the influence of LAS molecules on the gelation stage of the gelation process.

Therefore, the increase in the G' values during the gelation stage, was considered for a constant t_g value of 5 s in order to gain insights into the gelation rates of both gelling agents with increasing LAS concentrations.

The evolution of the G' values during the gelation stage of the gelation process, is summarized in Figure 6-71 for the ternary systems H₂O-LAS-DBC and H₂O-LAS-L-Tyr-L-Tyr.

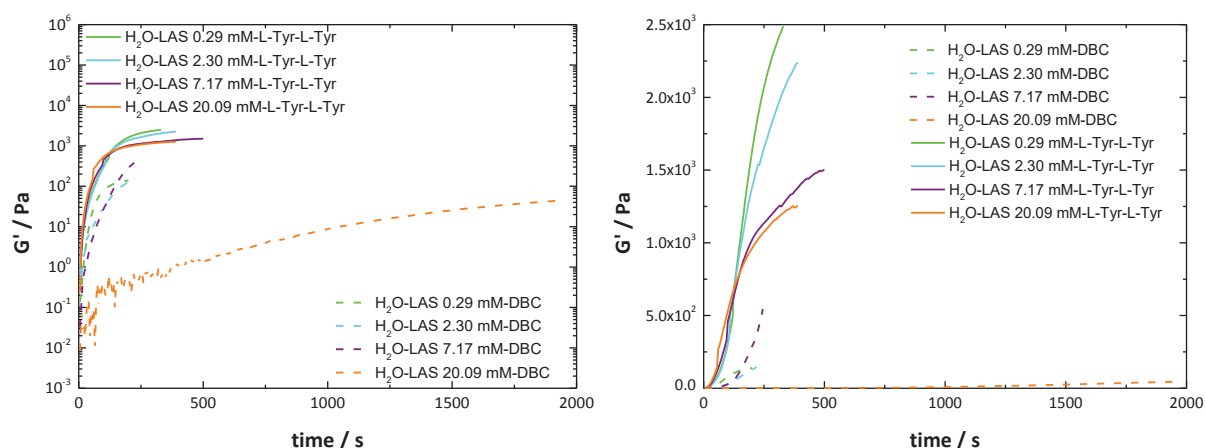


Figure 6-71 Log-linear (left) and linear-linear plots (right) of the storage modulus G' vs. time during the gelation stage of the ternary systems H₂O-LAS-DBC and H₂O-LAS-L-Tyr-L-Tyr with a gellant concentration of 6.69 mM and varied LAS concentrations, measured with oscillating shear rheometry, at a constant strain of 0.05 %, frequency of 1 Hz, and a cooling rate of 10 K/min, using a parallel plate geometry, with a gap of 800 μm .

By comparing the increase in the G' values of both gelling agents in the presence of LAS, it was clearly shown that higher gelation rates occurred for the L-Tyr-L-Tyr-in-LAS than for the DBC-in-LAS system, as demonstrated by the steeper increase in the L-Tyr-L-Tyr ternary's G' values, compared to those of the DBC ternary system.

The DBC gelation rate decreased with increasing LAS concentrations. The gelation rate for the ternary system H₂O-LAS-L-Tyr-L-Tyr was found to be identical of up to 130 s, and then it decreased slightly as the LAS concentration increased.

The lowest G' value that was achieved by both ternary systems, was $4 \times 10^{+01}$ Pa. The $t-t_g$ values were taken at this G' value in order to study the influence of LAS molecules on the gelling agents' gelation rates.

The data are summarized in Table 6-20.

Table 6-20 Rheological data applied from the analysis of the kinetic data of the ternary systems H₂O-LAS-DBC and H₂O-LAS-L-Tyr-L-Tyr with a gellant concentration of 6.69 mM and varied surfactant concentrations, measured at a cooling rate of 10 K/min. For the determination of the data for $t-t_g$, the time was taken at which the same G' value was obtained for all surfactant concentrations in the presence of the two gelling agents for varied surfactant concentrations (t_g - gelation time at $G'(0)$, fixed G' value – $4 \times 10^{+01}$ Pa).

c / mM	t-t _g / s	
	DBC	L-Tyr-L-Tyr
0.29	70	45
2.30	115	45
7.17	115	35
20.09	1855	30

The $t-t_g$ values increased from 70 to 1855 s with increasing LAS concentration, for the ternary system H₂O-LAS-DBC and were between 30 and 45 s for the L-Tyr-L-Tyr-in-LAS system.

A comparison of both gelling agents' gelation rates clearly showed that the gelation rate of L-Tyr-L-Tyr was greater than that of DBC, as shown by the lower $t-t_g$ values at which a G' value of $4 \times 10^{+01}$ Pa was achieved.

In a mixture with 20.09 mM LAS, the difference between the gelling agents' t_g values became more pronounced than it had been below this concentration.

It can be concluded that the addition of surfactant molecules has more influence on the gelation rate of DBC than on that of L-Tyr-L-Tyr, which became more evident at high LAS concentrations.

As the gelation rate of L-Tyr-L-Tyr was found to be greater than that of DBC, the hypothesis that the L-Tyr-L-Tyr network structure consists of solid fibers rather than fiber-like aggregates, appears to have been confirmed. The growth of solid fibers could be faster than the connection of aggregates into a fiber-like network structure.

In order to compare the influence of surfactant molecules on the quasi-equilibrium stage of the gelling agents, i.e. when the gel network formation was completed, the $G'(\infty)$ values were plotted against the DBC and L-Tyr-L-Tyr ternary systems' LAS concentrations, as presented in Figure 6-72.

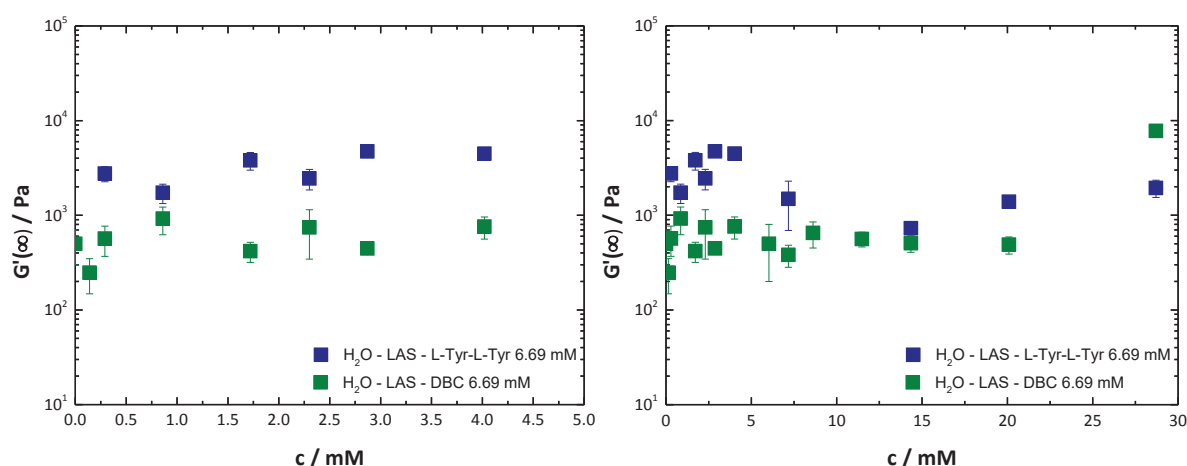


Figure 6-72 Storage modulus in the quasi-equilibrium stage $G'(\infty)$ (right) and the extract from the diagram at lower surfactant concentrations (left) of the ternary systems H₂O-LAS-DBC and H₂O-LAS-L-Tyr-L-Tyr with a gellant concentration of 6.69 mM as a function of LAS concentration, measured at 293 K, with oscillating shear rheometry at a frequency of 1 Hz, and a strain of 0.05 %, using a parallel plate geometry, with a gap of 800 μ m. The prepared sample was transferred into the rheometer at 353 K and was cooled to 293 K with 10 K/min. The error bars give the standard deviation for the average $G'(\infty)$ values determined for each surfactant concentration.

For LAS concentrations of up to 20.09 mM, the $G'(\infty)$ values for L-Tyr-L-Tyr were higher than those of DBC. The values ranged from $7 \times 10^{+02}$ to $5 \times 10^{+03}$ Pa, for the L-Tyr-L-Tyr-in-LAS system, and from $3 \times 10^{+02}$ to $1 \times 10^{+03}$ Pa, for the DBC-in-LAS system.

The opposite behavior was found in a mixture with 28.70 mM LAS, as the DBC $G'(\infty)$ value was greater than that of the L-Tyr-L-Tyr ternary system.

It can be concluded that, for LAS concentrations of up to 20.09 mM, a finer gel network could be formed by L-Tyr-L-Tyr, compared to DBC. This correlates with the cryo-TEM images as the thickness of the solid fibers or fiber-like aggregates of the L-Tyr-L-Tyr ternary system, was found to be lower than those of the DBC-in-LAS system. The thickness was found to be up to 60 nm for the L-Tyr-L-Tyr ternary system, and up to 280 nm for the DBC ternary system (Chapters 6.2.2.3 and 6.5.2.2).

The comparison of the two gelling agents, showed that LAS molecules had more influence on the DBC induction, gelation, and quasi-equilibrium stages, than on those of L-Tyr-L-Tyr. This could be attributed to the formation of fiber-like aggregates in the case of DBC, which seem to be more sensitive to surfactant molecules than the network structure composed of solid fibers, in the case of L-Tyr-L-Tyr.

This was concluded from the following results: 1) The gel network formation of DBC at high LAS concentrations, was delayed by being cooled at different rates, rather than only at a rate of 5 K/min, 2) the minimum of G' value during the transition from the induction to the gelation stage, was more pronounced for DBC than for the L-Tyr-L-Tyr ternary system, 3) the gelation rate of DBC decreased with an increase of the LAS concentration, whereas no clear trend was found for the L-Tyr-L-Tyr-in-LAS system, and 4) the $G'(\infty)$ values of DBC increased at high LAS concentrations, whereas no clear trend was found for L-Tyr-L-Tyr with an increase in the LAS concentration.

7 Outlook

The present study has shown a new way for a better understanding of the gelation properties of hydrogellants in the presence of surfactant molecules as systematical investigations were performed for two different types of LMWGs under defined shear and preparation conditions.

In addition, predictions for the gelation process in the presence of surfactant molecules can be made.

For the development of the mutual understanding of the gelation properties of hydrogellants in the presence of surfactant molecules, it would be beneficial, to study the influence of further parameters, such as the pH value or the electrolyte content.

Moreover, the proposed mechanism for gel network formation in a mixture with surfactant molecules should be verified by further investigations using rheology and imaging measurements.

It could also be interesting to find out whether the LMWGs' gelation ability could be enhanced by modifying the chemical structures, such as by the addition of further carboxyl or hydroxyl groups^[73].

For applications, it would be interesting to determine whether a surfactant system could be gelled by using LMWGs in such a way that the strength of the gel could be adjusted in a defined way.

As a further aspect, the gels' self-healing character could be studied by using rheology^[19], which is highly desirable for biological applications^[141]. For this, the gel phase would have to be sheared at high shear rates so that the evolution of the G' values could then be monitored.

Finally, the gel networks' morphology could also be visualized by using atomic force and scanning electron microscopy.

The $T_{\text{sol-gel}}$ values could also be determined by using differential scanning calorimetry (DSC) measurements, to gain insights into the structural behavior.

The studies could be completed with scattering (SAXS - small-angle X-ray scattering, SANS - small-angle neutron scattering) and spectroscopic methods (Fluorescence, UV/VIS, MS, NMR and IR).

8 Abbreviations

Latin abbreviations

c	concentration
cmc	critical micelle concentration
D	diffusion coefficient
d_h	hydrodynamic diameter of micelle
D_f	fractal dimension
G^*	complex modulus
G'	storage modulus
$G'(0)$	average G' values in the induction stage
$G'(\infty)$	average G' values in the quasi-equilibrium stage
G''	loss modulus
h	Planck's constant
I	intensity
i	complex number
k_B	Boltzmann constant
l	distance
m	mass
N_A	Avogadro constant
N_{AGG}	aggregation number
N_M	number of micelles
N_S	number of surfactant molecules
r	radius
T	temperature
t	time

t_g	gelation time
t_{gelation}	difference of the gelation time at $G'(0)$ and $G'(\infty)$
$T_{\text{sol-gel}}$	sol-gel transition temperature
v	velocity
V_M	volume of micelle

Greek abbreviations

α	scaling factor
β	correction factor
δ	phase shift angle
γ	wavelength
$\dot{\gamma}$	shear rate
γ_s	shear strain
η	viscosity
θ	scattering angle
σ	surface tension
τ	shear stress
τ_D	delayed time
ω	angular frequency
ψ	scaling exponent

9 List of Figures

Figure 4-1 Schematic illustration of the aggregates formed by surfactant molecules with increasing surfactant concentration or temperature (according to reference [61]).	28
Figure 4-2 Phase behavior study of the binary system H ₂ O-C ₁₂ E ₆ (data were taken from reference [62]) (cmc – critical micelle concentration, W – water, L ₁ – spherical micelles, H ₁ – hexagonal phase, V ₁ – cubic phase, L _α – lamellar phase, S – solid).	29
Figure 4-3 Schematic illustration of the hierarchical self-assembly of low molecular weight gellants (LMWGs) (according to reference [11]).	31
Figure 4-4 Schematic illustration of different types of junctions (according to references [51],[76]–[78]).	32
Figure 4-5 Schematic illustration of the electron beam of a transmission electron microscope (redrawn from reference [93]).	35
Figure 4-6 Visualization of the applied sinusoidal shear strain and shear stress response of samples showing viscous, elastic, and viscoelastic behaviors (according to reference [108]).	39
Figure 4-7 Illustration of the relationship between the complex modulus G*, storage modulus G' and loss modulus G'' (according to reference [108]).	40
Figure 5-8 Illustration of the thermomixer from the company Hettich Benelux and the vial consisting of a pressure relief cap from the company Dunn Labortechnik GmbH.	43
Figure 5-9 Illustration of the components of transmission electron microscope.	44
Figure 5-10 Illustration of the cryogenic working chamber.	44
Figure 5-11 Illustration of a rotational rheometer from Malvern Instruments.	46
Figure 6-12 Storage modulus G' and loss modulus G'' vs. temperature of the 6.69 mM binary system of H ₂ O-DBC measured with oscillating shear rheometry at a constant frequency of 1 Hz, a shear strain of 0.05 %, and a cooling rate of 10 K/min, using a parallel plate geometry with a gap of 800 μm.	49
Figure 6-13 Apparent sol-gel transition temperature for different cooling rates, T _{sol-gel} , vs. cooling rate of the binary system H ₂ O-DBC with 6.69 mM DBC, measured with oscillating shear rheometry at a constant frequency of 1 Hz, and a shear strain of 0.05 %, using a parallel plate geometry with a gap of 800 μm.	50

Figure 6-14 Optical microscopy image of the 6.69 mM binary system of H ₂ O-DBC. The sample was transferred onto the slide at 353 K and was allowed to cool to 298 K. The image was taken after 20 minutes (scale bar = 100 μ m).	51
Figure 6-15 Cryo-TEM image of the 6.69 mM binary system of H ₂ O-DBC. The sample was at first allowed to cool from 363 to 298 K. After standing at 298 K for 5 minutes, the sample was prepared for cryo-TEM.	52
Figure 6-16 Chemical structure of DBC.	54
Figure 6-17 Model calculations of the storage modulus G' vs. time for different D_f values, according to equation 6-3 (left), and fractal analysis of the kinetic data in terms of the <i>Dickinson</i> equation, according to equation 6-1 (right).	58
Figure 6-18 Evolution of the storage modulus G' of the 6.69 mM binary system of H ₂ O-DBC, measured with oscillating shear rheometry at a constant frequency of 1 Hz, a shear strain of 0.05 %, and a cooling rate of 10 K/min, using a parallel plate geometry with a gap of 800 μ m (I - Induction stage, G - Gelation stage, Q - Quasi-equilibrium stage).	59
Figure 6-19 Fractal analysis of the kinetic data in terms of the <i>Dickinson</i> equation, according to equation 6-1, of the 6.69 mM binary system of H ₂ O-DBC, measured with oscillating shear rheometry at a constant frequency of 1 Hz, a shear strain of 0.05 %, and a cooling rate of 10 K/min, using a parallel plate geometry with a gap of 800 μ m.	60
Figure 6-20 Log-log (left) and linear-linear plots (right) of the storage modulus in the quasi-equilibrium stage, $G'(\infty)$, of the binary system H ₂ O-DBC with varied gellant concentrations, measured at 293 K with oscillating shear rheometry, at a frequency of 1 Hz, and a strain of 0.05 %, using a parallel plate geometry with a gap of 800 μ m. The prepared sample was transferred into the rheometer at 353 K and was cooled to 293 K with a rate of 10 K/min.	62
Figure 6-21 Surface tension measurements of the binary system H ₂ O-LAS and the ternary system H ₂ O-LAS-DBC with 1.11 mM DBC and varied LAS concentrations, measured with a <i>Du Nouy</i> ring tensiometer, at 298 K. The samples were prepared individually for each surfactant concentration and adjusted to an initial pH of 3 (red), 5 (green), and 7 (blue).	64
Figure 6-22 Storage modulus G' and loss modulus G'' vs. temperature of the ternary system H ₂ O-LAS-DBC with a surfactant concentration of 7.17 mM and a gellant concentration of 6.69 mM, measured with oscillating shear rheometry, at a constant	

frequency of 1 Hz, a shear strain of 0.05 %, and a cooling rate of 10 K/min, using a parallel plate geometry with a gap of 800 μm	67
Figure 6-23 Apparent $T_{\text{sol-gel}}$ values for different cooling rates of the ternary system H_2O -LAS-DBC with a gellant concentration of 6.69 mM and varied surfactant concentrations, measured with oscillating shear rheometry, at a constant frequency of 1 Hz, a shear strain of 0.05 %, and cooling rates of 5 and 10 K/min, using a parallel plate geometry with a gap of 800 μm . Symbols marked with a double asterisk, **, indicate the temperature at which the gelation occurred by a long-term measurement.	68
Figure 6-24 Measurement of the temperature dependency of the storage modulus G' of the ternary system H_2O -LAS-DBC with a gellant concentration of 6.69 mM and varied surfactant concentrations, measured with a parallel plate geometry and a gap of 800 μm at 293 K with oscillating shear rheometry at a constant frequency of 1 Hz, a shear strain of 0.05 %, and a cooling rate of 5 K/min.	70
Figure 6-25 Correlation function of the binary system H_2O -LAS with a surfactant concentration of 28.70 mM, measured with Zetasizer Nano Series, at 298 K. The measurement was repeated at regular 5-minute intervals. For a clear display, the measurements were recorded after 5, 20, 40 and 60 minutes.....	72
Figure 6-26 Number distribution of the binary system H_2O -LAS with a surfactant concentration of 28.70 mM, measured with Zetasizer Nano Series, at 298 K. The measurement was repeated at regular 5-minute intervals. For a clear display, the measurements were recorded after 5, 20, 40 and 60 minutes.....	73
Figure 6-27 Optical microscopy image of the ternary system H_2O -LAS-DBC with a gellant concentration of 6.69 mM and a surfactant concentration of 0.29 mM. The sample was transferred onto the slide at 353 K and was allowed to cool to 298 K. The image was taken after 20 minutes (scale bar = 100 μm).	75
Figure 6-28 Optical microscopy image of the ternary system H_2O -LAS-DBC with a gellant concentration of 6.69 mM and a surfactant concentration of 20.09 mM. The sample was transferred onto the slide at 353 K and was allowed to cool to 298 K. The image was taken after 180 minutes (scale bar = 100 μm).	75
Figure 6-29 Cryo-TEM image of water.....	77
Figure 6-30 Cryo-TEM image of the binary system H_2O -LAS with a surfactant concentration of 20.09 mM.	78

Figure 6-31 Cryo-TEM image of the binary system H ₂ O-LAS with a surfactant concentration of 28.70 mM.	78
Figure 6-32 Cryo-TEM images of the ternary system H ₂ O-LAS-DBC with a surfactant concentration of 0.29 mM and a gellant concentration of 6.69 mM. The sample was at first allowed to cool from 363 to 298 K. After standing at 298 K for 5 minutes, the sample was prepared for cryo-TEM.	79
Figure 6-33 Cryo-TEM images of the ternary system H ₂ O-LAS-DBC with a surfactant concentration of 20.09 mM and a gellant concentration of 6.69 mM. The sample was at first allowed to cool from 363 to 298 K. After standing at 298 K for 5 minutes, the sample was prepared for cryo-TEM.	80
Figure 6-34 Cryo-TEM image of the ternary system H ₂ O-LAS-DBC with a surfactant concentration of 20.09 mM and a gellant concentration of 6.69 mM. The sample was at first allowed to cool from 363 to 298 K. After standing at 298 K for 60 minutes, the sample was prepared for cryo-TEM.	81
Figure 6-35 Cryo-TEM images of the ternary system H ₂ O-LAS-DBC with a surfactant concentration of 28.70 mM and a gellant concentration of 6.69 mM. The sample was at first allowed to cool from 363 to 298 K. After standing at 298 K for 5 (left) and 60 minutes (right), the sample was prepared for cryo-TEM.	82
Figure 6-36 Evolution of the storage modulus G' of the ternary system H ₂ O-LAS-DBC with 0.29 mM LAS and 6.69 mM DBC, measured with oscillating shear rheometry, at a constant frequency of 1 Hz, a shear strain of 0.05 %, and a cooling rate of 10 K/min, using a parallel plate geometry with a gap of 800 μ m (I- Induction stage, G - Gelation stage, Q - Quasi-equilibrium stage).	84
Figure 6-37 Fractal analysis of the kinetic data in terms of the <i>Dickinson</i> equation, according to equation 6-1, of the ternary system H ₂ O-LAS-DBC with a surfactant concentration of 0.29 mM and a gellant concentration of 6.69 mM, measured with oscillating shear rheometry at a constant frequency of 1 Hz, a shear strain of 0.05 %, and a cooling rate of 10 K/min, using a parallel plate geometry with a gap of 800 μ m.	85
Figure 6-38 Storage modulus G' and loss modulus G'' vs. temperature of the ternary system H ₂ O-LAS-DBC with a surfactant concentration of 28.70 mM and a gellant concentration of 6.69 mM, measured with oscillating shear rheometry, at a constant frequency of 1 Hz, a shear strain of 0.05 %, and a cooling rate of 10 K/min, using a parallel plate geometry with a gap of 800 μ m.	90

- Figure 6-39** Storage modulus G' vs. time (left) and fractal analysis of the kinetic data in terms of the *Dickinson* equation, according to equation 6-1 (right), of the ternary system H_2O -LAS-DBC with 28.70 mM LAS and 6.69 mM DBC, measured with oscillating shear rheometry, at a constant strain of 0.05 %, frequency of 1 Hz, and a cooling rate of 10 K/min, using a parallel plate geometry with a gap of 800 μm (I - Induction stage, G - Gelation stage, Q - Quasi-equilibrium stage). 91
- Figure 6-40** Storage modulus G' vs. time (right) and the extract from the diagram (left) of the ternary system H_2O -LAS-DBC with 6.69 mM DBC and varied LAS concentrations, for the illustration of the minimum during the gelation process. The data were taken from temperature-sweep measurement for a surfactant concentration of 11.48 mM LAS, and from the combination of temperature-sweep and time-sweep measurements, for LAS concentrations above 20.09 mM. The samples were cooled from 353 to 293 K at a rate of 10 K/min (below the minimum of G' - induction stage, above the minimum of G' - gelation stage). 93
- Figure 6-41** Log-linear plot of the storage modulus G' vs. time (right) and the extract from the diagram (left) during the gelation stage of the ternary system H_2O -LAS-DBC with a gellant concentration of 6.69 mM and varied surfactant concentrations, measured with oscillating shear rheometry, at a constant strain of 0.05 %, frequency of 1 Hz, and a cooling rate of 10 K/min, using a parallel plate geometry, with a gap of 800 μm 94
- Figure 6-42** Linear-linear plot of the storage modulus G' vs. time (right) and the extract from the diagram (left) during the gelation stage of the ternary system H_2O -LAS-DBC with a gellant concentration of 6.69 mM and varied surfactant concentrations, measured with oscillating shear rheometry, at a constant strain of 0.05 %, frequency of 1 Hz, and a cooling rate of 10 K/min, using a parallel plate geometry, with a gap of 800 μm 95
- Figure 6-43** Schematic illustration of the gel network formation of the ternary system H_2O - LAS - DBC with 6.69 mM DBC and varied LAS concentration. The $t-t_g$ values were taken from the analysis of the kinetic data, measured at a cooling rate of 10 K/min. For the determination of the $t-t_g$ values, the time was taken at which the same G' value was obtained for all surfactant concentrations (t_g - gelation time, G' value for a cooling rate of 10 K/min – $5 \times 10^{+01}$ Pa). The gelation rate is decreased with the increase of LAS concentration which could be related to the adsorption of surfactant molecules on the surface of the gellant aggregates, leading to a decrease in the interfacial tension

between the gellant aggregates and the water phase, so that a finer gel network could be formed.	98
Figure 6-44 Storage modulus in the induction stage $G'(0)$ (right) and the extract from the diagram at lower surfactant concentrations (left) of the ternary system H_2O -LAS-DBC with a gellant concentration of 6.69 mM, as a function of LAS concentration, measured at 293 K with oscillating shear rheometry at a frequency of 1 Hz, and a strain of 0.05 %, using a parallel plate geometry with a gap of 800 μm . The prepared sample was transferred into the rheometer at 353 K and was cooled to 293 K at rates of 5 and 10 K/min. The error bars give the standard deviation for the average $G'(0)$ values determined for each surfactant concentration.	99
Figure 6-45 Storage modulus in the quasi-equilibrium stage $G'(\infty)$ (right) and the extract from the diagram at lower surfactant concentrations (left) of the ternary system H_2O -LAS-DBC with a gellant concentration of 6.69 mM, as a function of surfactant concentration, measured at 293 K with oscillating shear rheometry at a frequency of 1 Hz, and a strain of 0.05 %, using a parallel plate geometry with a gap of 800 μm . The prepared sample was transferred into the rheometer at 353 K and was cooled to 293 K at rates of 5 and 10 K/min. The error bars give the standard deviation for the average $G'(\infty)$ values determined for each surfactant concentration.	100
Figure 6-46 Surface tension of the ternary system H_2O - $C_{12-18}E_7$ -DBC with a gellant concentration of 0.00 and 1.11 mM and varied surfactant concentrations, measured with a <i>De Nouy</i> ring tensiometer, at 298 K. The samples were prepared individually for each surfactant concentration and adjusted to an initial pH of 5. The values correspond to the first measured value, when the ring get in contact with the surface of the liquid.	103
Figure 6-47 Storage modulus G' and loss modulus G'' vs. temperature of the ternary system H_2O - $C_{12-18}E_7$ -DBC with a surfactant concentration of 0.08 mM and a gellant concentration of 6.69 mM, measured with oscillating shear rheometry at a constant frequency of 1 Hz, a shear strain of 0.05 %, and a cooling rate of 10 K/min, using a parallel plate geometry, with a gap of 800 μm	105
Figure 6-48 Measurement of the temperature dependency of the storage modulus G' of the ternary system H_2O - $C_{12-18}E_7$ -DBC with a gellant concentration of 6.69 mM and varied surfactant concentrations, measured with a parallel plate geometry, and a gap of 800 μm , at 293 K with oscillating shear rheometry at a constant frequency of 1 Hz, a shear strain of 0.05 %, and a cooling rate of 10 K/min.	106

Figure 6-49 Storage modulus in the quasi-equilibrium stage $G'(\infty)$ of the ternary system $\text{H}_2\text{O}-\text{C}_{12-18}\text{E}_7\text{-DBC}$ with 6.69 mM DBC as a function of surfactant concentration, measured at 293 K with oscillating shear rheometry, at a frequency of 1 Hz, and a strain of 0.05 %, using a parallel plate geometry with a gap of 800 μm . The prepared sample was transferred into the rheometer at 353 K and was cooled to 293 K at a rate of 10 K/min. The error bars give the standard deviation for the average $G'(\infty)$ values determined for each surfactant concentration.	109
Figure 6-50 Storage modulus in the quasi-equilibrium stage $G'(\infty)$ vs. surfactant concentration of the ternary systems $\text{H}_2\text{O}-\text{C}_{12-18}\text{E}_7\text{-DBC}$ and $\text{H}_2\text{O}-\text{LAS}-\text{DBC}$ with 6.69 mM DBC, measured at 293 K with oscillating shear rheometry, at a frequency of 1 Hz, and a strain of 0.05 %, using a parallel plate geometry, with a gap of 800 μm . The prepared sample was transferred into the rheometer at 353 K and was cooled to 293 K at a rate of 10 K/min. The error bars give the standard deviation for the average $G'(\infty)$ values determined for each surfactant concentration.	112
Figure 6-51 Chemical structure of L-Tyr-L-Tyr.	114
Figure 6-52 Storage modulus G' and loss modulus G'' vs. temperature of the 6.69 mM binary system of $\text{H}_2\text{O}-\text{L-Tyr-L-Tyr}$, measured with oscillating shear rheometry, at a constant frequency of 1 Hz, a shear strain of 0.05 %, and a cooling rate of 10 K/min, using a parallel plate geometry, with a gap of 800 μm	115
Figure 6-53 Optical microscopy image of the binary system $\text{H}_2\text{O}-\text{L-Tyr-L-Tyr}$ with a gellant concentration of 6.69 mM. The sample was transferred onto the slide at 353 K and was allowed to cool to 298 K. The image was taken after 20 minutes (scale bar = 100 μm).	116
Figure 6-54 Storage modulus G' and loss modulus G'' vs. temperature of the ternary system $\text{H}_2\text{O}-\text{LAS}-\text{L-Tyr-L-Tyr}$ with a surfactant concentration of 7.17 mM and a gellant concentration of 6.69 mM, measured with oscillating shear rheometry, at a constant frequency of 1 Hz, a shear strain of 0.05 %, and a cooling rate of 10 K/min, using a parallel plate geometry, with a gap of 800 μm	117
Figure 6-55 Apparent $T_{\text{sol-gel}}$ values for different cooling rates (right) and the extract from the diagram at lower surfactant concentrations (left) of the ternary system $\text{H}_2\text{O}-\text{LAS}-\text{L-Tyr-L-Tyr}$ with 6.69 mM L-Tyr-L-Tyr and varied LAS concentrations, measured with oscillating shear rheometry, at a constant frequency of 1 Hz, a shear strain of 0.05 %, and cooling rates of 5 and 10 K/min, using a parallel plate geometry,	

with a gap of 800 μm . Symbols marked with a double asterisk, **, indicate the temperature at which the gelation occurred by a long-term measurement.	119
Figure 6-56 Measurement of the temperature dependency of the storage modulus G' of the ternary system H_2O -LAS-L-Tyr-L-Tyr with a gellant concentration of 6.69 mM and varied surfactant concentrations, measured with a parallel plate geometry, and a gap of 800 μm , at 293 K with oscillating shear rheometry, at a constant frequency of 1 Hz, a shear strain of 0.05 %, and a cooling rate of 5 K/min.	120
Figure 6-57 Optical microscopy image of the ternary system H_2O -LAS-L-Tyr-L-Tyr with a gellant concentration of 6.69 mM and a surfactant concentration of 0.29 mM. The sample was transferred onto the slide at 353 K and was allowed to cool to 298 K. The image was taken after 20 minutes (scale bar = 100 μm).	121
Figure 6-58 Optical microscopy image of the ternary system H_2O -LAS-L-Tyr-L-Tyr with a gellant concentration of 6.69 mM and a surfactant concentration of 20.09 mM. The sample was transferred onto the slide at 353 K and was allowed to cool to 298 K. The image was taken after 180 minutes (scale bar = 100 μm).	122
Figure 6-59 Cryo-TEM images of the ternary system H_2O -LAS-L-Tyr-L-Tyr with a surfactant concentration of 0.29 mM and a gellant concentration of 6.69 mM. The sample was at first allowed to cool from 363 to 298 K. After standing at 298 K for 5 minutes, the sample was prepared for cryo-TEM.	123
Figure 6-60 Cryo-TEM image of the ternary system H_2O -LAS-L-Tyr-L-Tyr with a surfactant concentration of 0.29 mM and a gellant concentration of 6.69 mM. The sample was at first allowed to cool from 363 to 298 K. After standing at 298 K for 45 minutes, the sample was prepared for cryo-TEM.	124
Figure 6-61 Cryo-TEM images of the ternary system H_2O -LAS-L-Tyr-L-Tyr with a surfactant concentration of 20.09 mM and a gellant concentration of 6.69 mM. The sample was at first allowed to cool from 363 to 298 K. After standing at 298 K for 5 minutes, the sample was prepared for cryo-TEM.	124
Figure 6-62 Cryo-TEM image of the ternary system H_2O -LAS-L-Tyr-L-Tyr with a surfactant concentration of 20.09 mM and a gellant concentration of 6.69 mM. The sample was at first allowed to cool from 363 to 298 K. After standing at 298 K for 45 minutes, the sample was prepared for cryo-TEM.	125
Figure 6-63 Storage modulus G' vs. temperature (left) and storage modulus G' vs. time at a temperature of 293 K (right) of the ternary system H_2O -LAS-L-Tyr-L-Tyr with a surfactant concentration of 28.70 mM and a gellant concentration of 6.69 mM,	

measured with oscillating shear rheometry, at a constant frequency of 1 Hz, a shear strain of 0.05 %, and a cooling rate of 10 K/min, using a parallel plate geometry, with a gap of 800 μm	126
Figure 6-64 Combination of temperature-sweep and time-sweep measurements (left) and the fractal analysis of the kinetic data in terms of the <i>Dickinson</i> equation, according to equation 6-1 (right), of the ternary system H_2O -LAS-L-Tyr-L-Tyr with 28.70 mM LAS and 6.69 mM L-Tyr-L-Tyr, measured with oscillating shear rheometry, at a constant frequency of 1 Hz, a shear strain of 0.05 %, and a cooling rate of 10 K/min, using a parallel plate geometry, with a gap of 800 μm (I - Induction stage, G - Gelation stage, Q - Quasi-equilibrium stage).....	127
Figure 6-65 Storage modulus G' vs. time (right) and the extract from the diagram (left) of the ternary system H_2O -LAS-L-Tyr-L-Tyr with 6.69 mM L-Tyr-L-Tyr and varied surfactant concentrations. The data were taken from the combination of temperature-sweep and time-sweep measurements. The samples were cooled from 353 to 293 K at a rate of 10 K/min (below the minimum of G' - induction stage, above the minimum of G' - gelation stage).	130
Figure 6-66 Log-linear (left) and linear-linear plots (right) of the storage modulus G' vs. time during the gelation stage of the ternary system H_2O -LAS-L-Tyr-L-Tyr with 6.69 mM L-Tyr-L-Tyr and varied surfactant concentrations, measured with oscillating shear rheometry, at a constant strain of 0.05 %, frequency of 1 Hz, and a cooling rate of 10 K/min, using a parallel plate geometry, with a gap of 800 μm	132
Figure 6-67 Storage modulus in the quasi-equilibrium stage $G'(\infty)$ (right) and the extract from the diagram at lower surfactant concentrations (left) of the ternary system H_2O -LAS-L-Tyr-L-Tyr with 6.69 mM L-Tyr-L-Tyr as a function of LAS concentration, measured at 293 K with oscillating shear rheometry, at a frequency of 1 Hz, and a strain of 0.05 %, using a parallel plate geometry, with a gap of 800 μm . The prepared sample was transferred into the rheometer at 353 K and was cooled to 293 K with 5 and 10 K/min. The error bars give the standard deviation for the average $G'(\infty)$ values determined for each surfactant concentration.....	134
Figure 6-68 Apparent $T_{\text{sol-gel}}$ values for a cooling rate of 10 K/min (right) and the extract from the diagram at lower surfactant concentrations (left) of the ternary systems H_2O -LAS-DBC and H_2O -LAS-L-Tyr-L-Tyr with a gellant concentration of 6.69 mM and varied surfactant concentrations, measured with oscillating shear rheometry, at a constant frequency of 1 Hz, and a shear strain of 0.05 %, using a parallel plate	

geometry, with a gap of 800 μm . Symbols marked with a double asterisk, **, indicate the temperature at which the gelation occurred by a long-term measurement. 136

Figure 6-69 Measurement of the temperature dependency of the storage modulus G' of the ternary systems H_2O -LAS-DBC and H_2O -LAS-L-Tyr-L-Tyr with a gellant concentration of 6.69 mM and varied surfactant concentrations, measured with a parallel plate geometry, and a gap of 800 μm at 293 K with oscillating shear rheometry at a constant frequency of 1 Hz, a shear strain of 0.05 %, and a cooling rate of 5 K/min. 138

Figure 6-70 Storage modulus G' vs. time of the ternary systems H_2O -LAS-DBC and H_2O -LAS-L-Tyr-L-Tyr with a gellant concentration of 6.69 mM and varied surfactant concentrations for the illustration of the minimum during the gelation process. The data were taken from the combination of temperature-sweep and time-sweep measurements. The samples were cooled from 353 to 293 K at a rate of 10 K/min (below the minimum of G' - induction stage, above the minimum of G' - gelation stage). 139

Figure 6-71 Log-linear (left) and linear-linear plots (right) of the storage modulus G' vs. time during the gelation stage of the ternary systems H_2O -LAS-DBC and H_2O -LAS-L-Tyr-L-Tyr with a gellant concentration of 6.69 mM and varied LAS concentrations, measured with oscillating shear rheometry, at a constant strain of 0.05 %, frequency of 1 Hz, and a cooling rate of 10 K/min, using a parallel plate geometry, with a gap of 800 μm 141

Figure 6-72 Storage modulus in the quasi-equilibrium stage $G'(\infty)$ (right) and the extract from the diagram at lower surfactant concentrations (left) of the ternary systems H_2O -LAS-DBC and H_2O -LAS-L-Tyr-L-Tyr with a gellant concentration of 6.69 mM as a function of LAS concentration, measured at 293 K, with oscillating shear rheometry at a frequency of 1 Hz, and a strain of 0.05 %, using a parallel plate geometry, with a gap of 800 μm . The prepared sample was transferred into the rheometer at 353 K and was cooled to 293 K with 10 K/min. The error bars give the standard deviation for the average $G'(\infty)$ values determined for each surfactant concentration. 143

10 List of Tables

Table 4-1 Different classes of surfactants taken from reference [61].	27
Table 5-2 Used chemicals with their trade names, purities and suppliers. The compound L-Tyr-L-Tyr was synthesized by <i>Dominik Goebel</i> , one of Prof. <i>Nachtsheims's</i> PhD students at the university of Bremen.	42
Table 6-3 Surface tension of water and of the binary system H ₂ O-DBC with a gellant concentration of 1.11 mM at pH values of 3 and 5, measured with a Du Nouy ring tensiometer, at 298 K. The samples were prepared individually for each pH.	53
Table 6-4 Indications for different D_f values according to references [52],[13],[119]–[122]......	56
Table 6-5 Parameters taken from the kinetic data of the 6.69 mM binary system of H ₂ O-DBC for applying the <i>Dickinson</i> equation (equation 6-1) (t_g – gelation time at $G'(0)$, $G'(0)$ - average values of G' in the induction stage, $G'(\infty)$ - average values of G' in the quasi-equilibrium stage).....	60
Table 6-6 Cmc values of LAS-in-water system and in mixture with 1.11 mM DBC, determined with a <i>Du Nouy</i> ring tensiometer, at 298 K.	65
Table 6-7 Hydrodynamic diameter of particles in the binary system H ₂ O-LAS with surfactant concentrations of 20.09 and 28.70 mM, measured from the number distribution with ZetaSizer Nano Series, at 298 K. The measurement was repeated at regular 5-minute intervals.	73
Table 6-8 Thicknesses of the fiber-like aggregates, or solid fibers, determined from cryo-TEM images of the ternary system H ₂ O-LAS-DBC with a gellant concentration of 6.69 mM and varied surfactant concentrations.	82
Table 6-9 Parameters taken from the kinetic data of the ternary system H ₂ O-LAS-DBC with 0.29 mM LAS and 6.69 mM DBC for applying the <i>Dickinson</i> equation, according to equation 6-1 (t_g – gelation time at $G'(0)$, $G'(0)$ - average values of G' in the induction stage, $G'(\infty)$ - average values of G' in the quasi-equilibrium stage). The error bars give the standard deviation for the average $G'(0)$ and $G'(\infty)$ values determined for this surfactant concentration.	84
Table 6-10 Rheological data applied from temperature-sweep measurements of the ternary system H ₂ O-LAS-DBC with 6.69 mM DBC and varied LAS concentrations, measured at a cooling rate of 10 K/min ($T_{sol-gel}$ - apparent sol-gel transition temperature for a cooling rate of 10 K/min, $G'(0)$ - average values of G' in the induction stage, $G'(\infty)$ - average values of G' in the quasi-equilibrium stage, t_g - gelation time at $G'(0)$	

and t_{gelation} - difference of the gelation time at $G'(\infty)$ and $G'(0)$. Symbols marked with a double asterisk, **, indicate the temperature at which the gelation occurred by a long-term measurement). The error bars give the standard deviation for the average $G'(0)$ and $G'(\infty)$ values determined for each surfactant concentration. 86

Table 6-11 Rheological data applied from temperature-sweep measurements of the ternary system H₂O-LAS-DBC with 6.69 mM DBC and varied LAS concentrations, measured at a cooling rate of 5 K/min ($T_{\text{sol-gel}}$ - apparent sol-gel transition temperature for a cooling rate of 5 K/min, $G'(0)$ - average values of G' in the induction stage, $G'(\infty)$ - average values of G' in the quasi-equilibrium stage, t_g - gelation time at $G'(0)$ and t_{gelation} - difference of the gelation time at $G'(\infty)$ and $G'(0)$. Symbols marked with a double asterisk, **, indicate the temperature at which the gelation occurred by a long-term measurement). The error bars give the standard deviation for the average $G'(0)$ and $G'(\infty)$ values determined for each surfactant concentration. 88

Table 6-12 Fractal analysis of the kinetic data of the ternary system H₂O-LAS-DBC with 6.69 mM DBC and varied LAS concentrations, acquired by time-sweep measurements, in terms of the *Dickinson* equation, according to equation 6-1, at 293 K. The prepared samples were transferred into the rheometer at 353 K and were cooled to 293 K at a rate of 10 K/min (T - measuring temperature, $G'(0)$ - average values of G' in the induction stage, $G'(\infty)$ - average values of G' in the quasi-equilibrium stage, t_g - gelation time at $G'(0)$ and t_{gelation} - difference of the gelation time at $G'(\infty)$ and $G'(0)$). The error bars give the standard deviation for the average $G'(0)$ and $G'(\infty)$ values determined for each surfactant concentration. 92

Table 6-13 Rheological data applied from the analysis of the kinetic data of the ternary system H₂O-LAS-DBC with a gellant concentration of 6.69 mM and varied surfactant concentrations, measured at cooling rates of 5 and 10 K/min. For the determination of the t - t_g values, the time was taken at which the same G' value was obtained for all surfactant concentrations (t_g - gelation time, fixed G' value for a cooling rate of 5 K/min – $3 \times 10^{+02}$ Pa and fixed G' value for a cooling rate of 10 K/min – $5 \times 10^{+01}$ Pa). 96

Table 6-14 Cmc values of the H₂O-C₁₂₋₁₈E₇ binary system and H₂O-C₁₂₋₁₈E₇-DBC ternary system with 1.11 mM DBC, determined with a *Du Nouy* ring tensiometer, at 298 K and pH 5. 104

Table 6-15 Parameters taken from the kinetic data of the ternary system H₂O-LAS-L-Tyr-L-Tyr with a surfactant concentration of 28.70 mM and 6.69 mM L-Tyr-L-Tyr for applying the *Dickinson* equation, according to equation 6-1 (t_g – gelation

time at $G'(0)$, $G'(\infty)$ - average values of G' in the induction stage, $G'(\infty)$ - average values of G' in the quasi-equilibrium stage). The error bars give the standard deviation for the average $G'(0)$ and $G'(\infty)$ values determined for this surfactant concentration. 127

Table 6-16 Fractal analysis of the kinetic data of the ternary system H_2O -LAS-L-Tyr-L-Tyr with 6.69 mM L-Tyr-L-Tyr and varied surfactant concentrations, acquired by dynamic rheological measurements, in terms of the *Dickinson* equation, according to equation 6-1. The prepared samples were transferred into the rheometer at 353 K and were cooled to 293 K at a rate of 10 K/min ($T_{sol-gel}$ - apparent sol-gel transition temperature for a cooling rate of 10 K/min, $G'(0)$ - average values of G' in the induction stage, $G'(\infty)$ - average values of G' in the quasi-equilibrium stage, t_g - gelation time at $G'(0)$ and $t_{gelation}$ - difference of the gelation time at $G'(\infty)$ and $G'(0)$). The error bars give the standard deviation for the average $G'(0)$ and $G'(\infty)$ values determined for each surfactant concentration..... 129

Table 6-17 Fractal analysis of the kinetic data of the ternary system H_2O -LAS-L-Tyr-L-Tyr with 6.69 mM L-Tyr-L-Tyr and varied surfactant concentrations, acquired by dynamic rheological measurements, in terms of the *Dickinson* equation, according to equation 6-1. The prepared samples were transferred into the rheometer at 353 K and were cooled to 293 K at a rate of 5 K/min ($T_{sol-gel}$ - apparent sol-gel transition temperature for a cooling rate of 5 K/min, $G'(0)$ - average values of G' in the induction stage, $G'(\infty)$ - average values of G' in the quasi-equilibrium stage, t_g - gelation time at $G'(0)$ and $t_{gelation}$ - difference of the gelation time at $G'(\infty)$ and $G'(0)$). The error bars give the standard deviation for the average $G'(0)$ and $G'(\infty)$ values determined for each surfactant concentration..... 131

Table 6-18 Rheological data applied from the analysis of the kinetic data of the ternary system H_2O -LAS-L-Tyr-L-Tyr with a gellant concentration of 6.69 mM and varied surfactant concentrations, measured at cooling rates of 5 and 10 K/min. For the determination of the $t-t_g$ values, the time was taken at which the same G' value was obtained for all surfactant concentrations (t_g - gelation time at $G'(0)$, fixed G' value for a cooling rate of 5 K/min – $8 \times 10^{+02}$ Pa and fixed G' value by cooling at a rate of 10 K/min – $7 \times 10^{+02}$ Pa). 133

Table 6-19 Fractal analysis of the kinetic data of the ternary systems H_2O -LAS-DBC and H_2O -LAS-L-Tyr-L-Tyr with a gellant concentration of 6.69 mM and varied surfactant concentrations, acquired by temperature and time-sweep measurements, in terms of the *Dickinson* equation, according to equation 6-1. The prepared samples

were transferred into the rheometer at 353 K and were cooled to 293 K at a rate of 10 K/min ($T_{\text{sol-gel}}$ - apparent sol-gel transition temperature for a cooling rate of 10 K/min, t_g - gelation time at $G'(0)$ and t_{gelation} - difference of the gelation time at $G'(\infty)$ and $G'(0)$. Symbols marked with a double asterisk, **, indicate the temperature at which the gelation occurred by a long-term measurement at a constant temperature)..... 140

Table 6-20 Rheological data applied from the analysis of the kinetic data of the ternary systems H₂O-LAS-DBC and H₂O-LAS-L-Tyr-L-Tyr with a gellant concentration of 6.69 mM and varied surfactant concentrations, measured at a cooling rate of 10 K/min. For the determination of the data for $t-t_g$, the time was taken at which the same G' value was obtained for all surfactant concentrations in the presence of the two gelling agents for varied surfactant concentrations (t_g - gelation time at $G'(0)$, fixed G' value – $4 \times 10^{+01}$ Pa). 142

11 References

- [1] Adhikari, B. et al., Pyrene-containing peptide-based fluorescent organogels, *Chemistry (Weinheim an der Bergstrasse, Germany)* **2011**, 17, 11488–11496.
- [2] Erdogan, H. et al., Laser-triggered degelation control of gold nanoparticle embedded peptide organogels, *Langmuir* **2013**, 29, 6975–6982.
- [3] Geng, H. et al., Low-Molecular-Weight Organo- and Hydrogelators Based on Cyclo(l-Lys-l-Glu), *Langmuir* **2016**, 32, 4586–4594.
- [4] Liu, X. et al., Transformation of Dipeptide-Based Organogels into Chiral Crystals by Cryogenic Treatment, *Angewandte Chemie (International ed. in English)* **2017**, 56, 2660–2663.
- [5] Baddeley, C. et al., Structure-function studies of modular aromatics that form molecular organogels, *The Journal of organic chemistry* **2007**, 72, 7270–7278.
- [6] Xing, P. et al., Superstructure Formation and Topological Evolution Achieved by Self-Organization of a Highly Adaptive Dynamer, *ACS nano* **2016**, 10, 2716–2727.
- [7] Bartocci, S. et al., Solvent-tunable morphology and emission of pyrene-dipeptide organogels, *Journal of peptide science : an official publication of the European Peptide Society* **2015**, 21, 871–878.
- [8] Jang, K. et al., Organogels from functionalized T-shaped pi-conjugated bisphenazines, *Langmuir* **2010**, 26, 13630–13636.
- [9] Löfman, M. et al., Bile acid alkylamide derivatives as low molecular weight organogelators, *Journal of colloid and interface science* **2011**, 360, 633–644.
- [10] Zhang, L. et al., Self-Assembly and Drug Release Capacities of Organogels via Some Amide Compounds with Aromatic Substituent Headgroups, *Materials (Basel, Switzerland)* **2016**, 9.
- [11] Estroff, L. A. et al., Water Gelation by Small Organic Molecules, *Chem. Rev.* **2004**, 104, 1201–1217.
- [12] Abdallah, D. J. et al., Organogels and Low Molecular Mass Organic Gelators, *Advanced Materials* **2000**, 12, 1237–1247.
- [13] Huang, X. et al., Distinct kinetic pathways generate organogel networks with contrasting fractality and thixotropic properties, *Journal of the American Chemical Society* **2006**, 128, 15341–15352.

- [14] Meunier, J. A., Sur les composés que la mannite et la sorbite forment avec les aldéhydes, par M.J. Meunier,, *Gauthier-Villars et fils* **1891**.
- [15] Brenzinger, K., Zur Kenntnis des Cystins und des Cysteins, *Z. Physiol. Chem.* **1892**, 16, 537.
- [16] Cortner, R. A., NOTE, *Journal of the American Chemical Society* **1921**, 43, 2199–2202.
- [17] Zsigmondy, R. et al., Ueber Gallerten, *Zeitschrift für Chemie und Industrie der Kolloide* **1912**, 11, 145–157.
- [18] Schacht, K. et al., Controlled hydrogel formation of a recombinant spider silk protein, *Biomacromolecules* **2011**, 12, 2488–2495.
- [19] Lescanne, M. et al., Thixotropic Organogels Based on a Simple N -Hydroxyalkyl Amide, *Langmuir* **2004**, 20, 3032–3041.
- [20] Terech, P. et al., Low Molecular Mass Gelators of Organic Liquids and the Properties of Their Gels, *Chem. Rev.* **1997**, 3133–3159.
- [21] Skilling, K. J. et al., Insights into low molecular mass organic gelators: a focus on drug delivery and tissue engineering applications, *Soft matter* **2014**, 237–256.
- [22] McNeice, P. et al., Low molecular weight gelators (LMWGs) for ionic liquids, *Green Chemistry* **2017**, 19, 4690–4697.
- [23] Lloyd, G. O. et al., Anion-tuning of supramolecular gel properties, *Nature chemistry* **2009**, 1, 437–442.
- [24] Li, J.-L. et al., Control of crystallization in supramolecular soft materials engineering, *Soft matter* **2013**, 9, 435–442.
- [25] Che, X. et al., Gelation behaviour and gel properties of two-component organogels containing a photoresponsive gelator, *New J. Chem.* **2017**, 41, 8614–8619.
- [26] Heeres, A. et al., Orthogonal self-assembly of low molecular weight hydrogelators and surfactants, *Journal of the American Chemical Society* **2003**, 125, 14252–14253.
- [27] Xing, P. et al., Switchable and orthogonal self-assemblies of anisotropic fibers, *New J. Chem.* **2013**, 37, 3949.
- [28] Tang, S. et al., Producing Supramolecular Functional Materials Based on Fiber Network Reconstruction, *Advanced Functional Materials* **2009**, 19, 2252–2259.

- [29] Nebot, V. J. et al., Interplay of molecular hydrogelators and SDS affords responsive soft matter systems with tunable properties, *Langmuir* **2013**, 29, 9544–9550.
- [30] Menger, F. M. et al., Anatomy of a Gel. Amino Acid Derivatives That Rigidify Water at Submillimolar Concentrations, *Journal of the American Chemical Society* **2000**, 122, 11679–11691.
- [31] Xing, B. et al., Hydrophobic interaction and hydrogen bonding cooperatively confer a vancomycin hydrogel, *Journal of the American Chemical Society* **2002**, 124, 14846–14847.
- [32] Drury, J. L. et al., Hydrogels for tissue engineering, *Biomaterials* **2003**, 24, 4337–4351.
- [33] Li, J. L. et al., Engineering of Small Molecule Organogels by Design of the Nanometer Structure of Fiber Networks, *Advanced Materials* **2006**, 18, 2574–2578.
- [34] Brizard, A. M. et al., Self-assembled interpenetrating networks by orthogonal self assembly of surfactants and hydrogelators, *Faraday Discussions* **2009**, 143, 345.
- [35] Behanna, H. A. et al., Modulation of fluorescence through coassembly of molecules in organic nanostructures, *Journal of the American Chemical Society* **2007**, 129, 321–327.
- [36] Chen, J.-Y. et al., Synergistic Coassembly of Two Structurally Different Molecular Gelators, *Langmuir* **2016**, 32, 12175–12183.
- [37] Fleming, S. et al., Insights into the coassembly of hydrogelators and surfactants based on aromatic peptide amphiphiles, *Biomacromolecules* **2014**, 15, 1171–1184.
- [38] Chen, J.-Y. et al., Manipulating the fractal fiber network of a molecular gel with surfactants, *Journal of colloid and interface science* **2018**, 526, 356–365.
- [39] Moffat, J. R. et al., Controlled self-sorting in the assembly of 'multi-gelator' gels, *Chemical Communications* **2009**, 316–318.
- [40] Laibinis, P. E. et al., Orthogonal self-assembled monolayers, *science* **1989**, 245, 845–847.
- [41] Laupheimer, M. et al., Studying orthogonal self-assembled systems, *Soft matter* **2013**, 9, 3661.
- [42] Laupheimer, M., Gelled Bicontinuous Microemulsions, *Springer International Publishing* **2014**.

- [43] Laupheimer, M. et al., Studying orthogonal self-assembled systems, *Soft matter* **2014**, 10, 8744–8757.
- [44] Fu, C. et al., Fluorescent sensitization of gemini surfactant micellar-hybridized supramolecular hydrogels, *Journal of Luminescence* **2017**, 181, 8–13.
- [45] Koitani, S. et al., Gelling Lamellar Phases of the Binary System Water-Didodecyldimethylammonium Bromide with an Organogelator, *Langmuir* **2017**, 33, 12171–12179.
- [46] Jinno, Y. et al., Ionic surfactants induce amphiphilic tris(urea) hydrogel formation, *Chemistry, an Asian journal* **2012**, 7, 1768–1771.
- [47] Murata, K. et al., Thermal and Light Control of the Sol-Gel Phase Transition in Cholesterol-Based Organic Gels. Novel Helical Aggregation Modes As Detected by Circular Dichroism and Electron Microscopic Observation, *Journal of the American Chemical Society* **1994**, 116, 6664–6676.
- [48] Abdallah, D. J. et al., The Influence of the Cationic Center, Anion, and Chain Length of Tetra-n-alkylammonium and -phosphonium Salt Gelators on the Properties of Their Thermally Reversible Organogels, *Chemistry of Materials* **2000**, 12, 406–413.
- [49] Lam, R. et al., A molecular insight into the nature of crystallographic mismatches in self-assembled fibrillar networks under non-isothermal crystallization conditions, *Soft matter* **2010**, 6, 404–408.
- [50] Du, X. et al., Supramolecular Hydrogelators and Hydrogels, *Chemical reviews* **2015**, 115, 13165–13307.
- [51] Yuan, B. et al., Size invariance of fibrous networks of supramolecular soft materials during formation under critical volume confinement, *Soft matter* **2012**, 8, 5187.
- [52] Atencia, J. et al., Controlled microfluidic interfaces, *Nature* **2005**, 437, 648–655.
- [53] Liu, X. Y. et al., Creating New Supramolecular Materials by Architecture of Three-Dimensional Nanocrystal Fiber Networks, *Journal of the American Chemical Society* **2002**, 124, 15055–15063.
- [54] Liu, X. Y. et al., Mechanism of the Formation of Self-Organized Microstructures in Soft Functional Materials, *Advanced Materials* **2002**, 421–426.
- [55] Chen, J. Y. et al., Controlling the Supramolecular Architecture of Molecular Gels with Surfactants, *Langmuir* **2016**, 32, 1171–1177.

- [56] Hanabusa, K. et al., Physical Gelation by Low-Molecular-Weight Compounds and Development of Gelators, *Bulletin of the Chemical Society of Japan* **2016**, 89, 174–182.
- [57] Wang, L. et al., Synthesis and gelation capability of mono- and disubstituted cyclo(L-Glu-L-Glu) derivatives with tyramine, tyrosine and phenylalanine, *Colloid and Polymer Science* **2017**, 295, 1549–1561.
- [58] Xie, Z. et al., Organo- and hydrogels derived from cyclo(L-Tyr-L-Lys) and its ϵ -amino derivatives, *Soft matter* **2009**, 5, 1474.
- [59] Li, Y. et al., Ultrasound induced formation of organogel from a glutamic dendron, *Tetrahedron* **2007**, 63, 7468–7473.
- [60] Zhai, Z. et al., Mechanically-sensitive hydrogels formed from β -cyclodextrin and an anionic surfactant containing a biphenyl group, *Soft matter* **2016**, 12, 2715–2720.
- [61] Wang, J. et al., Visible-light/temperature dual-responsive hydrogel constructed by α -cyclodextrin and an azobenzene linked surfactant, *Soft matter* **2017**, 13, 6490–6498.
- [62] Kleinsmann, A. J. et al., Phenylalanine-containing cyclic dipeptides--the lowest molecular weight hydrogelators based on unmodified proteinogenic amino acids, *Chemical communications (Cambridge, England)* **2013**, 49, 7818–7820.
- [63] Dörfler, H.-D., Grenzflächen und kolloid-disperse Systeme, *Springer* **2002**.
- [64] Mitchell, D. J. et al., Phase behaviour of polyoxyethylene surfactants with water. Mesophase structures and partial miscibility (cloud points), *Journal of the Chemical Society, Faraday Transactions 1: Physical Chemistry in Condensed Phases* **1983**, 79, 975.
- [65] Clint, J. H., Surfactant Aggregation, *Springer Netherlands* **2012**.
- [66] Toerne, K. et al., Thermal Stability of Nonionic Surfactant Aggregates, *Langmuir* **2001**, 17, 6119–6121.
- [67] Demyanchuk, I. et al., Percolation-to-droplets transition during spinodal decomposition in polymer blends, morphology analysis, *The Journal of chemical physics* **2004**, 121, 1141–1147.
- [68] Guo, C. et al., Toward a Quantitative Model and Prediction of the Cloud Point of Normal Nonionic Surfactants and Novel Gemini Surfactants with Heuristic Method and Gaussian Process, *Journal of Dispersion Science and Technology* **2012**, 33, 1401–1410.

- [69] Abdallah, D. J. et al., The Quest for the Simplest Possible Organogelators and Some Properties of their Organogels, *J. Braz. Chem. Soc.* **2000**, 11, 209–218.
- [70] Piepenbrock, M.-O. M. et al., Metal- and anion-binding supramolecular gels, *Chemical reviews* **2010**, 110, 1960–2004.
- [71] Aggeli, A. et al., Hierarchical self-assembly of chiral rod-like molecules as a model for peptide β -sheet tapes, ribbons, fibrils, and fibers, *Proceedings of the National Academy of Sciences of the United States of America* **2001**, 98, 11857–11862.
- [72] Smith, D. K., Supramolecular gels, *Nature chemistry* **2010**, 2, 162–163.
- [73] van Esch, J. H., We Can Design Molecular Gelators, But Do We Understand Them?, *Langmuir* **2009**, 8392–8394.
- [74] Lan, Y. et al., To gel or not to gel, *Chemical Society reviews* **2015**, 44, 6035–6058.
- [75] Weiss, R. G., The past, present, and future of molecular gels. What is the status of the field, and where is it going?, *Journal of the American Chemical Society* **2014**, 136, 7519–7530.
- [76] Albert, R. et al., Statistical mechanics of complex networks, *Reviews of Modern Physics* **2002**, 74, 47–97.
- [77] Wang, R. et al., Real-time observation of fiber network formation in molecular organogel, *The journal of physical chemistry. B* **2006**, 110, 7275–7280.
- [78] Xu, W. et al., Sol–gel transition of poly(3-hexylthiophene) revealed by capillary measurements, *Soft matter* **2012**, 8, 726–733.
- [79] Wang, R.-Y. et al., Architecture of fiber network, *The journal of physical chemistry. B* **2006**, 110, 25797–25802.
- [80] Tan, G. et al., Nucleation and growth characteristics of a binary low-mass organogel, *Langmuir* **2006**, 22, 7416–7420.
- [81] Shi, J. H. et al., Spherulitic networks, *The journal of physical chemistry. B* **2009**, 113, 4549–4554.
- [82] Yuan, B. et al., Volume confinement induced microstructural transitions and property enhancements of supramolecular soft materials, *Soft matter* **2011**, 7, 1708–1713.

- [83] Lescanne, M. et al., Structural Aspects of the Gelation Process Observed with Low Molecular Mass Organogelators, *Langmuir* **2003**, 19, 2013–2020.
- [84] SCHRAMM, G. A. et al., A Practical Approach to Rheology and Rheometry, *Haake* **1994**.
- [85] Rogers, M. A. et al., Solvent-modulated nucleation and crystallization kinetics of 12-hydroxystearic acid, *Langmuir* **2009**, 25, 8556–8566.
- [86] Liu, X. Y., Interfacial Effect of Molecules on Nucleation Kinetics †, *J. Phys. Chem. B* **2001**, 105, 11550–11558.
- [87] Vintiloiu, A. et al., Organogels and their use in drug delivery--a review, *Journal of controlled release : official journal of the Controlled Release Society* **2008**, 125, 179–192.
- [88] Raeburn, J. et al., The importance of the self-assembly process to control mechanical properties of low molecular weight hydrogels, *Chemical Society reviews* **2013**, 42, 5143–5156.
- [89] Buerkle, L. E. et al., Supramolecular gels formed from multi-component low molecular weight species, *Chem. Soc. Rev.* **2012**, 41, 6089–6102.
- [90] Sangeetha, N. M. et al., Supramolecular gels: Functions and uses, *Chem. Soc. Rev.* **2005**, 34, 821–836.
- [91] Yang, Z. et al., Conjugates of naphthalene and dipeptides produce molecular hydrogelators with high efficiency of hydrogelation and superhelical nanofibers, *Journal of Materials Chemistry* **2007**, 17, 850–854.
- [92] Mahler, A. et al., Rigid, Self-Assembled Hydrogel Composed of a Modified Aromatic Dipeptide, *Advanced Materials* **2006**, 18, 1365–1370.
- [93] Brizard, A. et al., Preparation of Nanostructures by Orthogonal Self-Assembly of Hydrogelators and Surfactants, *Angewandte Chemie* **2008**, 120, 2093–2096.
- [94] BROGLIE, L. de, Waves and Quanta, *Nature* **1923**, 112, 540.
- [95] Hawkes, P. W. et al., Transmission Electron Microscopy, *Springer Berlin Heidelberg* **1993**.
- [96] Roos, N. et al., Cryopreparation of thin biological specimens for electron microscopy, *Oxford Univ. Press* **1990**.
- [97] Costello, M. J., Cryo-electron microscopy of biological samples, *Ultrastructural pathology* **2006**, 30, 361–371.

- [98] Egelhaaf, S. U. et al., New controlled environment vitrification system for cryo-transmission electron microscopy, *Journal of Microscopy* **2000**, 200, 128–139.
- [99] Friedrich, H. et al., Imaging of self-assembled structures, *Angewandte Chemie (International ed. in English)* **2010**, 49, 7850–7858.
- [100] Mie, G., Beiträge zur Optik trüber Medien, speziell kolloidaler Metallösungen, *Annalen der Physik* **1908**, 330, 377–445.
- [101] Cummins, H. Z.; Pike, E. R., Photon Correlation and Light Beating Spectroscopy, *Springer US* **1974**.
- [102] Chu, B., Laser light scattering, *Academic Press* **1991**.
- [103] Everett, D. H., Grundzüge der Kolloidwissenschaft, *Steinkopff* **1992**.
- [104] Stetefeld, J. et al., Dynamic light scattering, *Biophysical reviews* **2016**, 8, 409–427.
- [105] Pecora, R., Dynamic Light Scattering, *Springer US* **1985**.
- [106] Kasapis, S. et al., Rheology and Food Microstructure, 7–46.
- [107] Irgens, F., Rheology and Non-Newtonian Fluids, *Springer International Publishing* **2014**.
- [108] Mezger, T. G., The Rheology Handbook, *Vincentz Network* **2014**.
- [109] Malkin, A. J. et al., Rheology, *ChemTec Publ* **2012**.
- [110] Tadros, T. F., Rheology of Dispersions, *Wiley* **2011**.
- [111] Winter, H. H., Can the gel point of a cross-linking polymer be detected by the G?, *Polymer Engineering and Science* **1987**, 27, 1698–1702.
- [112] Ranjan, R. et al., Folic acid supramolecular ionogels, *Physical chemistry chemical physics : PCCP* **2017**, 19, 22934–22945.
- [113] Boekhoven, J. et al., Bio-inspired supramolecular materials by orthogonal self-assembly of hydrogelators and phospholipids, *Chemical science* **2016**, 7, 6021–6031.
- [114] Friggeri, A. et al., Entrapment and release of quinoline derivatives using a hydrogel of a low molecular weight gelator, *Journal of controlled release : official journal of the Controlled Release Society* **2004**, 97, 241–248.
- [115] Gould, T. J. et al., Optical nanoscopy, *Annual review of biomedical engineering* **2012**, 14, 231–254.

- [116] Friggeri, A. et al., Charge-Transfer Phenomena in Novel, Dual-Component, Sugar-Based Organogels, *Journal of the American Chemical Society* **2002**, 124, 10754–10758.
- [117] Hauner, I. M. et al., The Dynamic Surface Tension of Water, *The journal of physical chemistry letters* **2017**, 8, 1599–1603.
- [118] Guo, Y.-j. et al., Solution Property Investigation of Combination Flooding Systems Consisting of Gemini–Non-ionic Mixed Surfactant and Hydrophobically Associating Polyacrylamide for Enhanced Oil Recovery, *Energy & Fuels* **2012**, 26, 2116–2123.
- [119] Dickinson, E., On gelation kinetics in a system of particles with both weak and strong interactions, *Journal of the Chemical Society, Faraday Transactions* **1997**, 93, 111–114.
- [120] Ziff, R. M. et al., The kinetics of cluster fragmentation and depolymerisation, *Journal of Physics A: Mathematical and General* **1985**, 18, 3027–3037.
- [121] Brinker, C. J. et al., Sol-Gel Science, *Elsevier Science* **1990**.
- [122] Huang, X. et al., Kinetics of 5 α -cholestan-3 β -yl N-(2-naphthyl)carbamate/n-alkane organogel formation and its influence on the fibrillar networks, *Journal of the American Chemical Society* **2005**, 127, 4336–4344.
- [123] Liu, X. Y. et al., Formation kinetics of fractal nanofiber networks in organogels, *Applied Physics Letters* **2001**, 79, 3518–3520.
- [124] Khalkhal, F. et al., Scaling behavior of the elastic properties of non-dilute MWCNT–epoxy suspensions, *Rheologica Acta* **2011**, 50, 717–728.
- [125] Wang, R.-Y. et al., From kinetic-structure analysis to engineering crystalline fiber networks in soft materials, *Physical chemistry chemical physics : PCCP* **2013**, 15, 3313–3319.
- [126] Shih, W.-H. et al., Scaling behavior of the elastic properties of colloidal gels, *Physical Review A* **1990**, 42, 4772–4779.
- [127] Terech, P. et al., Rheological Properties and Structural Correlations in Molecular Organogels, *Langmuir* **2000**, 16, 4485–4494.
- [128] MacKintosh et al., Elasticity of semiflexible biopolymer networks, *Physical review letters* **1995**, 75, 4425–4428.

- [129] Chen, Y.-Y. et al., The Effect of Sodium Dodecylbenzenesulfonate (SDBS) Micelles on a Belousov □ Zhabotinsky Oscillating System Catalyzed with a Tetraazamacrocyclic Copper(II) Complex, *Helvetica Chimica Acta* **2014**, 97, 237–244.
- [130] Mysels, K. J. et al., Light Scattering by Some Laurylsulfate Solutions, *The Journal of Physical Chemistry* **1959**, 63, 1696–1700.
- [131] Li, J.-L. et al., Architecture of Supramolecular Soft Functional Materials: From Understanding to Micro-/Nanoscale Engineering, *Advanced Functional Materials* **2010**, 3196–3216.
- [132] Watanabe, H. et al., Rheological and Morphological Behavior of Styrene-Butadiene Diblock Copolymer Solutions in Selective Solvents, *Journal of Rheology* **1982**, 26, 153–179.
- [133] Vlasenko, A. S. et al., Dissociation constants and micelle–water partition coefficients of hydroxybenzoic acids and parabens in surfactant micellar solutions, *Journal of Molecular Liquids* **2009**, 145, 182–187.
- [134] Sood, A. K. et al., Evaluation of micellar properties of sodium dodecylbenzene sulphonate in the presence of some salts, *Journal of Chemical Sciences* **2018**, 130, 60.
- [135] Rai, R. et al., Ionic liquid-induced unprecedented size enhancement of aggregates within aqueous sodium dodecylbenzene sulfonate, *Langmuir* **2010**, 26, 17821–17826.
- [136] Palazzesi, F. et al., A molecular dynamics investigation of structure and dynamics of SDS and SDBS micelles, *Soft matter* **2011**, 7, 9148.
- [137] Patterson, J. P. et al., The analysis of solution self-assembled polymeric nanomaterials, *Chemical Society reviews* **2014**, 43, 2412–2425.
- [138] Henkel KGaA Düsseldorf, Fatty Alcohols - Raw Materials, Processes, Application, *ZR-Fettchemie* **1982**.
- [139] Tanaka, M. et al., Recommended table for the density of water between 0 C and 40 C based on recent experimental reports, *Metrologia* **2001**, 38, 301–309.
- [140] Liu, Y. et al., Identify kinetic features of fibers growing, branching, and bundling in microstructure engineering of crystalline fiber network, *CrystEngComm* **2014**, 16, 5402.

- [141] Dawn, A. et al., Low Molecular Weight Supramolecular Gels Under Shear, *Chemistry (Weinheim an der Bergstrasse, Germany)* **2018**, 24, 762–776.

12 List of Presentations

1. Poster presentation at *Zsigmondy-Kolloquium* 2017; „Self-assembly of Low Molecular Weight Gellants in Presence of Surfactants“; F. Yapici, A. Klemmer, P. Schmiedel, W. von Rybinski; Saarbrücken/Germany; April 2017
2. Poster presentation at *Kolloid-Tagung* 2017; “Self-assembly of Low Molecular Weight Gellants in Presence of Surfactants”; F. Yapici, P. Schmiedel, W. von Rybinski; München/Germany; October 2017
3. Poster presentation at *ECIS* 2018; “Impact of Surfactants on the Dynamics of the Gelation Process of Low Molecular Weight Hydrogellants”; F. Yapici, P. Schmiedel, C.A.M. Seidel, W. von Rybinski; Ljubljana/Slovenia; September 2018
4. Lecture at *IDC* 2019; “Impact of Surfactants on the Dynamics of the Gelation Process of Low Molecular Weight Hydrogellants”; F. Yapici, P. Schmiedel, W. von Rybinski, C.A.M. Seidel; Düsseldorf/Germany; April 2019

13 Acknowledgements

Throughout the writing of this dissertation I have received a great deal of support and assistance. I have been lucky enough to have a chance to spend a few years of my life holding this research.

First of all, I would like to express my sincere gratitude to *Prof. Dr. Wolfgang von Rybinski* for his support of my PhD study. Thank you so much for your excellent cooperation and help during my research.

Special thanks go also out to *Prof. Dr. Claus Seidel*, who provided me an opportunity to do my PhD thesis in cooperation with his institute, for his very valuable support and discussions.

My sincere thanks also goes to *Dr. Peter Schmiedel* (Henkel AG & Co. KGaA) for his immense knowledge, insightful comments and encouragement to successfully complete my PhD thesis. You supported me greatly and were always willing to help me.

In addition, I want to thank *Dr. Matthias Wegener*, *Dr. Benjamin Berntsson* and *Daniel Menham* for the revision of this manuscript and *Burkhard Eschen* for his enormous help concerning cryo-TEM measurements.

I also want to thank the company Henkel AG & Co. KGaA for the financial support during my PhD thesis.

I owe a huge debt of gratitude to my parents *Gülay* and *Nebi Yapici*, to my sisters *Nergis* and *Elif* and to my brother *Ahmet* for their continuous support, patience and love. You are always there for me.

14 Eidesstattliche Erklärung

Hiermit versichere ich an Eides statt, dass die Dissertation mit dem Thema

„Self-assembly of Low Molecular Weight Gellants in the Presence of Surfactants“

von mir selbstständig und ohne unzulässige fremde Hilfe unter Beachtung der „Grundsätze zur Sicherung guter wissenschaftlicher Praxis an der Heinrich-Heine-Universität Düsseldorf“ erstellt worden ist, sowie von mir in der vorgelegten oder in ähnlicher Form noch bei keiner anderen Institution eingereicht wurde.

Es existieren keine vorherigen Promotionsversuche.

Düsseldorf, den 21.01.2020

Filiz Yapici